UNIVERSITÀ
DEGLI STUDI
DI PADOVA

Università degli Studi di Padova

Dipartimento di Scienze Biomediche

CORSO DI DOTTORATO DI RICERCA IN SCIENZE BIOMEDICHE SPERIMENTALI

CICLO XXX

THE ROLE OF RAPTOR IN ADULT SKELETAL MUSCLE

Coordinatore: Ch.mo Prof. Paolo Bernardi

Supervisore: Ch.mo Prof. Bert Blaauw

Dottorando : Martina Baraldo

INDEX

SUMMARY

Skeletal muscle is the largest organ in the body comprising 40% of total body mass. Skeletal muscle mass is the result of an equilibrium between protein synthesis and protein breakdown. When protein synthesis overcomes protein degradation the result is muscle hypertrophy with increased fiber size. Better understanding of the signaling pathways controlling muscle mass and function is of great importance. Indeed so far there are no therapeutic approaches that can prevent or reduce muscle wasting, as seen in aging and muscular dystrophy. While various studies have identified important regulators of adult skeletal muscle mass, little is known about how these pathways can modulate muscle function. One of the main pathways regulating skeletal muscle is the Akt-mTOR pathway.

Under anabolic conditions, mTOR is activated, leading to increased protein synthesis through the phosphorylation of S6K1 and 4EBP1. On the other hand, mTOR activation can also lead to the inhibition of protein degradation through the phosphorylation of Ulk1, which is involved in the autophagosome formation.

mTOR assembles into two distinct multiprotein complexes, namely the rapamycin-sensitive complex mTORC1 and the rapamycin-insensitive complex mTORC2. While mTORC2 is mainly involved in cytoskeleton reorganization, mTORC1 plays a role in cell growth and protein synthesis. One of the key members of the mTORC1 is a 150kDa protein called Raptor, which has been shown to be able to recruit mTOR substrates S6K1 and 4EBP1 on mTORC1, promoting their phosphorylation (Hara et al., 2002) (Kim et al., 2002).

Mice lacking Raptor only in skeletal muscle from birth show a pronounced myopathy leading to premature death (Bentzinger et al., 2008). However, treating adult mice with the specific mTORC1 inhibitor rapamycin does not lead to a myopathic phenotype and even improves muscle physiology in aged mice (Harrison et al., 2009). So, we wondered what happens if Raptor is deleted in adult skeletal muscle.

We, therefore, generated an inducible muscle-specific Raptor knock-out mouse line (HSA-Raptor ko).

One month of Raptor deletion in adult muscle does not affect muscle mass or muscle morphology. In addition, also muscle force production is comparable between control and knock-out animals, confirming that at this time point there are no myopathies.

Since in literature it has been reported that deletion of Raptor from birth leads to premature death around 5-6 months of age, we decided to monitor mice lifespan and body weight for a longer period after deletion. We observed that body weight during these months is unchanged between wt and Raptor ko mice, so we decided to sacrifice mice 7 months after the beginning of the treatment to assess muscle histology.

At this time point, muscles from Raptor ko mice showed signs of a muscle myopathy, with centronucleated fibers, a high number of small and large muscle fibers, central structures and inflammation. In addition, we observed that Raptor knock-out muscles show a huge amount of spontaneous fibrillation spikes at rest, suggesting the presence of denervated fibers. Furthermore, mitochondrial membrane potential and respiratory chain complex activity are impaired upon Raptor deletion. These features result in compromised muscle performance and exercise intolerance.

Moreover, while metabolic characteristics upon Raptor deletion shift from oxidative to glycolytic fibers with glycogen accumulation, structural properties reveal the opposite behaviour, with a shift from fast- to slow-twitch fibers. This is likely linked to the increased activity of calcineurin-NFAT pathway seen in Raptor ko muscles.

Since understanding the key players in the regulation of muscle mass can be of therapeutic interest, we wanted to understand the role of Raptor during Akt-induced hypertrophy. So, we generate an inducible muscle-specific Akt-Raptor ko mouse line.

Akt overexpression results in a strong increase in cross-sectional area of muscle fibers, which is only partially reduced upon Raptor deletion.

Moreover, fiber hypertrophy is completely blunted when Akt-Raptor ko mice are treated with the mTORC1 inhibitor, rapamycin.

We also found that Akt-Raptor ko mice are significantly weaker than controls, meaning that Akt-induced hypertrophy in the absence of Raptor is not functional anymore. In addition, this effect is not reverted by rapamycin administration, as seen in Akt-S6K1 knock-out mice (Marabita et al., 2016).

RIASSUNTO

I muscoli scheletrici costituiscono il 40% di tutto l'organismo. Il tessuto muscolare è un tessuto molto plastico e dinamico che si adatta in relazione ai diversi stimoli. La massa muscolare è il risultato di un equilibrio tra sintesi e degradazione proteica: una maggior sintesi delle proteine muscolari porta infatti ad ipertrofia mentre una maggior degradazione associata ad una ridotta sintesi ha come conseguenza uno stato atrofico del muscolo. Una migliore conoscenza delle vie di segnale che regolano la crescita e la funzione muscolare diventano di particolare importanza terapeutica per prevenire la perdita di massa associata sia all'invecchiamento, che a diverse patologie, quali ad esempio distrofie e sclerosi. Una delle vie maggiormente implicate nella regolazione della crescita muscolare è la via Akt-mTOR.

In condizioni anaboliche, mTOR è attivo e promuove la sintesi proteica attraverso la fosforilazione di S6K1 e 4EBP1. Inoltre, mTOR va anche a bloccare la degradazione proteica attraverso l'inibizione di una proteina che partecipa alla formazione dell'autofagosoma, Ulk1.

mTOR esiste sotto forma di due complessi multiproteici: mTORC1, implicato nella crescita cellulare, e mTORC2, che regola la riorganizzazione del citoscheletro. Uno dei componenti principali di mTORC1 è la proteina Raptor, che è in grado di reclutare i substrati di mTORC1, quali ad esempio S6K1 e 4EBP1, promuovendone la fosforilazione (Hara et al., 2002) (Kim et al., 2002).

Topi in cui Raptor è assente nel muscolo scheletrico dalla nascita sviluppano una severa miopatia, risultante in una morte prematura degli animali (Bentzinger et al., 2008). Tuttavia, il trattamento di topi adulti con rapamicina, che inibisce selettivamente mTORC1, non porta a patologie muscolari e, anzi, migliora la fisiologia del muscolo di topi anziani (Harrison et al., 2009).

Considerando questi risultati contradditori, ci siamo chiesti quale sia il ruolo di Raptor nel muscolo adulto. Abbiamo, quindi, generato un modello

murino in cui Raptor viene deleto nel muscolo scheletrico in maniera inducibile.

Un mese di delezione di Raptor non ha effetti sulla morfologia o sulla funzionalità del muscolo. Considerando che in letteratura i topi knock-out per Raptor dalla nascita muoiono attorno ai 5-6 mesi, abbiamo deciso di monitorare il peso corporeo e la durata della vita per un periodo di tempo maggiore. Abbiamo notato che, durante questi mesi, il peso rimane invariato tra i topi controllo e i topi knock-out; abbiamo, quindi, deciso di sacrificare gli animali 7 mesi dopo l'inizio del trattamento per controllare l'istologia del muscolo.

A questo punto, i muscoli dei topi Raptor ko mostrano segni miopatici, con fibre centronucleate, fibre atrofiche e ipertrofiche, strutture centrali e infiammazione. Inoltre, abbiamo notato che i muscoli knock-out presentano fibrillazioni spontanee e quindi attività elettrica a riposo, suggerendo la presenza di fibre denervate. La delezione di Raptor, inoltre, ha portato ad una severa depolarizzazione mitocondriale e ad una ridotta attività di alcuni complessi della catena respiratoria. Tutti questi effetti sono facilmente collegabili alla significativa debolezza muscolare osservata in questi topi.

Dal momento che una più approfondita conoscenza dei mediatori maggiormente implicati nella crescita muscolare può essere di interesse terapeutico, abbiamo deciso di generare una nuova linea murina in cui Akt viene espresso e Raptor deleto solo nel muscolo scheletrico in maniera inducibile al fine di valutare quale sia il ruolo di Raptor nella crescita indotta dall'overespressione di Akt. Nei topi Akt-Raptor ko, l'ipertrofia delle fibre muscolari è solo parzialmente ridotta in confronto a quella osservata nei topi Akt. Incredibilmente, il trattamento con rapamicina significativamente diminuisce la crescita indotta da Akt, anche in assenza di Raptor. Inoltre, i topi Akt-Raptor ko mostrano una ridotta forza muscolare, suggerendo che l'ipertrofia dipendente da Akt in assenza di Raptor non è più funzionale. Quest'effetto non è normalizzato neanche

dalla somministrazione di rapamicina, com'era stato visto nei topi Akt-S6K1 ko (Marabita et al., 2016).

INTRODUCTION

1.1. Skeletal muscle structure and function

Skeletal muscle is the largest organ in the body, comprising 40% of total body mass and acting as a protein reservoir of our organism. It is responsible for body posture and movement and it is under 'voluntary' control of the somatic nervous system through the alpha motor neuron innervation. The morphological and contractile units that compose skeletal muscles are elongated, cylindrical and multinucleated cells, called muscle fibers. Each fiber is surrounded by a sarcolemma, which contains the cytoplasm, called sarcoplasm. The sarcolemma of each fiber is then surrounded by a basal lamina and reticular fibers in a layer called endomysium. Muscle fibers are organized in bundles and separated by specific membranes. Each bundle, called fasciculus, is surrounded by connective tissue, known as perimysium. Each muscle is then surrounded by another layer of connective tissue, called epimysium (Fig.1) (Light and Champion, 1984).

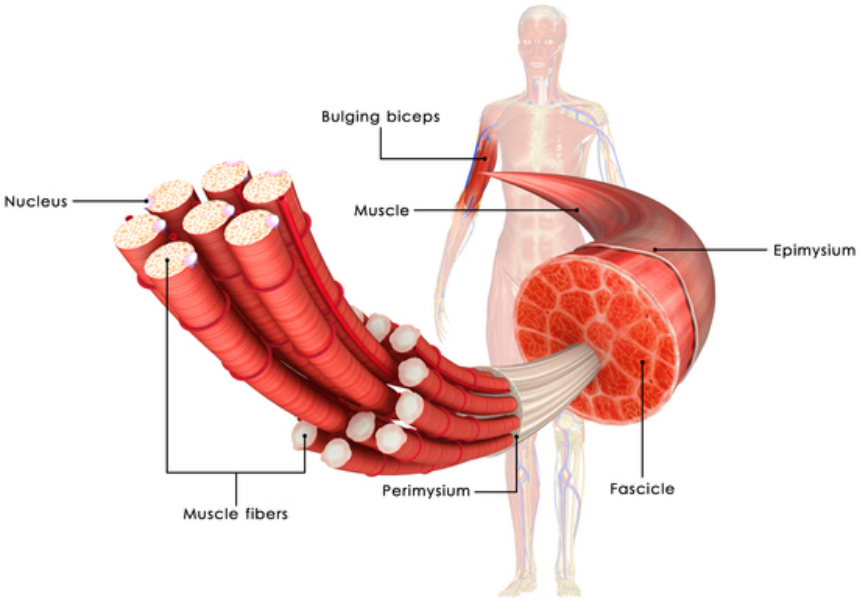

Fig. 1: Schematic representation of skeletal muscle structure

The sarcoplasm contains thousands of cylindrical structures, called myofibrils, responsible for muscle contraction. Myofibrils are composed of contractile proteins, which are organized in thin filaments and thick filaments. The contractile units of muscle fibers are called sarcomeres, which are associated in series to form the myofibrils, and in parallel, giving the striated pattern to muscle fibers. The structure of the sarcomere was described first thank to microscopy techniques that individuated isotropic (light band) and anisotropic (dark band) zones. Dark bands are also called A-bands and they contain the entire length of a single thick filament. A-band follows the light bands, or I-bands, which correspond to the zone in which thin filaments are not superimposed by thick filaments. Each I-band is divided by a thin line, the Z-line. The segment between two neighbouring Z-lines is the sarcomere. Within the A-band a paler region, called the H-zone, is defined, in which thick filaments are not superimposed by thin filaments. Finally, within the H-zone, the thin M-line delineates the middle of the sarcomere. These bands are not only morphological unit, but they also have a functional role since they are composed by different proteins, required for muscle contraction. Indeed, actin filaments (thin filaments) are the major component of the I-band and extend into the A-band. Myosin filaments, thick filaments, extend throughout the A-band and are thought to overlap in the M band (Fig.2). A big protein, titin, extends from the Z-line of the sarcomere to the M-line, where it is thought to interact with the thick filaments. In this way titin can keep myosin molecules centered in the sarcomere and maintain the resting tension, allowing a muscle to snap back if overextended. Many proteins important for the stability of the sarcomeric structure are present in the Z-line and in the M-band of the sarcomere. Actin filaments are cross-linked with titin molecules in the Z-disc via the Z-line protein alpha-actinin. In the M-band, myosin and M proteins bridge the thick filament system to the M-line part of titin (elastic filaments) (Barrett et al., 2010). Moreover, several regulatory proteins, such as tropomyosin and troponin,

bind actin and myosin molecules, modulating its contraction capability. Indeed, tropomyosin forms a complex with troponin and this complex is associated with two molecules of actin, acting as a regulator of skeletal muscle contraction. When the concentration of Ca^{2+} is low, the complex blocks the interaction of actin and myosin, so the muscle does not contract. At high concentration, Ca^{2+} binding to troponin shifts the position of the complex, relieving this inhibition and allowing contraction to proceed.

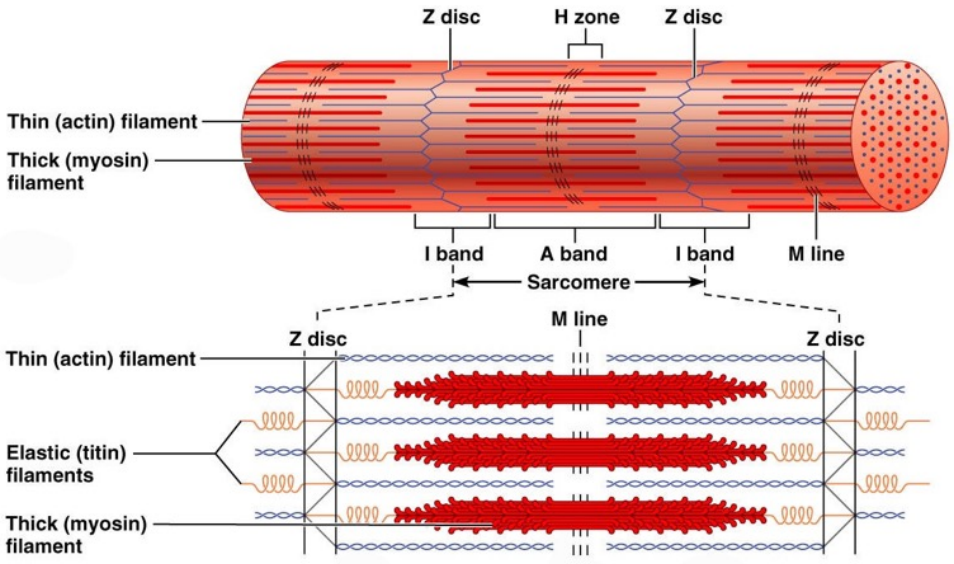

Fig. 2: Schematic representation of skeletal muscle sarcomere

Synaptic input from motor neurons is required to produce muscle contractions. A single motor neuron is able to innervate multiple muscle fibers, thereby causing the fibers to contract at the same time. Indeed, muscle contraction is due to the excitation-contraction coupling, by which an electrical stimulus is converted into mechanical contraction. In general, an action potential arrives to depolarize the cell membrane. This results in an increase in cytosolic calcium that is called a calcium transient. Ca^{2+} increases activates calcium sensitive contractile proteins that then use

ATP to cause cell shortening. Upon contraction, the A-bands do not change their length, whereas the I bands and the H-zone shorten. In other words, the thin filament slides over a thick filament to generate tension in the muscle. This is known as the sliding filament hypothesis. There are projections from the thick filaments, called cross-bridges, which contain the part (head) of myosin linked to actin. The binding of ATP to a myosin head detaches myosin from actin, thereby allowing myosin to bind to another actin molecule. Once attached, ATP is hydrolyzed by myosin, thus converting chemical energy into mechanical energy.

To allow the simultaneous contraction of all sarcomeres, the sarcolemma penetrates into the cytoplasm of the muscle cell between myofibrils, forming membranous tubules called transverse tubules (T-tubules) (Fig. 3). The T-tubules are electrically coupled with the terminal cisternae which continue into the sarcoplasmic reticulum. Thus, the sarcoplasmic reticulum, which contains the majority of calcium ions required for contraction, extends from both sides of T-tubules into the myofibrils. T-tubules form an anatomic structure with two SR cisternae that surround them; this structure is called triad and it allows the transmission of membrane depolarization from the sarcolemma to the SR. Skeletal muscle contraction is the result of an interaction between cellular and chemical components after motor neuron stimulation. The axon of a motor neuron is in contact with muscle fiber through a chemical synapse, which is called the neuromuscular junction (NMJ). Synaptic transmission starts when an action potential reaches the presynaptic terminal of a motor neuron, activating voltage-dependent calcium channels to allow calcium ions to enter the neuron and triggering neurotransmitter release from the neuron into the synaptic cleft. Acetylcholine, released from motor neurons, binds to the postsynaptic receptors located on the sarcolemma, resulting in muscle fiber depolarization and, thus, generating an action potential which propagates along the sarcolemma and reaches T-tubules and the SR. Here the action potential changes the permeability of the sarcoplasmic reticulum, allowing the flow of calcium ions into the cytosol between the

myofibrils. The release of calcium ions induces the myosin heads to interact with the actin, allowing the muscle contraction. The contraction process is ATP dependent, the energy is provided by mitochondria which are located closed to Z-line.

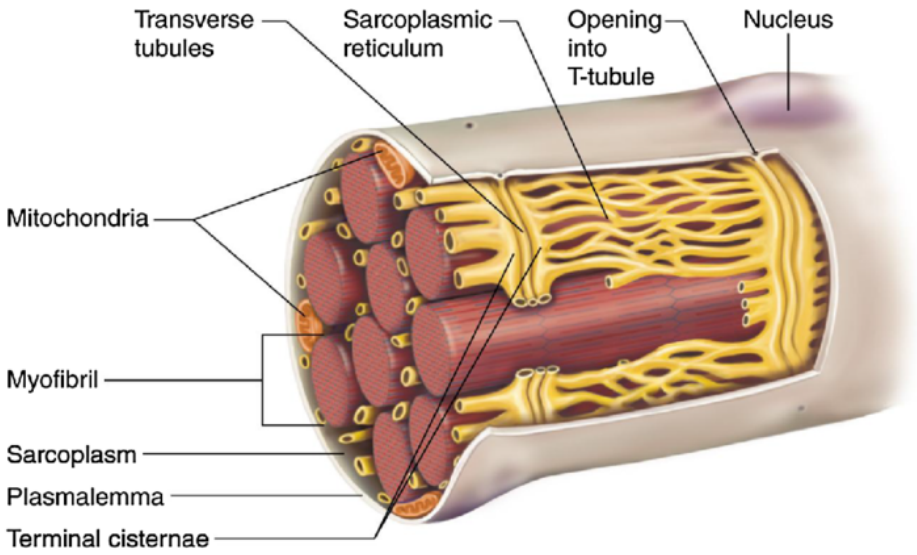

Fig. 3: Schematic representation of organization of T-tubules in skeletal muscle

The contraction properties of a muscle depend on the fiber type composition. Mammalian muscle fibers are divided into two different classes: type I, also called slow fibers, and type II, called fast fibers. This classification considers only mechanical properties. However, the different fibers types also show peculiar features, such as for example myosin ATPase enzymes, metabolism (oxidative or glycolytic), mitochondrial content and resistance to fatigue (Pette and Heilmann, 1979) (Schiaffino et al., 2007).There are four major fiber types: I, IIA, IIX and IIB, based on the presence of different myosin heavy chain (MyHC) isoforms (Ciciliot et al., 2013). Slow fibers (type I), which express slow isoform of MyHC, are red small fibers and they are resistant to fatigue. This is due to the high content of mitochondria of these fibers, which, thus, show an higher metabolic activity. Moreover, they appear red due to the high levels of

myoglobin and high capillary densities. These fibers, due to their high oxidative capacity, are also known as slow oxidative fibers.

Fast fibers (type II) are divided in three groups depending on which myosin is expressed. Type IIA fibers are faster than type I, but they are still relatively fatigue-resistant. They are slower compared to IIX and IIB, with higher oxidative metabolism due to the high content of mitochondria (Schiaffino and Reggiani, 1996) (Schiaffino and Reggiani, 2011). For these reasons, they are termed fast oxidative fibers. The IIX and the IIB fibers are known as fast glycolytic fibers due to a prominent glycolytic metabolism. They show few mitochondria, less myoglobin but high levels of glycogen, they exhibit fast contractility but less resistance to fatigue. Moreover, they appear big and white and they express MHC IIb and IIx. The content of the different fibers changes between different muscles, in accordance with their function. Muscles specialized in postural activity are mainly composed of slow fibers, while muscles involved in body movement display mainly fast fibers. Thus, contraction speed and contractile properties of a muscle can vary in accordance to the percentage of the different fiber types that compose it. Indeed, skeletal muscles can be classified in slow muscles, such as the soleus, and fast muscles, such as Tibialis Anterior.

The fiber-type composition of different muscles is initially established during development independently of neural influence, but nerve activity has a major role in the maintenance and modulation of its properties in adult muscle (Murgia et al., 2000). Indeed, during postnatal development and regeneration, a default nerve activity-independent pathway of muscle fiber differentiation, which is controlled by thyroid hormone, leads to the activation of a fast gene program. On the contrary, the postnatal maintenance of the slow gene program is dependent on slow motor neuron activity. Fiber-type changes during postnatal life, such as fiber-type switching, could be due to changes in nerve activity. Indeed, a loss of nerve activity in soleus muscle results in a fiber-type switching from slow to fast fibers.

The transcription of different fiber type-specific genes must be precisely regulated to maintain muscle function. Different signaling pathways control fiber type-specific gene programs. Among them, the most known regulators of slow-gene program are the calcineurin-dependent nuclear factor of activated T-cells (NFAT) transcription factors, that may act as activators or repressors of distinct MyHC genes.

1.2. Muscle atrophy and muscle hypertrophy

Motor neuron activity has a role not only in controlling muscle fiber differentiation, but also in maintaining muscle trophism. Indeed, a loss in neuromuscular transmission results in a progressive loss of skeletal muscle mass. On the contrary, an intense muscle activity can lead to an increase in fiber size. Skeletal muscle, thus, is a very plastic tissue that can adapt to different stimuli, such as physical activity, metabolism and hormones, or to variations in motor neuron activity. A decrease or an increase in skeletal muscle mass results, respectively, in muscle atrophy or muscle hypertrophy. Muscle atrophy is linked to different pathological conditions which lead to a reduction in fiber size. On the other hand, muscle hypertrophy is due to growth of pre-existing muscle fibers, thus resulting in an increase in skeletal muscle mass. The regulation of muscle mass and fiber size depends on protein turnover. Indeed, skeletal muscle mass is the result of an equilibrium between protein synthesis and protein breakdown. An increase in protein synthesis results in an accumulation of contractile and structural proteins in the sarcoplasma, leading to a bigger fiber size and, so, to muscle hypertrophy. On the contrary, if protein degradation overcomes protein synthesis, the results is a reduction in skeletal muscle mass, resulting in skeletal muscle atrophy.

1.2.1. Muscle atrophy

Many pathological conditions have been linked to a loss of skeletal muscle mass and, so, to muscle atrophy. During ageing there is a progressive decline of muscle mass, a condition referred to as sarcopenia. The rate of muscle loss with age appears to be fairly consistent, approximately 1%-2% per year past the age of 50 years, until reaching 15% around 70 years of age. Moreover, several diseases, such as cancer, AIDS, disuse, immobilization, denervation, sepsis, diabetes, heart and renal failure, have been associated with a loss of muscle tissue. It has been demonstrated that all these catabolic conditions are associated with transcriptional changes of a subset of specific genes, involved in protein degradation, energy production and growth-related process. This group of genes are called atrophy-related genes or “atrogenes” (ATG). Among the upregulated “atrogenes”, there is a subset of transcripts which are strongly involved in protein degradation. The two main pathways involved in this process are: the ubiquitin-proteasome system (UPS) and the autophagy-lysosome system.

1.2.1.1. Ubiquitin-proteasome system

The ubiquitin-proteasome system (UPS) controls the turnover of intracellular regulatory proteins involved in critical cellular processes, including cell cycle progression, cell growth and differentiation, gene transcription, signal transduction and apoptosis. It is responsible for the degradation of unneeded or damaged proteins, avoiding their accumulation and, thus, preventing the onset of related diseases. The importance of proteolytic degradation inside cells and the role of ubiquitin in UPS was acknowledged in the award of the 2004 Nobel Prize in Chemistry.

Protein degradation starts from attaching a chain of multiple ubiquitin molecules to target proteins. Ubiquitin is a protein of 76 amino acids and it

serves as a tag for degradation of targeted proteins through covalent binding of a lysine residue. This process requires the coordinated reaction of three enzymes. Firstly, an ubiquitin-activating enzyme (called E1) activates ubiquitin in an ATP-dependent manner by forming a thiol ester bond at its C terminus. This ubiquitin is then transferred from E1 to one of the ubiquitin-conjugating enzymes E2. In the last step, one of the ubiquitin ligases (E3) recognizes the specific proteins to be ubiquitinated and catalyzes the transfer of ubiquitin from E2 to a lysine residue of this target protein (Chen and Dou, 2010). Once a protein is tagged with a single ubiquitin molecule, this is a signal to other ligases to attach additional ubiquitin molecules, forming a polyubiquitin chain that is bound by the proteasome, allowing protein degradation. A target protein must be labeled with at least four ubiquitin monomers before being recognized by the proteasome lid. Ubiquitin contains seven lysine residues to which another ubiquitin molecule can bind, resulting in different types of polyubiquitin chains involved in different processes. The ones with a role in proteasome targeting are the chains in which additional ubiquitin are bound to Lysine 48 of the previous ubiquitin (Pickart and Fushman, 2004) (Xu et al., 2009). An ubiquitinated protein is then recognized by the 19S regulatory particle of the proteasome in an ATP-dependent binding step. Before entering the catalytic core of the proteasome, target proteins have to be deubiquitinated by thiol proteases and partially unfolded. The unfolding process occurs via conformational changes driven by ATP hydrolysis. Unfolded proteins can be translocated into the active sites of the proteasome where they are degraded in an ATP-independent manner by specific peptidases (Fig. 4) (Liu et al., 2006) (Nandi et al., 2006).

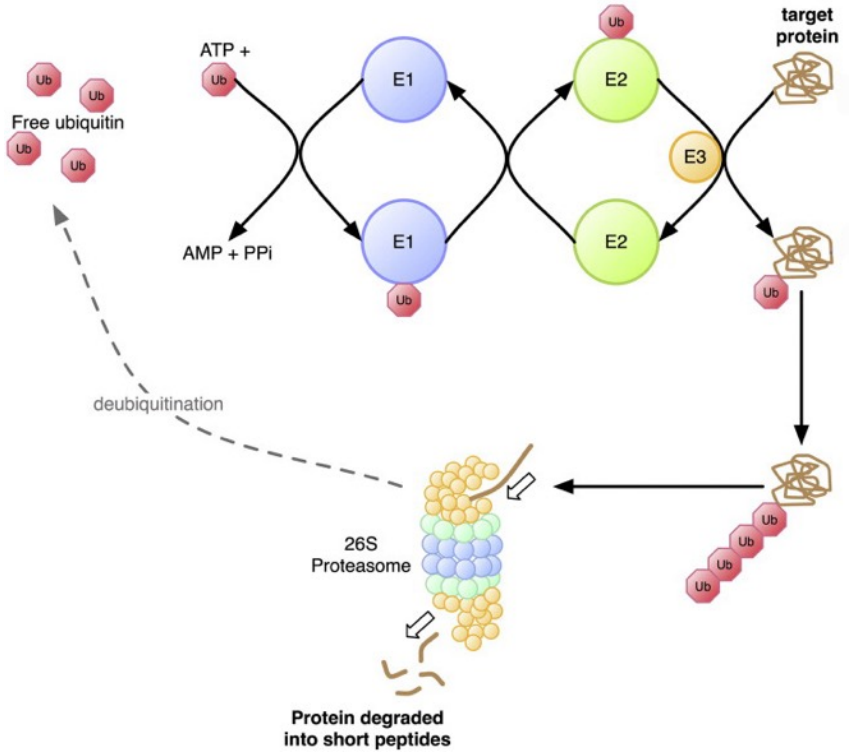

Fig. 4: Schematic representation of ubiquitin proteasome system

The ubiquitin-proteasome pathway is constitutively operative in normal skeletal muscle and is responsible for the turnover of most soluble and myofibrillar muscle proteins upon changes in muscle activity. Muscle mass loss can be linked to: (1) increased ubiquitination of muscle proteins; (2) increase proteasome activity; (3) increased protein degradation; and (4) upregulation of genes encoding ubiquitin, some E2 enzymes, few E3 enzymes and several proteasome subunits.

Among the known E3s, only few of them are expressed specifically in skeletal muscle and upregulated during atrophying conditions (Sacheck et al., 2007). The first to be identified were Atrogin-1/MAFbx and MuRF1, which are expressed specifically in smooth and striated muscles (Bdolah et al., 2007) (Bodine et al., 2001a) (Gomes et al., 2001). Their expression is under the control of a family of transcription factors, known as FoxO1, FoxO3 and FoxO4. FoxOs family members have a central role in regulating catabolic processes that lead to muscle atrophy.

Indeed, deletion of the three FoxO factors simultaneously protects from muscle atrophy, preventing the induction of many E3 ligases, including Atrogin1 and MuRF1 (Milan et al., 2015).

1.2.1.2. Autophagy-lysosome system

Autophagy is a catabolic process that targets different cellular components, including proteins, lipids, damaged organelles and pathogenes. It occurs at a basal levels to maintain intracellular homeostasis, but it can be accelerated by a variety of stresses such as starvation, accumulation of abnormal proteins, organelle damage and pathogene infection. Indeed, besides its function in intracellular protein clearance and in cell adaption to nutrient deprivation, autophagy has many other different physiological and pathophysiological roles, development, anti-aging, elimination of microorganisms, cell death, tumor suppression and antigen presentation. During autophagy, a small cisterna, called the isolation membrane or phagophore, elongates and surrounds a part of the cytoplasm to form a double-membraned structure, called autophagosome. Autophagosomes can either fuse with late endosomes to form amphisomes, which then fuse with lysosomes, or they can fuse directly with lysosomes (Nakamura and Yoshimori, 2017). Both the cytoplasm and the inner limiting membrane are degraded by lysososmal hydrolases, and the degraded contents are transported back to the cytoplasm where they can be reused for biosynthesis or energy production (Fig 5).

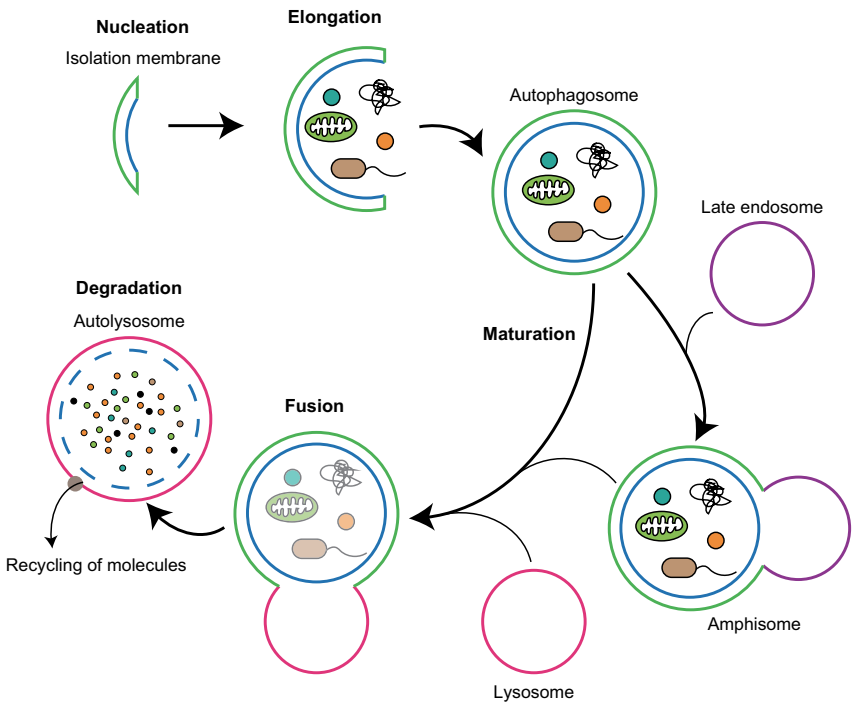

Fig. 5: Schematic representation of autophagy-lysosome system (Nakamura and Yoshimori, 2017)

Every step of this process requires the involvement of different ATGs proteins. Briefly, activation of the unc-51-like kinase 1 (Ulk1; Atg1 in yeast) complex is crucial for the initiation of autophagy, whereas, the mammalian homolog of Atg6, Beclin1 has a central role in the regulation of autophagy by forming a complex with Vps34, a class III phosphatidylinositol 3-kinase (PI3-kinase). In addition, UVRAG (UV irradiation resistance-associated gene) associates with Beclin1-Vps34 complex, enhancing autophagy. Further, Ambra1 binds to Beclin1, enhancing Vps34 kinase activity and promoting autophagosome formation. The subsequent elongation and closure of the isolation membrane are mediated by two ubiquitin-like ATG conjugation pathways, ATG12-ATG5 and LC3-phosphatidyletanolamine systems. Both assist autophagosome formation but only LC3 is present in sealed autophagosome (Eskelinen and Saftig, 2009). LC3 exists as LC3-I, which is localized in the cytoplasm, and LC3-II, in which LC3 is conjugated with phosphatidyletanolamine by an ubiquitination-like enzymatic reaction. This modification results in a change of molecular weight of LC3, allowing

us to distinguish by western blot between the two isoforms. Moreover, the lipidated form of LC3 associates with both the outer and the inner membranes of the autophagosomes. Lipidated LC3 contributes to the closure of the autophagosome and enables the docking of specific cargos and adaptor proteins, such as p62. Since p62 has an ubiquitin–binding domain, it has been proposed that ubiquitinated proteins and inclusion bodies are recruited to the autophagosome membrane via p62 (Bjorkoy et al., 2005). Moreover, it was shown that p62 prefers biding to Lys63-linked ubiquitinated proteins (Yao, 2010). The autophagosome, then, fuses with a lysosome through the actions of multiple proteins, including SNAREs and UVRAG. Following the fusion, the lipidated LC3 bound to the inner membrane and p62 are degraded with the cargo, while LC3-II attached to the outer membrane is cleaved off by Atg4 and recycled. For this reason, an increase in p62 levels can be associated with an autophagy impairment.

At the end, the degraded products are released in the cytoplasm through the action of permeases (Yang et al., 2006). This allows unneeded proteins to be degraded and the amino acids to be recycled for the synthesis of proteins that are essential for survival. Autophagy is mainly regulated by nutrient availability. In fact, in condition of nutrient deprivation, autophagy is induced to maintain the amino acid pool.

Autophagy needs to be properly regulated to maintain cellular homeostasis. Indeed, an activation or an inhibition of autophagy are correlated to muscle atrophy. The transcription factor FoxO3 regulates muscle atrophy and it was shown to be necessary and sufficient for autophagy induction in skeletal muscle. Indeed, the overexpression *in vivo* of constitutively active FoxO3 induced myofiber atrophy and this muscle loss requires autophagy (Mammucari et al., 2007) (Masiero et al., 2009). Moreover, many of the Atg proteins that take part in this process are under FoxO control.

1.2.2. Muscle hypertrophy

Muscle hypertrophy is mainly regulated by two different pathways: the myostatin-Smad2/3 axis as negative modulator and the IGF1-Akt-mTOR axis as positive regulator.

1.2.2.1. Myostatin

Myostatin is a growth factor and is a member of the TGFβ protein family. It inhibits muscle growth and differentiation during development. Indeed, it is secreted by myocytes and acts on muscle cells' autocrine function to block myogenesis. Animals that are knock-out for myostatin gene or that are treated with myostatin inhibitors show a huge increase in muscle mass (Amthor et al., 2007). The treatment of dystrophic mice with a peptide blocking myostatin, activates muscle growth and it ameliorates pathological conditions by improving tetanic muscle force. Myostatin inhibitors, thus, can be of therapeutic interest in diseases that are accompanied by skeletal muscle loss (Bogdanovich et al., 2005).

1.2.2.2. IGF1-Akt-mTOR pathway

IGF1-Akt pathway is activated when the growth factor IGF1 (insulin-like growth factor 1) binds to its receptor, IGF1r. As a consequence, it phosphorylates insulin receptor substrate (IRS), which can in turn activate PI3K. The function of this kinase is to phosphorylate membrane phospholipids, generating phosphatidylinositol-3,4,5-triphosphate (PIP3) from the phosphatidylinositol-4,5-biphosphate (PIP2). PIP3 is able to recruit PDK1 (phosphoinositide-dependent kinase 1) and Akt at the cell membrane, allowing the interaction between these two kinases. In this way, PDK1 can phosphorylate Akt at the Thr^{308}, leading to its activation.

Akt, thus, promotes protein synthesis, either by activation of mTOR (mammalian target of rapamycin) kinase or by inhibition of GSK3β (Glycogen Synthase Kinase 3β). On the other hand, Akt blocks protein degradation through the phosphorylation and inhibition of FoXOs transcription factors. Both these functions of Akt lead to muscle growth upon its activation.

The effect of Akt on mTOR is indirect; indeed, Akt inhibits Tuberous sclerosis complex 1 and 2 (TSC1/2), which act as GAP proteins (GTPase activating protein), inhibiting Rheb (Ras homolg enriched in brain), a G protein localized on lysosomal surface which is, in turn, able to activate mTOR (Fig.6).

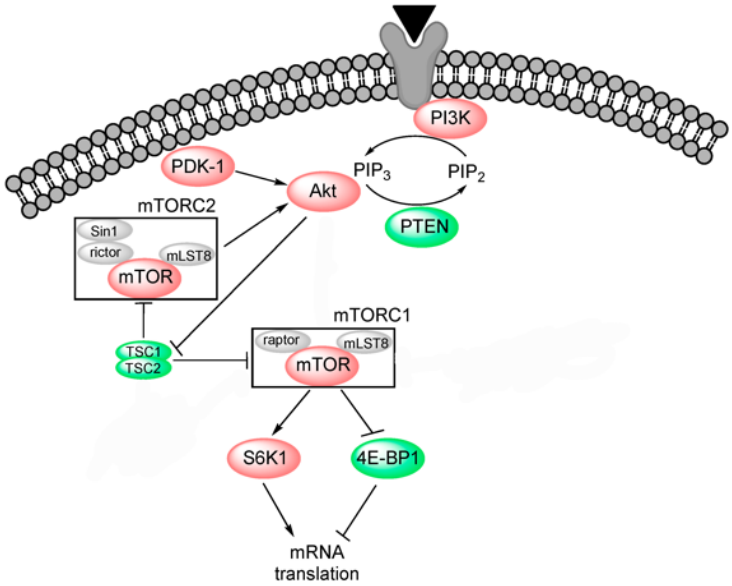

Fig. 6: Schematic representation of IGF1-Akt-mTOR pathway

Control of mTOR activity is critical for the cell since its dysregulation is correlated with cancer, metabolic disease and diabetes. mTOR exists as two multiprotein complexes: mTORC1, when it is bound to Raptor (regulatory-associated protein of mTOR), and mTORC2, when it is bound to Rictor (rapamycin-insensitive companion of mTOR). While mTORC2 is responsible for cell survival and cytoskeleton reorganization, through the phosphorylation of Protein kinase C (PKC) and SGK (Serum/Glucocorticoid-regulated kinase) and it is implicated in Akt

activation through the phosphorylation of Ser^{473} residue, mTORC1 is mainly involved in cell growth and ribosome biogenesis through the regulation of its downstream targets, such as Ulk1, whose phosphorylation and inhibition leads to autophagy block, S6 kinase (S6K) and eIF4E-binding proteins (4EBPs). S6K stimulates protein synthesis through the phosphorylation and activation of ribosomal protein S6, which seems to be involved in the transport of 5' TOP mRNA to the ribosome. These transcripts codify only for components of the translation machinery, such as ribosomal proteins and initiation and elongation factors. S6K induces cell growth also through its effect on eIF4B, involved in the translation of 5' TOP mRNA, and on eEF2k (eukaryotic elongation factor 2 kinase), inhibiting it and, thus, leading to eEF2 activation. On the other hand, eIF4E-binding proteins act as a repressor of protein synthesis through the binding to eIF4E, avoiding the formation of eIF4F complex. When 4EBPs are phosphorylated by mTORC1, they detach from eIF4E, allowing it to bind to eIF4G and eIF4A and, thus, generating eIF4F complex, involved in translational process (Hay and Sonenberg, 2004). The ratio eIF4E/4EBPs regulates the speed of cap-dependent translation. About 30% of tumors has been correlated with high levels of eIF4E and so to a high ratio eIF4E/4EBPs (Alain et al., 2012).

Akt stimulates cell growth also through the phosphorylation and inhibition of GSK3β. GSK3β is a serine-threonine kinase and it phosphorylates substrates that have already been phosphorylated by other kinases (priming phosphate). When GSK3β is phosphorylated, the phosphorylated residue goes in the binding site of priming phosphate, acting as a pseudosubstrate, and inhibiting its activity (Cohen and Frame, 2001). Among all its targets, GSK3β phosphorylates and inactivates eukaryotic initiation factor 2B (eIF2B). Thus, inhibition of GSK3β by Akt results in eIF2B activation and increased protein translation. Overexpression of dominant negative GSK3β results in myotubes hypertrophy, whereas overexpression of wildtype GSK3β in the heart leads to a decrease of about 30% in heart size (Rommel et al., 2001) (Schiaffino and

Mammucari, 2011). Moreover, GSK3β overexpression results in phosphorylation of NFAT transcription factors, preventing the Ca^{2+}-Calcineurin-induced nuclear translocation of these factors (Beals et al., 1997) (Hilioti et al., 2004). Furthermore, the first discovered action of GSK3β is the phosphorylation and inhibition of Glycogen Synthase, the enzyme catalyzing last step of glycogen synthesis.

The IGF1-Akt pathway is regulated by different feedback loops. S6K, through a negative feedback loop, phosphorylates IRS1, promoting its degradation. On the other hand, mTORC2, through a positive feedback loop, phosphorylates Akt on its Ser^{473} residue. This phosphorylation, together with the one on Thr^{308} residue done by PDK1, results in the complete activation of the kinase. Both these modification are required for its effect on FoXO transcription factors, but not for its action on S6K. Moreover, Akt takes part in other cellular processes, such as cell survival, angiogenesis, metabolism and cell cycle through the phosphorylation of a great variety of downstream targets. It has been shown that Akt can ameliorate pathological conditions of dystrophic mice by improving muscle force and by increasing the levels of proteins like utrophin and dysferlin, which can compensate in part for the lack of dystrophin, thus protecting sarcolemma from ruptures (Blaauw et al., 2008). Moreover, overexpression of Akt in skeletal muscle results in muscle hypertrophy with increased muscle mass and muscle force. This Akt-induced fiber growth does not require the downstream target S6K, which is instead essential for maintaining muscle structure and force production during hypertrophy. Simultaneous inhibition of mTOR signaling to both S6K and 4EBP1 is sufficient to reduce Akt-induced muscle growth and render it insensitive to a further inhibition of mTORC1 (Marabita et al., 2016). While S6K and 4EBP1 can be phosphorylated by several kinases and their role in the regulation of skeletal muscle mass has already been elucidated, the role of the upstream kinase mTORC1 in Akt-induced hypertrophy is still an open question. Since a great variety of diseases has been linked to muscle mass loss, it becomes very important understanding the real

players involved in muscle growth in order to potentially counteract muscle atrophy.

1.3. Different approaches to study the role of mTORC1

The role of mTORC1 in body homeostasis and in muscle mass has been investigated through two different approaches: the genetic one, by the deletion of Raptor gene, and the pharmacological one, by the treatment with the mTORC1 inhibitor rapamycin.

1.3.1. Genetic approach: deletion of Raptor

Raptor is a scaffold protein of 150 kDa and it is one of the key members of mTOR complex 1. It is able to interact with mTORC1 targets, such as S6K and 4EBPs, promoting the interaction between the kinase and its substrates. Indeed, in this way, mTOR is able to catalyze their phosphorylation. The binding of Raptor to mTOR can be avoided through the treatment with rapamycin, a well-known mTORC1 inhibitor, or by AMPK. Indeed, in a condition of low energy, AMPK is activated and phosphorylates Raptor, allowing its interaction with 14-3-3 proteins and, thus, inhibiting it. In this way, blocking mTORC1 activity, AMPK inhibits the energy demanding process of protein synthesis.

It has been published that the loss of mTORC1, through Raptor deletion, from birth is embryonically lethal, as observed in mTOR-deficient mice (Guertin et al., 2006). Deletion of Raptor only in skeletal muscle (RAmKO) from birth, instead, results in mice with no overt phenotype in the first weeks of life. However, around 5 weeks of age, they start to loose body weight even if food consumption is comparable to control mice. RAmKO mice developed a pronounced kyphosis around two months of age and they die prematurely at the age of 150-180 days. Kyphosis and early death

are often signs of muscle dystrophy. Indeed, soleus and extensor digitorum longus (EDL) RAmKO muscles showed a high number of small and large muscle fibers, centronucleated fibers and central core-like structures (Fig. 7). Premature death, however, might be due to respiratory failure of RAmKO mice since diaphragm muscle also showed extensive muscle wasting and high degree of fibrosis (Bentzinger et al., 2008).

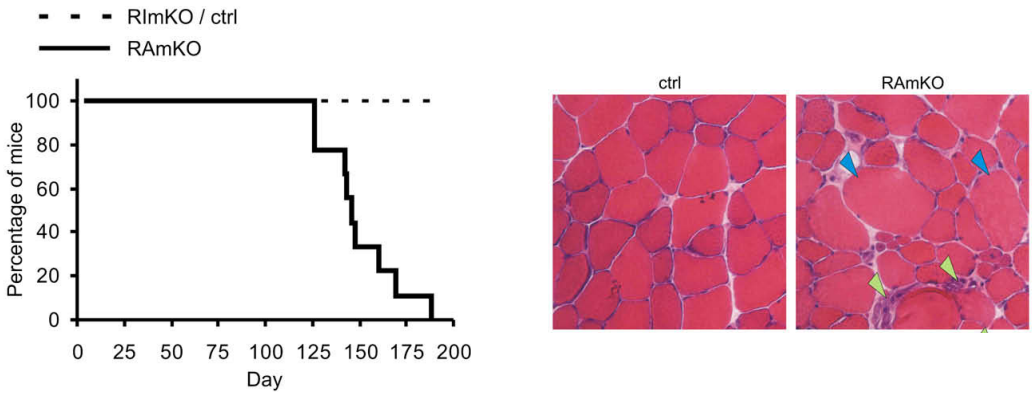

Fig. 7: RAmKO lifespan and muscle histology (Bentzinger et al., 2008)

Moreover, protein composition and function of the membrane compartments involved in excitation-contraction coupling (E-C coupling) is affected in RAmKO mice; this is a common feature of a group of several disorders, like core myopathies, which are characterized by the presence of core structures and fiber type switching towards a slow-twitch program, as observed in RAmKO mice (Lopez et al., 2015). Raptor deletion in adult heart results in a dilated cardiomyopathy and high mortality within 6 weeks after the deletion, demonstrating that Raptor is required for normal physiological heart function (Shende et al., 2011).

1.3.2. Pharmacological approach: rapamycin treatment

Rapamycin, also known as sirolimus, is a macrolide compound produced by bacterium *Streptomyces hygroscopicus* found in Easter Island, called also Rapa Nui. It has immunosuppressant functions, in fact it is used to

prevent organ transplant rejection. Its activity depends on the binding to specific cytosolic proteins, known as immunophilins. Rapamycin binds to the immunophilin FKBP12, inhibiting its isomerase activity. The complex rapamycin-FKBP12 prevents the interaction between mTOR and Raptor through the binding of rapamycin to FRB (FKBP12-rapamycin binding) sequence on mTOR. In this way, the complex inhibits mTORC1 activity and prevents the phosphorylation of its downstream targets (Sehgal, 1998). This action results in its immunosuppressant and anti-tumoral function. Indeed, rapamycin can either block the proliferation of T and B lymphocytes, reducing IgG, IgM and IgA production, or inhibit the proliferation of hepatocytes and fibroblasts, blocking cell cycle progression at G1 phase.

However, different mTORC1 targets showed different sensitivity to rapamycin treatment. This seems to be linked to different levels of mTORC1 activity towards a specific phosphorylation site. Indeed, if mTORC1 has a high affinity for a specific site, this results to be more resistant to rapamycin action and so to dephosphorylation, compared to ones with low affinity (Kang et al., 2013). Moreover, rapamycin can affect mTORC2 activity only with a long chronic treatment.

Rapamycin treatment, given to 600 days-old mice, is able to extend lifespan by about 14% in females and 9% in males. Indeed, it postpones death, without changing the distribution of presumptive causes of death. This can be due to a combination of anti-neoplastic effects and effects on cellular stress resistance that can result in delayed ageing (Fig.8) (Harrison et al., 2009).

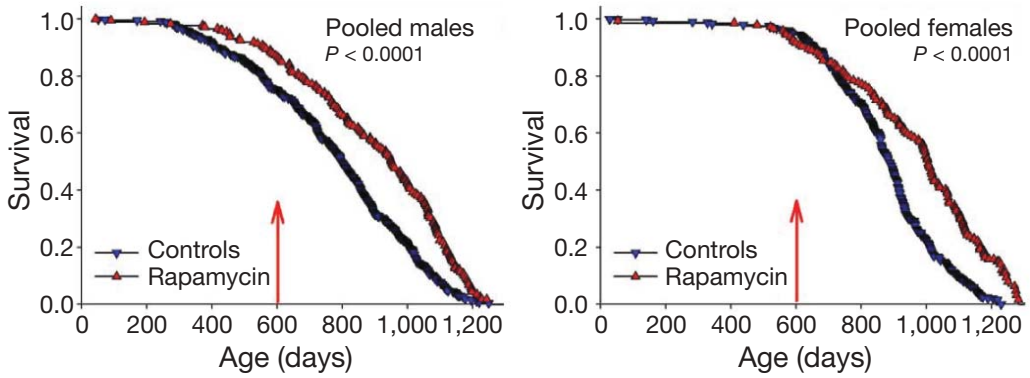

Fig. 8: Mice lifespan after rapamycin administration (Harrison et al, 2009)

Moreover, rapamycin treatment in aged mice significantly improved the behavior and spontaneous activity. Treated mice did not exercise harder, but with elevated frequency, meaning that treated mice may recover from fatigue more rapidly and are more energetic than untreated animals. These effects can be linked to the fact that rapamycin can prevent the loss of heart function associated with ageing, by reducing endogenous stress signaling in the heart and improving excitation-contraction coupling in mice (Flynn et al., 2013).

1.4. Aim of the work

Many pathological conditions have been linked to a loss of skeletal muscle mass, such as cancer, AIDS, muscular dystrophy and also ageing. So far, there are no therapeutic approaches that can prevent muscle wasting. Indeed, better understanding of the signaling pathways controlling muscle mass and function is of great importance. While various studies have identified important regulators of adult skeletal muscle mass, little is known about how these pathways can modulate muscle function. The two main pathways regulating skeletal muscle mass are the Akt-mTOR axis and the myostatin-BMP-Smad pathway. Akt overexpression or BMP stimulation leads to a strong muscle growth. In both cases, hypertrophy is significantly reduced after the treatment with the mTORC1 inhibitor rapamycin (Bodine et al., 2001b) (Winbanks et al., 2013). These studies reveal the key role of mTORC1 signaling in the regulation of skeletal muscle mass. Its function has been investigated through two different approaches: the genetic inhibition of mTORC1, through Raptor deletion, and the pharmacological treatment with the mTORC1 inhibitor, rapamycin.

Mice lacking Raptor only in skeletal muscle from birth show a pronounced myopathy leading to premature death (Bentzinger et al., 2008). However, treating adult mice with the specific mTORC1 inhibitor rapamycin does not lead to a myopathic phenotype and even improves muscle physiology and extends lifespan of aged mice (Harrison et al., 2009). Considering these contradictory results, we decided to address the role of Raptor in adult skeletal muscle. Therefore, to investigate its physiological role in muscle homeostasis, during my PhD, we generated an inducible muscle-specific Raptor knock-out mouse line (HSA-Raptor ko). To understand if there are time-dependent effects upon Raptor deletion, we analyzed muscles at two different time points: in the early stage (one month after the beginning of the treatment) and in the late stage. Since Bentzinger et al. showed that conditional muscle-specific Raptor ko mice died around 6 months of age,

we decided to sacrifice mice and assess muscle state 7 months after the beginning of the treatment, using it as the latter time point.
In addition, in order to evaluate the role of mTORC1 during Akt-induced hypertrophy, we generated a line in which Akt is overexpressed and activated in Raptor ko skeletal muscles (Akt-Raptor ko).

2. MATERIALS AND METHODS

2.1. Animal handling and generation of inducible muscle-specific Raptor ko mice

Animals were handled by specialized personnel under the control of inspectors of the Veterinary Service of the Local Sanitary Service (ASL 16 - Padova), the local officers of the Ministry of Health. All procedures are specified in the projects approved by the Italian Ministero Salute, Ufficio VI (authorization numbers 1060/2015PR). Muscles were removed at various time periods and frozen in liquid nitrogen for subsequent analysis.

Inducible muscle-specific Raptor knock-out mice were generated crossing mice expressing Raptor gene between two LoxP sites (Raptor$^{fl/fl}$) with mice carrying Cre recombinase fused to a mutated estrogen receptor (ER) domain under the control of human skeletal actin promoter (HSA) (Schuler et al., 2005) (Fig.1). Tamoxifen-induced Cre LoxP recombination was activated by oral administration of tamoxifen-containing chow (Tam400/Cre-ER Harlan), which was administered for 3 weeks. For 1-month-treated mice, muscles were collected 1 week after the tamoxifen diet finished, whereas for long-term mice, muscles were collected 7 months from the beginning of the treatment.

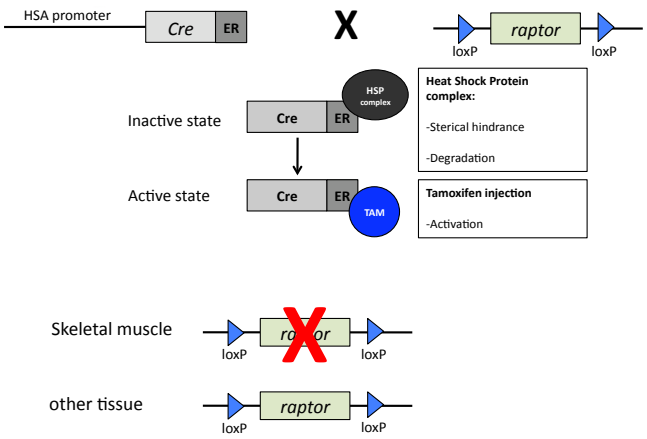

Fig.1: Schematic Representation of HSA-Raptor ko mouse model

Inducible muscle-specific Akt-Raptor knock-out mice were generated crossing mice carrying Raptor gene between two LoxP sites (Raptor$^{fl/fl}$) with mice expressing Akt-ER only after the deletion of an upstream DNA sequence by the Cre recombinase. Intramuscular injection of AAV9 for the Cre recombinase was performed to cleave loxP sites on Raptor and Akt genes (Fig. 2). Tamoxifen treatment by tamoxifen-containing chow oral administration started one month after viral injection and lasted for 3 weeks. Muscles were collected at the end of the treatment.

Rapamycin treatment was performed by intraperitoneal injections at 2 mg/Kg body weight every day for 3 weeks.

In order to analyze muscle mass, muscle-weight/body-weight was measured in all the models. Results are expressed as mean±SEM.

Adult mice of the same sex and age (3 months-old) were used for each individual experiment.

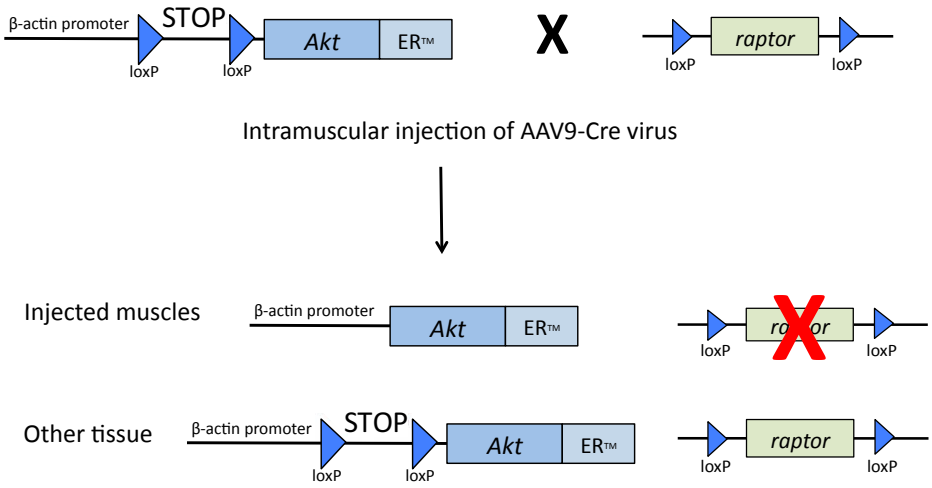

Fig. 2: Schematic Representation of Akt-Raptor ko mouse model

2.1.1. Genotyping of muscle-specific Raptor knock-out mice

Mice were identified by analyzing the presence of Cre-recombinase on genomic DNA by PCR. DNA was extracted using a lysis buffer containing Tris-HCL 1M pH 7.5 and Proteinase K 10mg/mL (Life Technologies). The samples were denatured by incubation for 1 hour at 57°C and then

proteinase K was inactivated at 99°C for 5 minutes. For the PCR reaction we used the following primers:

Cre Forward - NSP-780: CACCAGCCAGCTATCAACTCG

Cre Reverse - NSP-979: TTACATTGGTCCAGCCACCAG

We prepared a 20µl total volume mix for each sample with:

Template DNA: 2µl

Primer NSP-780 (10µM): 0.2µl Primer

NSP-979 (10µM): 0.2µl

GoTaq Green master mix 2X (Promega): 10µl

Water

Program:

step 1: 94° C for 3 minutes

step 2: 94° C for 45 seconds

step 3: 61° C for 30 seconds

step 4: 72° C 1 minute

step 5: go to step 2 for 40 times

We detected Cre-recombinase DNA (200 bp) with a 1% agarose gel.

The genotyping analysis of Akt allele were performed by using the following primers:

Akt Forward: ACTATCCCGACCGCCTTACT

Akt Reverse: TAGCGGCTGATGTTGAACTG

We prepared a 11µl total volume mix for each sample with:

Template DNA: 1µl

Primer FW (10µM): 0.5µl

Primer RV (10µM): 0.5µl

GoTaq Green master mix 2X (Promega): 5µl

Water

Program:

step 1: 94° C for 5 minutes

step 2: 94° C for 45 seconds

step 3: 60° C for 30 seconds

step 4: 72° C for 1:45 minutes

step 5: go to step 2 for 29 times

step 6: 72°C for 10 minutes

We detected Akt DNA (300 bp) with a 1% agarose gel.

The genotyping analysis of Raptor floxed allele were performed by using the following primers:

Raptor Forward: CTCAGTAGTGGTATGTGCTCAG

Raptor Reverse: GGGTACAGTATGTCAGCACAG

We prepared a 10µl total volume mix for each sample with:

Template DNA: 2µl

Primer FW (20µM): 0.6µl

Primer RV (20µM): 0.6µl

GoTaq Green master mix 2X (Promega): 5µl

Water

Program:

step 1: 94° C for 3 minutes

step 2: 94° C for 30 seconds

step 3: 58° C for 30 seconds

step 4: 72° C for 30 seconds

step 5: go to step 2 for 35 times

step 6: 72°C for 2 minutes

We detected Raptor DNA (Mutant= 180 bp; heterozygote: 141 bp & 180 bp; wild-type: 141 bp) with a 2% agarose gel.

2.2. Virus Injection

Mice were anesthetized and Gastrocnemius muscles were injected with $2*10^{10}$ vg of AAV-9 for the Cre recombinase, brought to 30µl with physiological solution. One month after the injection, tamoxifen treatment starts. 3 weeks after the administration of tamoxifen, mice were sacrificed and muscles analyzed.

2.3. *In vivo* muscle force measurements

Gastrocnemius muscle force was measured in living mice as previously described (Blaauw et al., 2008). Briefly, animals were anesthetized and muscle contractile performance was measured *in vivo* using a 305B muscle lever system (Aurora Scientific Inc.). Contraction was elicited by electrical stimulation of the sciatic nerve. Common peroneal nerve was cut and the torque developed during isometric contractions was measured at stepwise increasing stimulation frequency, with pauses of at least 30 seconds between stimuli to avoid effects due to fatigue. Duration of the trains never exceeded 600ms. Force was normalized to the muscle mass as an estimate of specific force. Time to peak, half time to peak and relaxation time of the twitch were also measured. Animals were then sacrificed by cervical dislocation and muscles were dissected, weighted and frozen.

2.4. Skinned fiber force measurements

Tibialis Anterior muscles were collected and skinned following the procedure of Thomas et al. (Lowe et al., 2001) with some adjustment in the buffer compositions. Freshly dissected muscle bundles were pinned on a polystyrene support placed in a 15ml tube. Tubes were gently mixed at 4°C in skinning buffer 1 (potassium propionate 60mM, TES [*N*-tris[hydroxymethyl]methyl-2-aminoethanesulphonic acid] 25mM, Magnesium acetate 2mM, EGTA 9mM, sodium azide 1mM, 0,05% Triton X-100, DTT 1mM, ATP 4mM, 1 Complete protease inhibitor tablet in 250ml, 25% glycerol). After 4÷6 hours, polystyrene supports were transferred in a new 15ml tube containing skinning buffer 2 (potassium propionate 60mM, TES buffer 25mM, Magnesium acetate 2mM, EGTA 1mM, sodium azide 1mM, DTT 1mM, ATP 4mM, 1 Complete protease inhibitor tablet in 250ml, 50% glycerol). Single fibers were dissected from bundles in skinning buffer 2 and a T-clip was mounted at each end. The

mounted fiber was transferred to an Aurora Scientific Permealized Fibers setup and attached to a tensiometer on one end and to a feedback motor at the other end. Fiber is washed from glycerol and equilibrated in Relax buffer (Table 1). Sarcomere length was measured in Preactivating solution (Table 1) using a video optical system and adjusted to 2.4 to 2.6μm at the beginning of the experiment. A full contraction in Activating buffer was performed and SL was adjusted again to 2.4 to 2.6μm. The whole experiment was performed in a temperature controlled bath set at 16°C. In calcium titration experiment, solutions listed in Table 2 were used and exchanged every other measurement.

	Imidazole	**EGTA**	**Ca^{2+} - EGTA**	**HDTA**	**KP**	**MgAc**	**ATP**	**CP**	**GSH**
Relax	25	10	0	0	11,8	6,89	5,56	20	10
Preactivating	25	0,1	0	9,9	11,7	6,48	5,56	20	10
Activating	25	0	10	0	11,7	6,39	5,65	20	10

Table 1. *All concentrations are in mM. ATP, adenosine 5'-triphosphate; EGTA, ethylene glycol-bis-(β-aminoethyl ether)-N,N,N',N'-tetraacetic acid; HDTA, 1,6 diaminohexane-N,N,N',N'-tetraacetic acid; CP, N-[Imino(phosphonoamino) methyl]-N-methylglycine; GSH, glutathione; KP, potassium propionate; MgAc, magnesium acetate. pH (adjusted with 2M KOH) was 7.1 at 11°C. Ionic strength, 150÷180 mM. HDTA was obtained from TCI EUROPE – Tokyo Chemical Industry (Zwijndrecht, Belgium), other chemicals from Sigma (St. Louis, MO). Solution adopted from Fusi et al. (Fusi et al., 2015).*

%ACT	0	15	37,5	45	50	55	58	62,5	68,75	75	80	85	90	94	100
pCa	8,97	7,57	7,04	6,91	6,82	6,73	6,68	6,6	6,48	6,34	6,22	6,07	5,87	5,63	4,69

Table 2. *Percentage of Activating solution added to Relax solution to obtain controlled calcium concentration buffers, pCa content has been estimated and suggested by Dr. Luca Fusi using a software provided by Dr E. Homsher.*

2.5. Electromyography analysis

This experiment was made in collaboration with Prof. Aram Megighian (University of Padova). Resting EMGraphic activity was recorded by inserting one needle electrode in the middle region of TA muscle and the second electrode close to the tendon region. Ground electrode was placed around the tail. Recordings were made at room temperature (20-22° C). Calibration bars in knock-out mice is the same as in wild-type mice.

2.6. Measurement of *in vivo* protein synthesis

In vivo protein synthesis was measured by using the SUnSET technique (Goodman et al., 2011b) (Schmidt et al., 2009). Mice were anesthetized and then given an intraperitoneal injection of 0.040µmol/g puromycin dissolved in 100µl of physiological solution. 30 min after injection, muscles were harvested and frozen in liquid nitrogen for Western Blot analysis. A mouse IgG2a monoclonal anti-puromycin antibody (clone 12D10, 1:500) was used to detect puromycin incorporation.

2.7. Colchicine treatment

We monitored autophagic flux in basal and 24 hours of starvation condition using colchicine (Ju et al., 2010). Briefly, control and Raptor knock-out mice were treated with 0,4mg/kg of colchicine or vehicle by intraperitoneal injection and starved. The treatment was repeated 12 hours prior to muscle collection.

2.8. FDB single fiber isolation

Animals were sacrificed through cervical dislocation. FDB muscles collected with their tendons and digested in a tube with collagenase (3mg/ml GIBCO-Life Technologies) in DMEM (GIBCO-Life Technologies) for 1 hour and 30 minutes at 37° C. Meanwhile coverslips were coated with 10% matrigel (Bdolah et al.) in Tyrode's buffer. After digestion the muscles were removed from collagenase, washed to inactivate the collagenase and dissected.

2.9. Mitochondrial membrane potential analysis

Mitochondrial membrane potential was measured in isolated fibers from FDB muscles as previously described (Mammucari et al., 2007) (Zhao et al., 2007). This experiment was made in collaboration with Vanina Romanello (VIMM, Padova). Briefly, FDB myofibers were placed for 15 minutes at 37°C in 1ml Tyrode's buffer and loaded with 2,5nM Tetramethylrhodamine (TMRM) (Molecular Probes), which is a cell-permeant, cationic, red-orange fluorescent dye that is readily sequestered by active mitochondria in a potential-dependent manner. The solution contains also glucose (3,5g/l), to sustain the fibers during the experiment, and Cyclosporin H (8mM) (Enzo Life Science), to block mitochondrial pumps, that would transport TMRM outside the mitochondria. Myofibers were then observed at Olympus IMT-2 inverted microscope (Melville, NY) equipped with a CellR imaging system. Sequential images of TMRM fluorescence were acquired every 60s with a 4X 0.5 UPLANSL N A objective (Olympus). At the times indicated by arrows, oligomycin (Olm, 5μM) (Sigma-Aldrich) or the protonophore carbonyl cyanide-p-trifluoromethoxyphenylhydrazone (FCCP, 4μM) (Sigma) were added to the cell culture medium. We used oligomycin to inhibit ATP-synthase. Otherwise, it can reversely transport protons across the inner

mitochondrial membrane, thus maintaining the potential also in dysfunctional mitochondria. For this reason, only this treatment allows us to detect real dysfunctional mitochondria, that would inevitably dissipate the potential, losing TMRM signal. Images were acquired, stored and analysis of TMRM fluorescence over mitochondrial regions of interest was performed using ImageJ software (http://rsb.info.nih.gov/ij/).

2.10. Measurements of respiratory chain complex activity

This experiment was performed in collaboration with Prof. Leonardo Salviati (University of Padova). Muscle mitochondria from the indicated genotype were isolated from quadriceps muscles as described (Frezza et al., 2007). The enzymatic activities of RC complexes I–IV were assayed spectrophotometrically, and the results were commonly normalized to the activity of citrate synthase (CS), a mitochondrial matrix enzyme, as described (Spinazzi et al., 2012).

2.11. Exhaustion exercise

Raptor knock-out and wild-type mice performed one day of concentric exercise on a treadmill (LE 8710 Panlab Technology 2B, Biological Instruments), at increasing velocity, according to the protocol of acute exercise previously described (He et al., 2012).

Briefly, exercise consists in 17 cm/sec for 40 minutes, 18 cm/sec for 10 min, 20 cm/sec for 10 min, 22 cm/sec for 10 min, and then increasing velocity of 1 cm/sec and of 2 cm/sec alternatively every 5 minutes, until they were exhausted. Exhaustion was defined as the point at which mice spent more than 5 s on the electric shocker without attempting to resume running.

Total running distance and time were recorded for each mouse. All

procedures are specified in the projects approved by the Italian Ministero Salute, Ufficio VI (authorization numbers 1060/2015PR).

2.12. Histological analysis and immunofluorescence stainings

Collected muscles were directly frozen in liquid nitrogen. Then, muscles were cut in 10μm thick cryosections (or 2μm for mTOR staining) by using Cryostat (Leica CM 1950) and used for different analysis. Images were collected with an epifluorescence Leica DM5000B microscope, equipped with a Leica DFC300-FX digital charge-coupled device camera, by using Leica DC Viewer software.

2.12.1. Haematoxylin & Eosin staining (H&E)

Haematoxylin is a basic dye which binds to basophilic substrates, such as DNA and RNA contained in ribosomes and nuclei, thus staining them violet. Eosin colors eosinophilic structures, such as intracellular and extracellular proteins, staining them pink.

Material	Time
Mayer Haematoxylin (Sigma-Aldrich)	1 minute
Wash in tap water	2 minutes
Eosin Y Solution Alcoholic (Sigma-Aldrich)	1 minute
Ethanol 50%	30 seconds
Ethanol 70%	30 seconds
Ethanol 100%	5 minutes
Ethanol 100%	10 minutes
Xilen	3 minutes
Mount with Eukitt (Sigma-Aldrich)	

2.12.2. Periodic Acid-Schiff staining (PAS)

PAS staining is a method to detect polysaccharides such as glycogen and glycoproteins. Periodic Acid oxidizes vicinal diols of these sugars, breaking up the bond between two adjacent carbons and creating a pair of aldehydes. These aldehydes, then, react with Schiff reagent, giving a purple-magenta color.

Material	Time
Carnoy's solution	10 minutes
Wash in distilled water	5-6- times
Periodic Acid 0,5% (Merck)	5 minutes
Wash in distilled water	5-6- times
Schiff reagent (Merck)	15 minutes
Wash in running tap water	5 minutes
Mount with Elvanol	

Carnoy's solution is a fixative composed of 60% ethanol, 30% chloroform and 10% glacial acetic acid.

Elvanol is a saturated solution of polyvinyl alcohol in Phosphate Buffered Saline (PBS), 20% glycerol and 1mM sodium azide.

2.12.3. SDH staining

Succinate dehydrogenase is an enzyme which forms complex II of respiratory chain and it is localized in the inner mitochondrial membrane. Colorimetric evaluation of the staining is used either to assess approximately the quantity and the distribution of mitochondria within muscle fibers or to evaluate oxidative activity of the enzyme. The reaction gives a purple coloration in the oxidative fibers, whereas glycolytic ones appear white. The sections were incubated for 30 minutes at 37°C with SDH solution (0.2M sodium succinate) (Sigma-Aldrich), 0.2M phosphate

buffer (Sigma) pH 7.4 and 50mg of nitro blue tetrazolium (NBT) (Sigma-Aldrich). After the incubation, sections were washed with distilled water for 5 times and then mounted with Elvanol solution.

2.12.4. Immunofluorescence analysis

Muscle cryosections were fixed in 4% paraformaldehyde for 10 minutes, treated with 0,1% Triton in PBS for 2 minutes and blocked with blocking solution (0,5% Bovine Serum Albumin BSA, 10% goat serum in PBS) for 30 minutes RT. Samples were then incubated with primary antibodies in 0,5% BSA, 4% goat serum in PBS at 4°C over-night. Then the sections were washed with PBS three times for 5 minutes and incubated with secondary antibodies (dilution 1:200) and WGA (Wheat Germ Agglutinin-Invitrogen), to label plasma membrane, 1:100 in 0,5% BSA, 4% goat serum in PBS at 37°C for 1 hour. After the washes, slides were mounted with Elvanol.

Primary antibody	Company	Dilution primary antibody	Secondary antibody
P-Akt	Cell Signaling	1:800	Anti-rabbit-594-conjugated
LC3	Cell Signaling	1:100	Anti-rabbit-594-conjugated
LAMP1	Hybridoma Bank	1:100	Anti-rat-488-conjugated
p62	Sigma-Aldrich	1:100	Anti-rabbit-594-conjugated
Dystrophin	abcam	1:100	Anti-rabbit-594-conjugated
GFP	Lifetech	1:100	Anti-rabbit-594-conjugated

Table 3: Antibodies used for immunofluorescence

Dystrophin staining is then used to fiber CSA measurement, by using ImageJ software (National Institutes of Health). All data are expressed as the mean±SEM (error bars). Comparisons were made by using t test, with $p<0.05$ being considered statistically significant.

2.12.5. Neural Cell Adhesion Molecule (NCAM) staining

NCAM is localized at NMJ level in a normal muscle, whereas it diffuses throughout myofibers when an impairment in the communication nerve-muscle occurs. Therefore, NCAM staining is used as a sign of muscle denervation.

Muscle cryosections were fixed with Methanol -20°C and incubated in blocking solution (10% goat serum in PBS) at room temperature (RT) for 1 hour. Samples were then incubated with the primary antibody against NCAM (Millipore) (dilution 1:100 in 2% goat serum in PBS) at 4°C over-night. Then the sections were washed with PBS three times for 5 minutes and incubated with the anti-rabbit-594-conjugated secondary antibody (dilution 1:200 in 2% goat serum in PBS) at 37°C for 1 hour (Jackson ImmunoResearch). After washing and incubation with DAPI, that labels nuclei, slides were mounted with Elvanol solution.

2.12.6. IgG staining

Cryosections were incubated in blocking solution (0.5% BSA, 10% goat serum in PBS) at RT for 20 minutes. Samples were then incubated with anti-mouse-594-conjugated secondary antibody (dilution 1:200) at 37°C for 1 hour (Jackson ImmunoResearch). After the wash and incubation with DAPI, slides were mounted with Elvanol.

2.12.7. mTOR-LAMP1 co-staining

2 μm muscle cryosections were used for the co-staining. They were fixed

in acetone at -20°C for 10 minutes. After one wash in PBS for 15 minutes, samples were treated with 0,3% CHAPS (GE Healthcare), 5% goat serum in PBS for 30 minutes at RT. Then the sections were washed with PBS three times for 5 minutes and incubated with primary antibodies anti-mTOR (Cell Signaling) and anti-LAMP1 (Hybridoma bank) 1:100 in 0,3% CHAPS, 0,5% BSA in PBS for 1 hour at RT. After the washes, cryosections were incubated with secondary antibodies (anti-rabbit-594-conjugated and anti-rat-488-conjugated) 1:200 with WGA 1:100 in 0,3% CHAPS, 0,5% BSA in PBS for 1 hour at RT. After the washes, samples were mounted with Elvanol.

2.12.8. Myosin staining

Muscles cryosections were blocked with mouse-on-mouse (MOM-Vector Laboratories) for 1 hour at RT. Then, primary antibodies were put (anti-BAD5, anti-SC71, anti BFF3) 1:100 (Hybridoma Bank) in BSA 1% for 1 hour at 37°C. After washes, secondary antibodies were added (DyLight 549-conjugated anti-mouse IgM and 488-conjugated anti-mouse IgG 1:200 and 405-conjugated anti-mouse IgG2b 1:100) in BSA 1% for 1 hour at 37°C. Then, samples were mounted with Elvanol.

2.12.9. Transcription factor EB (TFEB) staining

Muscles cryosections were treated with Methanol and 0,3% hydrogen peroxide for 30 minutes at RT. They were, then, washed 5 minutes for 5 times with PBS and treated with 0,2% Triton for 5 minutes. After 5 washes, samples were blocked with blocking solution (5% BSA, 10% fetal bovine serum in PBS) for 1 hour at RT. Sections were, then, incubated with anti-TFEB antibody (Bethyl) 1:200 in blocking solution diluted 1:10 at 4°C over-weekend.

We, then, did 3 washes in PBS-Tween 0,1% for 5 minutes and one wash in PBS. Biotinylated anti-rabbit (1:500 in blocking buffer diluted 1:10) was added for 1 hour at RT. We did 3 washes in PBS-Tween 0,1% for 5

minutes and one wash in PBS. After the addition of Vectastain ABC (Vector Laboratories) for 1 hour and NovaRed (Vector Laboratories) for 20 minutes, sections were mounted with Elvanol.

2.13. Immunoblotting

Cryosections of 20μm of TA muscles were lysed in 100μl of a buffer containing 50mM Tris pH 7.5, 150mM NaCl, 10mM $MgCl_2$, 0.5mM DTT, 1mM EDTA, 10% glycerol, 2% SDS, 1% Triton X-100, Roche Complete Protease Inhibitor Cocktail and Roche Phospho-Stop Phosphatase Inhibitor Cocktail. To detect Lys63 and Lys48 polyubiquitin chain content, samples were also added to two proteasome inhibitors: MG132 (Tocris bioscience) and NEM (Sigma-Aldrich).
Lysates were incubated at 70°C for 10 minutes and centrifuged at 13.300 rpm for 15 minutes at 4°C. Concentration of surnatant protein was, then, measured using BCA protein assay kit (Pierce) following manufacturer's instructions.

2.13.1. Protein gel electrophoresis

Extracted proteins were solubilized in a buffer containing 5μl of 4X NuPAGE® LDS Sample Buffer (Life Technologies), 1μl of 20X DTT (Life Technologies) and water, until reaching 20μl of volume. After 10 minutes of denaturation at 70°C, samples were loaded on SDS 4-12% or SDS 3-8% precast polyacrylamide gels (Life Technologies), according to molecular weight of the protein to be analyzed. The electrophoresis was run in 1x MES/MOPS or 1X Tris-Acetate Running buffer, respectively (Life Technologies), starting from a voltage of 90V until reaching 150V when samples entered the wells.

2.13.2. Transfer of the protein to the nitrocellulose membrane

Proteins were now transferred from gels to nitrocellulose membranes. For the transfer, we used a Semi-dry method (Bio-Rad). Membrane and blotting paper (Bio-Rad) were equilibrated with Transfer Buffer, composed by 20% Methanol and 1X Tris-Glycine (SERVA). Transfer was obtained by applying a current of 2mA/cm^2, according to the dimension of the gel, for 1 hour at RT. To evaluate the efficiency of the transfer, proteins were stained with Red Ponceau 1X (Sigma-Aldrich). The staining was easily reversed by washing with distilled water.

2.13.3. Incubation with antibodies

After the transfer of proteins into nitrocellulose membranes, the membranes were saturated with Blocking Buffer (5% no-fat milk powder or BSA solubilized in TBS 1X with 0,1% TWEEN) for 1 hour at RT and incubated over-night with different primary antibodies at 4°C listed in Table 4). Tris-buffer saline (TBS) is composed by 50mM Tris and 150mM NaCl in water, adjusted to pH 7.6.

Membranes were then washed 3 times with TBS 1X with 0,1% TWEEN at RT and incubated with secondary HRP-conjugated antibody for 1 hour at RT. Immunoreaction was revealed by Clarity Chemiluminescent substrate (Bio-Rad) and developed with ImageQuant LAS 4000 Mini (GE Healthcare).

Stripping Solution was made wth 25mM glycine and 1% SDS, pH 2.

Antibody	Costumer	Dilution
Rabbit anti-Raptor	Cell Signaling #2280	1:1000
Rabbit anti-mTOR	Cell Signaling #2983	1:1000
Rabbit anti-phospho-Akt (Ser473)	Cell Signaling #4060	1:1000
Rabbit anti-Akt	Cell Signaling #9272	1:1000

Rabbit anti-phospho-S6	Cell Signaling #2215	1:1000
Rabbit anti-S6	Cell Signaling #2217	1:1000
Rabbit anti-phospho-4Ebp1 (Thr37/46)	Cell Signaling #9459	1:1000
Rabbit anti-phospho-4Ebp1 (Ser65)	Cell Signaling #9455	1:1000
Rabbit anti-4Ebp1	Cell Signaling #9452	1:1000
Rabbit anti-phospho-GSK3β (Ser9)	Cell Signaling #9323	1:1000
Rabbit anti-GSK3β	Cell Signaling #9315	1:1000
Rabbit anti-LC3	Sigma L7543	1:1000
Rabbit anti-p62	Sigma P0067	1:1000
Rabbit anti-phospho-eIF2α	Abcam ab 32157	1:1000
Rabbit anti-eIF2α	Cell Signaling #9722	1:1000
Mouse anti-BiP/GRP78	BD 610979	1:5000
Mouse anti-puromycin	Millipore MABE343	1:1000
Rabbit anti-TOM20	Abcam ab14734	1:10000
Mouse anti-Porin1	SantaCruz Sc-11415	1:10000
Mouse anti-Lys48	Millipore 04-263	1:5000
Rabbit anti-Lys63	Millipore 05-1308	1:2000
Mouse anti-GAPDH	Abcam ab 8245	1:10000
Mouse anti-actin	SantaCruz sc-56459	1:5000
Goat anti-mouse IgG	Bio-Rad 1706516	1:2000
Goat anti-rabbit IgG	Bio-Rad 1706515	1:2000

Table 4: Antibodies used for Western Blot

2.13.4. Quantification of Immunoblotting

Quantification of the signal obtained through immunoreaction was measured with ImageJ software. Signal of interested protein was

normalized for levels of an housekeeping protein, representative of gel loading. As housekeeping proteins we used either Actin or GAPDH, since their content did not change during experimental conditions. Results are expressed as mean±SEM.

2.14. Gene expression analysis

2.14.1. RNA extraction

Total RNA was extracted from Gastrocnemius muscle by using Trizol (Life Technologies) according to manufacturer's instructions.

2.14.2. Reverse Transcription

400 ng of total RNA was reversely transcribed to obtain cDNA using SuperScript™ IV (Life Technologies) in the following mix:

Random primer hexamers (50ng/μl): 1μl
dNTPs 1mM: 1μl
The volume was brought to 13μl with RNase-free water.

Samples were denatured at 65°C for 5 minutes to avoid secondary structures of RNA. After the denaturation, samples were added to the following components:
DTT 100mM: 1μl
Rnase OUT (Life Technologies): 1μl
SuperScript™ IV (Life Technologies): 1μl
RNase-free water: 0,5μl

The reaction program was:

Step 1: 23°C for 10 minutes
Step 2: 50°C for 10 minutes

Step 3: 80°C for 10 minutes

At the end of the reaction, the volume of each sample was brought to 50µl with RNase-free water.

2.14.3. Real-Time PCR reaction

Quantitative real-time PCR was performed using SYBR Green chemistry (Applied Biosystems). SYBR Green is a fluorescent dye used as nucleic acid stain. Indeed, it intercalates into double-strand DNA, producing a fluorescent signal. Real-time PCR products accumulate during PCR cycles, creating an amplification plot, which is the plot of fluorescence signal versus cycle number, and, thus, allowing their detection through real-time PCR machine. At the beginning of PCR, the little change in fluorescent signal defines the baseline for the amplification plot. An increase in fluorescent signal above the baseline indicates the detection of PCR products. A fixed fluorescence threshold can be set above the baseline. Ct (threshold cycle) is defined as the fractional cycle number at which the fluorescence passes the fixed threshold. So, lower Ct value indicates an higher amount of the sample which can be therefore detected earlier through PCR process.

1µl of diluted cDNAs was amplified in 10µl PCR reactions in an ABI Prism 7000 (Applied Biosystem) thermocycler, coupled with an ABI Prism 7000 Sequence Detection System (Applied Biosystems) in 384-wells plates (Micro Amp Optical, Applied Biosystems). In each well 5µl sample mix and 5µl reaction mix were mixed.

Sample mix was prepared as follows:
cDNA: 1µl
RNase-free water: 4µl
SYBR Green was added to primer mix as follows:
SYBR Green qPCR (Applied Biosystems): 4,8µl

Forward/Reverse primer mix (50mM): 0,2µl

The PCR cycle used for the Real-Time PCR was:
Step 1: 95° C for 15 minutes
Step 2: 95° C for 25 seconds
Step 3: 58° C for 1 minute
Step 4: go to step 2 for 40 times

2.14.4. Quantification of the PCR products

Pfaffl in 2001 described a quantification method to evaluate the differences in gene expression, by measuring the ratio between a test sample and a housekeeping gene (Pfaffl, 2001). The relative expression ratio of a target gene is calculated based on the primer efficiency (E) and the threshold cycle deviation (∆Ct) of unknown sample versus a control, and expressed in comparison to a reference gene.
The mathematical model is defined with this equation:

$$\text{Ratio} = \frac{(E_{\text{target}})^{\Delta Ct}}{(E_{\text{reference}})^{\Delta Ct}}$$

The reference gene used in our real-time PCR was HPRT, which did not change under experimental conditions.

2.14.5. Primer pair design

Gene-specific primer pairs were selected with Primer Blast software (http://www.ncbi.nlm.nih.gov/tools/primer-blast/). Primer pairs were selected in a region close to the 3'-end of the transcript, and amplified fragments of 150-250bp in length. To avoid the amplification of contaminant genomic DNA, the target sequences were chosen on distinct

exons, separated by a long (more than 1000bp) intron. The melting temperature was chosen to be of about 58-60° C. The sequences of the primer pairs are listed in Table 5.

	Forward primer (5'-3')	Reverse primer (3'-5')
Raptor	GCCTGGAGTCACACTGGATT	CAGTTCAGCTCTCCCAGAGG
Atrogin1	GCAAACACTGCCACATTCTCTC	CTTGAGGGGAAAGTGAGACG
MUSA1	TCGTGGAATGGTAATCTTGC	CCTCCCGTTTCTCTATCACG
MURF-1	ACCTGCTGGTGGAAAACATC	ACCTGCTGGTGGAAAACATC
Fbxo21	TCAATAACCTCAAGGCGTTC	GTTTTGCACACAAGCTCCA
Ambra1	CCTCCTCTTCTTCCTCAGACA	AAATCCCAGCATAAGGCAAGT
LC3	CACTGCTCTGTCTTGTGTAGGTTG	TCGTTGTGCCTTTATTAGTGCATC
BNIP3	TTCCACTAGCACCTTCTGATGA	GAACACCGCATTTACAGAACAA
CathepsinL	GTGGACTGTTCTCACGCTCAAG	TCCGTCCTTCGCTTCATAGG
p62	CCCAGTGTCTTGGCATTCTT	AGGGAAAGCAGAGGAAGCTC
Ulk1	CCGTCAAATGCATTAACAAGA	GCATAGTGTGCAGGTAGTCAG
Beclin1	TGGAAGGGTCTAAGACGT	GGCTGTGGTAAGTAATGGA
MYH7	AGCAGGAGCTGATTGAGACC	TGTGATAGCCTTCTTGGCCT
MHC 2A	TTGGTGGATAAACTCCAGGC	CAGCTTGTTGACCTGGGACT
MHC 2X	ACCTTGTGGACAAACTGCAA	AGCTTGTTGACCTGGGACTC
MHC 2B	ACAGACTAAAGTGAAAGCCTACAA	CACATTTTGTGATTTCTCCTGTCAC
RCAN1	GTGTGGCAAACGATGATGTC	AGGAACTCGGTCTTGTGCAG
TFEB	AACAGTGCTCCCAACAGTCC	GGCGCATAATGTTGTCAATG
LAMP1	TCTGACCACCTACGAGACTG	ACATATGCTGGACACTGTAACG
nNOS	CCAAAGCAGAGATGAAAGACAC	TCTTGGTAGGAGACTGTTTGC

	A	
Tbc1d1	GTCCCGGGGTAATAAAGCCA	TTGTCACCCATGGACAGCTC
Tbc1d4	AGGGGCGGCCATTATTTCAA	CAAGCCGACCTCTCATCCTG
Glut1	AGCAGCAAGAAGGTGACG	CACGGAGAGAGACCAAAGC
Glut4	CCGCGGCCTCCTATGAGATACT	AGGCACCCCGAAGATGAGT
mTOR	CCTTCGTGCCTGTCTGAT	CCCATGAGGTCTTTGCAGTA
HPRT	GTTTGTTGTTGGATATGCCCTTG	GGCAACATCAACAGGACTCC

Table 5: Primers used for quantitative RT-PCR

Data were normalized to HPRT expression. Results are expressed as mean±SEM.

2.15. Statistical analysis

Generally, to reduce the standard deviation, we minimized physiological variation by using mice with same sex and same age. Comparisons were made by using two-tail Student's t-test, with $p \leq 0.05$ considered statistically significant. For all graphs data are represented as mean±SEM.

3. RESULTS

PART I

3.1. Generation of HSA-Raptor ko mouse line

Mammalian target of rapamycin complex 1 (mTORC1) plays a central role in cell growth. One of the key members of the mTORC1 complex is Raptor, which recruits mTOR substrates S6K1 and 4EBP1. Mice lacking Raptor only in skeletal muscle from birth show a pronounced myopathy (Bentzinger et al., 2008). However, treating adult mice with the specific mTORC1 inhibitor rapamycin does not lead to a myopathic phenotype and even extends lifespan (Harrison et al., 2009). Considering these contradictory results and the fact that deletion of a gene from birth can cause compensatory mechanisms, we wondered what happens if we delete Raptor in the adult skeletal muscle. To do this, we crossed Raptor floxed mice with mice expressing Cre recombinase (CRE) fused to a mutated estrogen receptor (ER) domain under a muscle specific promoter: the human skeletal actin promoter (HSA). In these mice CRE is constantly degraded due to heat-shock proteins (HSPs) binding to ER domain. When tamoxifen is administrated, it is able to bind to estrogen receptor thus preventing CRE degradation. In this way, tamoxifen treatment can delete Raptor only in skeletal muscle and not in other tissues. We treated 3-months-old mice for 3 weeks with tamoxifen and one month after the beginning of the treatment we checked if deletion occurred. By quantitative RT-PCR analysis on RNA extracts from skeletal muscle, we observed that Raptor mRNA is strongly reduced in Raptor knock-out (ko) animals (Fig. 1A). This result is confirmed by Western blot analysis, which shows that Raptor protein is decreased in skeletal muscle of ko mice, but not in liver and heart of the same mice (Fig. 1B).

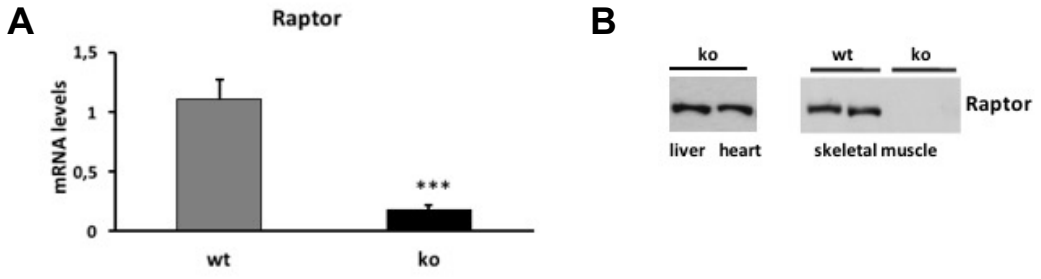

Fig. 1: Validation of Raptor knock-out model. A) *Raptor mRNA expression levels analyzed by RT-PCR in muscles of Raptor ko and control mice. n=4 mice each group.* ***B)*** *Representative Western Blot analysis for Raptor protein levels in skeletal muscle, liver and heart. n=15 mice each group for skeletal muscle; n=4 for liver and heart.* ***p≤0.001.*

3.2. Skeletal muscle-specific Raptor deletion does not affect muscle mass or muscle function at this time point

To check if Raptor deletion affects muscle mass, we measured muscle weight over body weight, which is a good indicator of changes in muscle mass, of wildtype and knock-out animals one month after the beginning of the treatment. Surprisingly, we did not find any significant changes between the two groups in all muscles examined (Fig. 2A).

Since Raptor deletion in skeletal muscle from birth leads to a myopathic phenotype, with central nuclei and either small and big fibers (Bentzinger et al., 2008), we did an H&E staining to assess muscle state in our mouse model. At this early time point, morphological analysis of Tibialis Anterior did not show any signs of a muscle pathology and, even, knock-out muscles are comparable to wild-type ones (Fig. 2B).

To check if Raptor deletion can impinge on glycogen content or on mitochondria function, we performed, respectively, a PAS staining and a succinate dehydrogenase (SDH) staining. However, also in this case morphological analysis did not reveal any difference between wild-type and knock-out muscles (Fig. 2C and 2D).

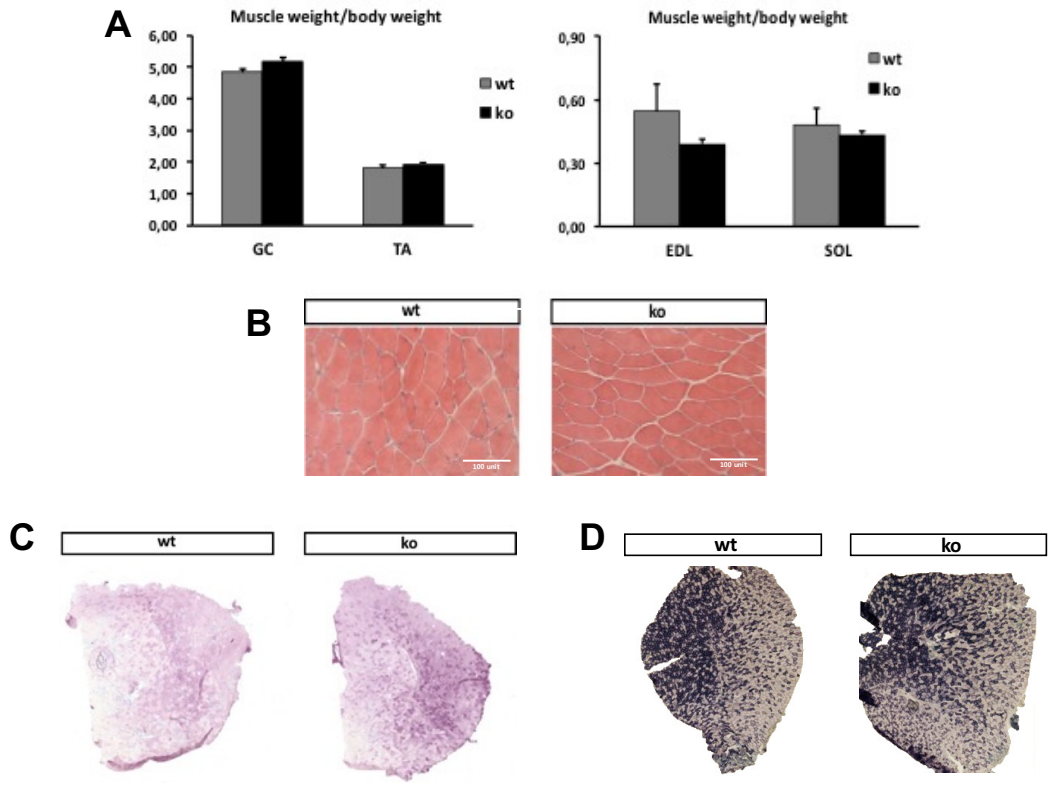

Fig 2: One month of deletion of Raptor does not affect muscle mass and muscle histology. A) *Muscle weight over body weight measurements of Gastrocnemius (GA), Tibialis Anterior (TA), EDL and Soleus of Raptor ko and control mice. n=3 mice each group.* ***B)*** *Representative image of Hematoxylin and eosin staining (H&E) on Tibialis Anterior of Raptor ko and control mice. n=6 mice each group.* ***C)*** *Representative image of PAS staining on Tibialis Anterior of Raptor ko and control mice. n=6 mice each group.* ***D)*** *Representative image of Succinate dehydrogenase staining (SDH) on Tibialis Anterior of Raptor ko and control mice. n=6 mice each group.*

To understand if Raptor deletion can affect muscle performance, we measured force production of Gastrocnemius muscle using an *in vivo* approach. Normalized force, which is the absolute force normalized for the muscle weight, was unaffected by Raptor deletion (Fig. 3A). Moreover time to peak, half time to peak and relaxation time of the twitch were unaltered in Raptor ko mice (Fig. 3B). These functional data are in line with morphological analysis, thus confirming the absence of a myopathic phenotype in one month-treated Raptor knock-out mice.

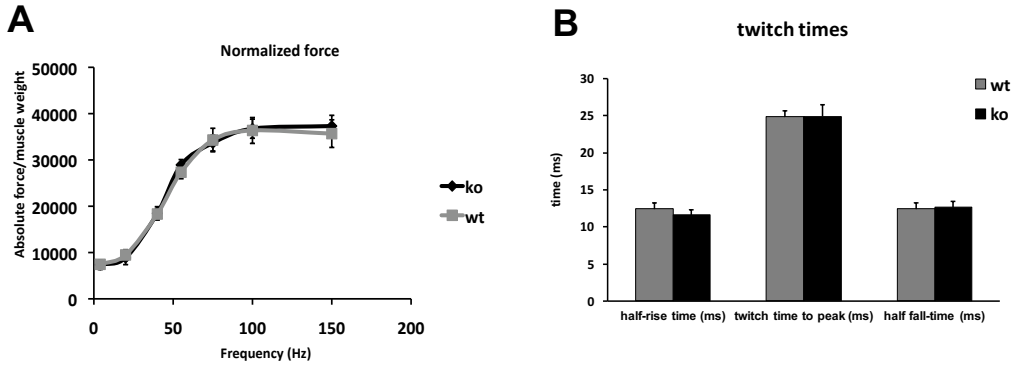

Fig. 3: Raptor deletion does not affect muscle performance. A) *Normalized force of Gastrocnemius muscle in wild-type and knock-out mice. n=4 mice each group.* ***B)*** *Twitch times analysis of wild-type and knock-out mice. n=4 mice each group.*

3.3. Deletion of Raptor affects Akt-mTOR signaling

To check how the absence of Raptor affects Akt-mTOR signaling, we performed Western blot analysis for different proteins involved in this pathway. We observed that mTOR protein levels are reduced by about 50% in knock-out animals (Fig. 4A). Moreover, we checked mTOR localization in wild-type and knock-out muscles, through a mTOR-LAMP1 co-staining, where LAMP1 is a marker of lysosomes. In wild-type Tibialis Anterior mTOR and LAMP1 sometimes co-localize, as expected, whereas in knock-out muscles both the proteins are poorly detectable, maybe for the reduced protein levels observed in these mice (Fig. 4B).

Phosphorylation of downstream targets of mTORC1, such as the ribosomal protein S6 and 4EBP1, are strongly reduced or, even, blunted in knock-out mice. Moreover, Raptor deletion results in the hyperphosphorylation and, thus, activation of Akt (Fig. 4C).

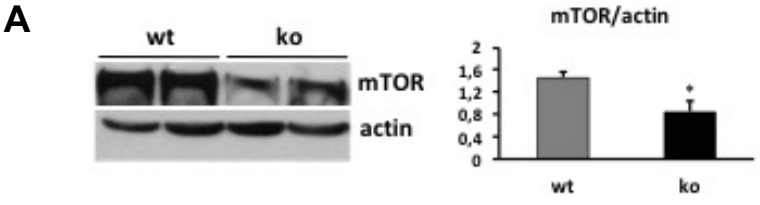

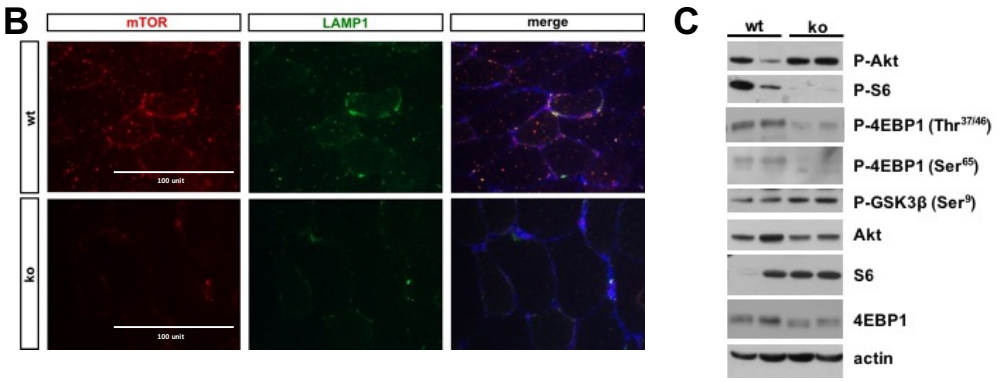

Fig. 4: Raptor deletion affects Akt-mTOR signaling. A) *Representative Western blot analysis and quantification of mTOR protein levels in Raptor ko mice. n=4 mice each group.* ***B)*** *Representative image of mTOR-LAMP1 co-staining (mTOR: red, LAMP1: green, co-localization: yellow, WGA: blue). n=3 mice each group.* ***C)*** *Representative Western blot analysis of Akt-mTOR axis. n=8 mice each group. *p*≤0.05**.**

3.4. Ubiquitin-Proteasome system (UPS) and Autophagy-Lysosome system are impaired upon Raptor deletion

It has been suggested that mTORC1 is the dominant regulator of autophagy induction, independently from FoxO3 activation levels. Indeed, activation of mTORC1 leads to a block in autophagy, even if FoxO3 is active, while Raptor deletion results in autophagy induction, regardless of FoxO inhibition (Castets et al., 2013) (Bentzinger et al., 2008).

To check what happens to UPS and to autophagy when we delete Raptor in adult skeletal muscle, we extracted mRNA from muscle tissue and we performed quantitative RT-PCR for different E3-ubiquitin ligases and for several “atrogenes”. We found that some genes involved in autophagy, like Ulk1, LC3, Cathepsin L, and in mitophagy (BNIP3) are strongly reduced in knock-out mice. Different E3 ubiquitin ligases, such as Atrogin-1, Murf-1, MUSA and Fbxo21, showed a tendency to decrease upon Raptor deletion (Fig. 5A and B).

One factor driving the expression of autophagy and lysosomal genes is the transcription factor EB (TFEB). Nuclear localization of TFEB results in its activation and, thus, in transcription of its target genes, while mTORC1-dependent phosphorylation on Ser^{211} of TFEB prevents its nuclear translocation and function (Settembre et al., 2011). We transfected wild-type and knock-out Tibialis Anterior with a construct codifying for TFEB fused to a green fluorescent peptide (TFEB-GFP). Through an immunofluorescence for GFP peptide, we can easily localize TFEB within the muscle. After 10 days from the electroporation, we found that in wild-type mice, in a rest state, TFEB preferentially localized in the cytoplasm, whereas, as expected, it was mainly present in the nuclei upon Raptor deletion. Indeed, quantification of the immunofluorescence revealed a 6-fold increase in TFEB-positive nuclei in Raptor ko muscles (Fig. 5C). TFEB activation is strongly in contrast with quantitative RT-PCR data where many genes involved in lysosome biogenesis are downregulated upon Raptor deletion.

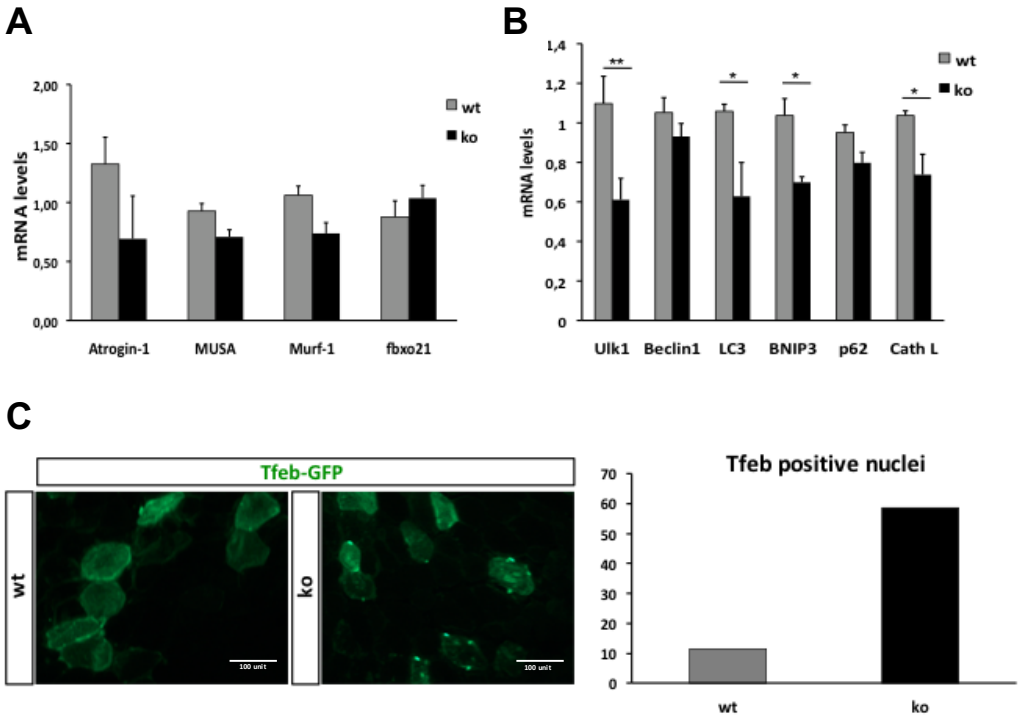

Fig. 5: Reduction of autophagy-related genes upon Raptor deletion. A) *Quantitative RT-PCR for E3 ubiquitin ligases Atrogin-1, MUSA, Murf-1 and Fbxo21. n=3 mice each group* ***B)*** *Quantitative RT-PCR for "atrogenes" Ulk1, Beclin-1, LC3, BNIP3, p62 and Cathepsin L. n=3 mice each group* ***C)*** *Representative image of TFEB-GFP immunofluorescence and quantification. n=2 mice each group *p≤0.05; **p≤0.01.*

To understand if Raptor deletion could affect autophagy induction, we placed Raptor ko mice under starvation, a condition known to strongly activate autophagy. 24-hours of starvation results in body weight loss to a similar extent in wild-type and knock-out mice, without affecting muscle histology (Fig. 6A and B). As expected, phosphorylation of mTORC1 target, Ulk1, is reduced in Raptor ko mice in both fed and starved condition (Fig. 6C). Low levels of P-Ulk1 are associated with autophagy induction and autophagosome formation (Kim et al., 2011). Therefore, we checked mRNA levels of different autophagy-related genes through quantitative RT-PCR. Many of them are not or only slightly induced after starvation in Raptor ko mice, meaning that autophagy stimulation is impaired upon Raptor deletion (Fig. 6D). However, lipidated LC3 (LC3-II) protein levels normalized for actin was increased in starved group without differences between wild-type and knock-out animals, whereas, p62 was only mildly reduced in Raptor ko mice both in fed and starved conditions (Fig. 6E).

In control mice, the increase in LC3-II compared to LC3-I levels indicates an accumulation of autophagosomes, due to autophagy induction during starvation. However, the lipidated form of LC3, bound to the inner autophagosome membrane, is degraded together with the cargo upon lysosome fusion. Indeed, the increase in LC3-II levels can also be associated to an impairment in autophagy degradation. In order to distinguish between these two possibilities, we treated wild-type and knock-out mice with an inhibitor of autophagosome-lysosome fusion, colchicine. If the amount of LC3-II further accumulates in the presence of colchicine, this would indicate enhancement of the autophagic flux. On the contrary, if the LC3-II levels remain unchanged, it is likely due to inhibition

of autophagic degradation (Mizushima and Yoshimori, 2007).

We found that both LC3-II and p62 tend to accumulate upon colchicine treatment. However, when we normalized for GAPDH, we did not find huge differences between the groups, likely meaning that autophagy flux is not impaired at this time point (Fig. 6F).

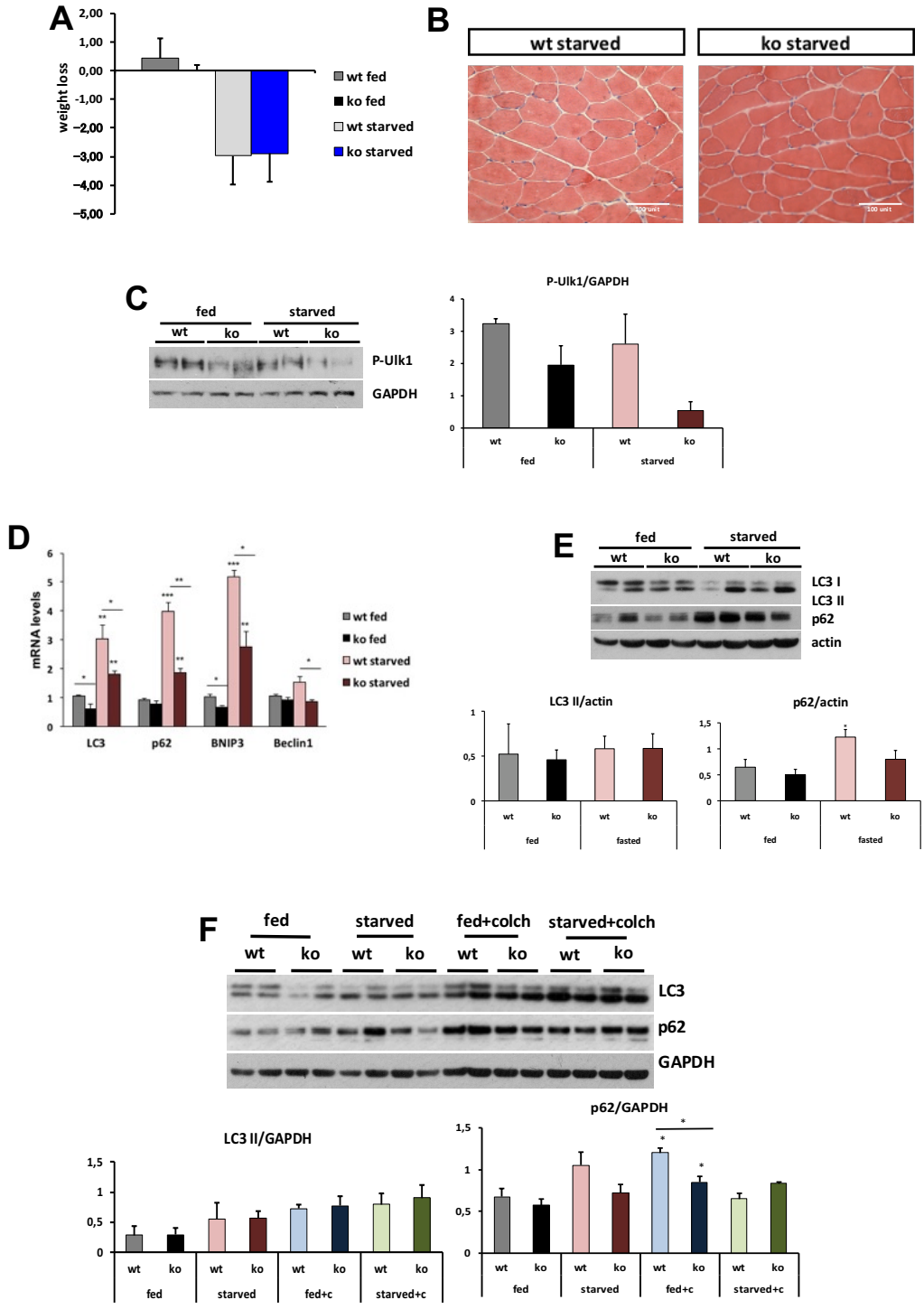

Fig. 6: Induction of autophagy-related genes is affected by Raptor deletion. A) *Body weight loss after 24 hours of starvation. n=3 mice each group* ***B)*** *Representative image of Hematoxylin and Eosin staining of wild-type and knock-out starved mice. n=3 mice each group* ***C)*** *Representative Western blot analysis of Ulk1 and relative quantification on GAPDH. n=2 mice each group* ***D)*** *Quantitative RT-PCR for "atrogenes" LC3, p62, BNIP3 and Beclin-1. n=7 fed mice; n=6 fasted mice* ***E)*** *Representative Western blot analysis of LC3 and p62 protein levels. n=6 mice each group* ***F)*** *Representative Western blot analysis for LC3 and p62 protein levels after colchicine administration. n=4 mice each group. *p≤0.05; **p≤0.01; ***p≤0.001.*

3.5. Rapamycin administration affects muscle histology and muscle performance of Raptor ko mice

Rapamycin prevents the interaction between Raptor and mTOR, blocking the formation of mTOR complex 1 and, thus, its activity. Indeed, it is a well-known specific inhibitor of mTORC1. However, it has been published that some functions of mTOR are rapamycin-sensitive but not strictly dependent on mTORC1 or mTORC2 (Patursky-Polischuk et al., 2009) (Luo et al., 2015).

To understand what happens in the absence of Raptor, we treated wild-type and knock-out mice for 3 weeks with intraperitoneal injections of rapamycin. Muscle histology of Tibialis Anterior is compromised in Raptor ko mice upon rapamycin administration, with no obvious differences in glycogen content or mitochondrial function after the treatment (Fig. 7A, B and C). Since Hematoxylin and Eosin staining revealed signs of muscle damage, we monitored inflammation and we found a strong increase in IgG-positive fibers in rapamycin-treated knock-out mice (Fig. 7D). Moreover, to verify if these compromised muscles were still functional, we measured *in vivo* force production of Gastrocnemius muscles. No differences were observed in wild-type mice upon rapamycin administration, whereas rapamycin-treated Raptor ko animals displayed a significant drop in normalized force compared to vehicle-treated knock-out mice (Fig. 7E), meaning that rapamycin can, in some way, affect muscle

homeostasis in the absence of Raptor.

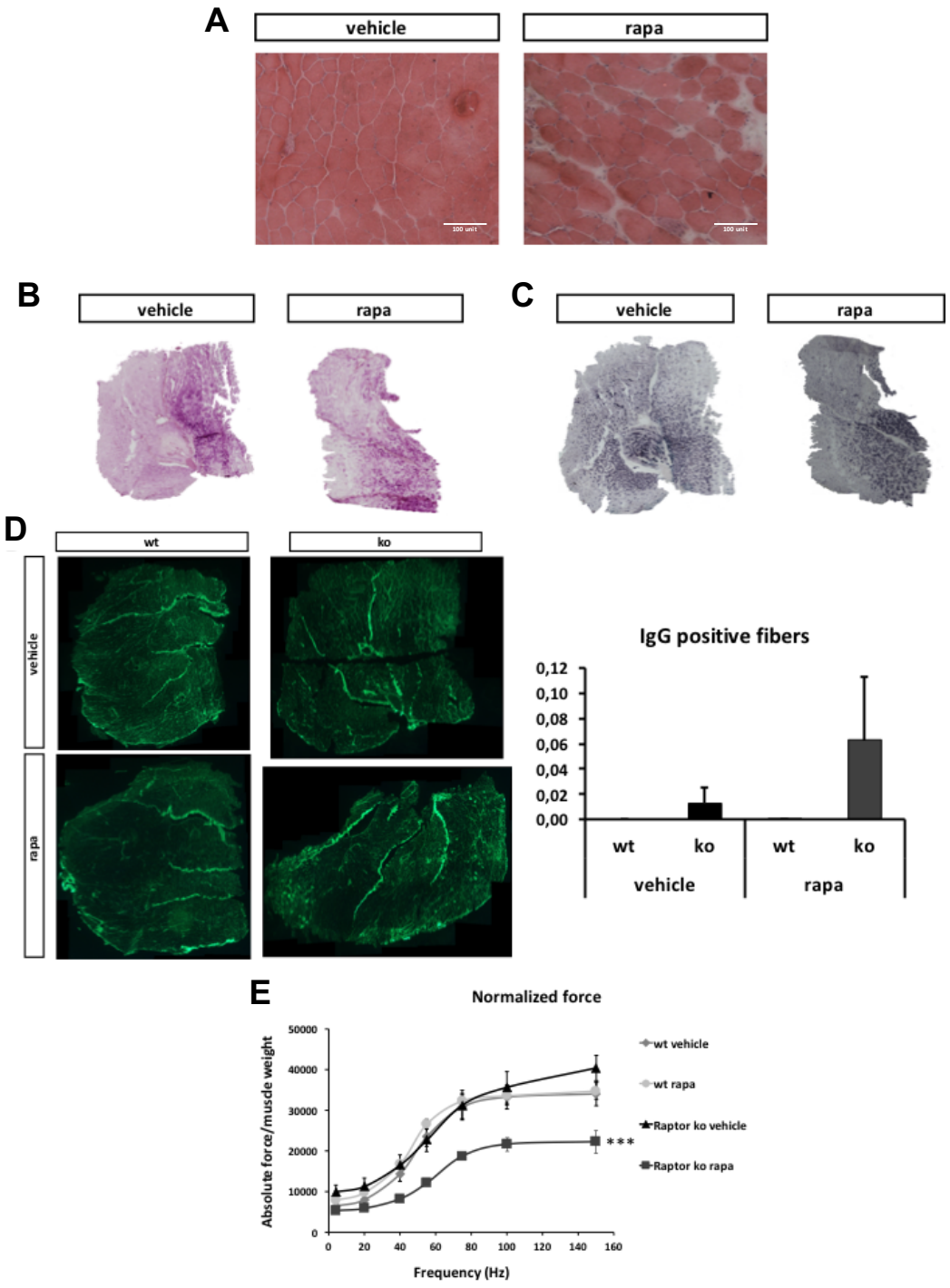

Fig. 7: Rapamycin affects muscle homeostasis in the absence of Raptor. A) *Representative image of Hematoxylin and Eosin staining in vehicle- and rapamycin-treated Raptor ko Tibialis Anterior. n=2 vehicle- and n=3 rapa-treated wt; n=5 vehicle- and n=5 rapa-treated Raptor ko* ***B)*** *Representative image of PAS staining in vehicle- and rapamycin-treated Raptor ko Tibialis Anterior. n=2 vehicle- and n=3 rapa-treated wt; n=5*

vehicle- and n=5 rapa-treated Raptor ko ***C)*** *Representative image of SDH staining in vehicle- and rapamycin-treated Raptor ko Tibialis Anterior. n=2 vehicle- and n=3 rapa-treated wt; n=5 vehicle- and n=5 rapa-treated Raptor ko* ***D)*** *Representative image of IgG staining in vehicle- and rapamycin-treated control and Raptor ko mice and relative quantification. n=2 vehicle- and n=3 rapa-treated wild-type mice; n=3 vehicle- and n=2 rapa-treated Raptor ko mice* ***E)*** *Normalized muscle force in vehicle- and rapamycin-treated control and Raptor ko mice n=2 vehicle- and n=3 rapa-treated wt; n=5 vehicle- and n=5 rapa-treated Raptor ko. ***p≤0.001.*

3.6. Long-term deletion of Raptor results in myopathic features and glycogen accumulation

Since one-month-old Raptor ko mice and control animals are comparable for muscle morphology and performance, we analyzed the effect of Raptor deletion for a longer period.

Deletion of Raptor in skeletal muscle from birth leads to decreased body weight starting at 2 months of age and results in premature death around 6 months of age (Bentzinger et al., 2008). Therefore, we decided to treat adult control and Raptor$^{fl/fl}$ mice for 3 weeks with tamoxifen to monitore lifespan and body weight after the deletion.

We found that body weight did not differ between wild-type and knock-out animals over time, and, loss of Raptor did not reduce lifespan (Fig. 8A). Thus, we decided to sacrifice animals at 7 months after Raptor deletion to assess muscle state. Muscle-weight/body-weight measurements revealed that Tibialis Anterior was only slightly, but not significantly, reduced in Raptor ko mice, whereas, knock-out Gastrocnemius muscles were significantly smaller compared to control (Fig. 8B). Moreover, Hematoxylin and Eosin staining showed several myopathic features in knock-out muscles (Fig. 8C), with either small and big fibers (Fig. 8D) and with 6% of centrally nucleated myofibers (Fig. 8E). Raptor ko Tibialis Anterior showed signs of inflammation, with increased IgG-positive fibers characterized by central core-like structures (Fig. 8F). PAS staining revealed a higher glycogen content in knock-out Tibialis Anterior, with either big puncta

accumulated in some fibers or small fibers with no glycogen inside (Fig. 8G). To test for changes in mitochondrial function, we used a SDH staining. Indeed, the activity of oxidative enzymes appeared lower in Raptor ko mice (Fig. 8H). In both cases, through SDH staining or through PAS staining, we found many central core-like structures, as previously observed with IgG staining.

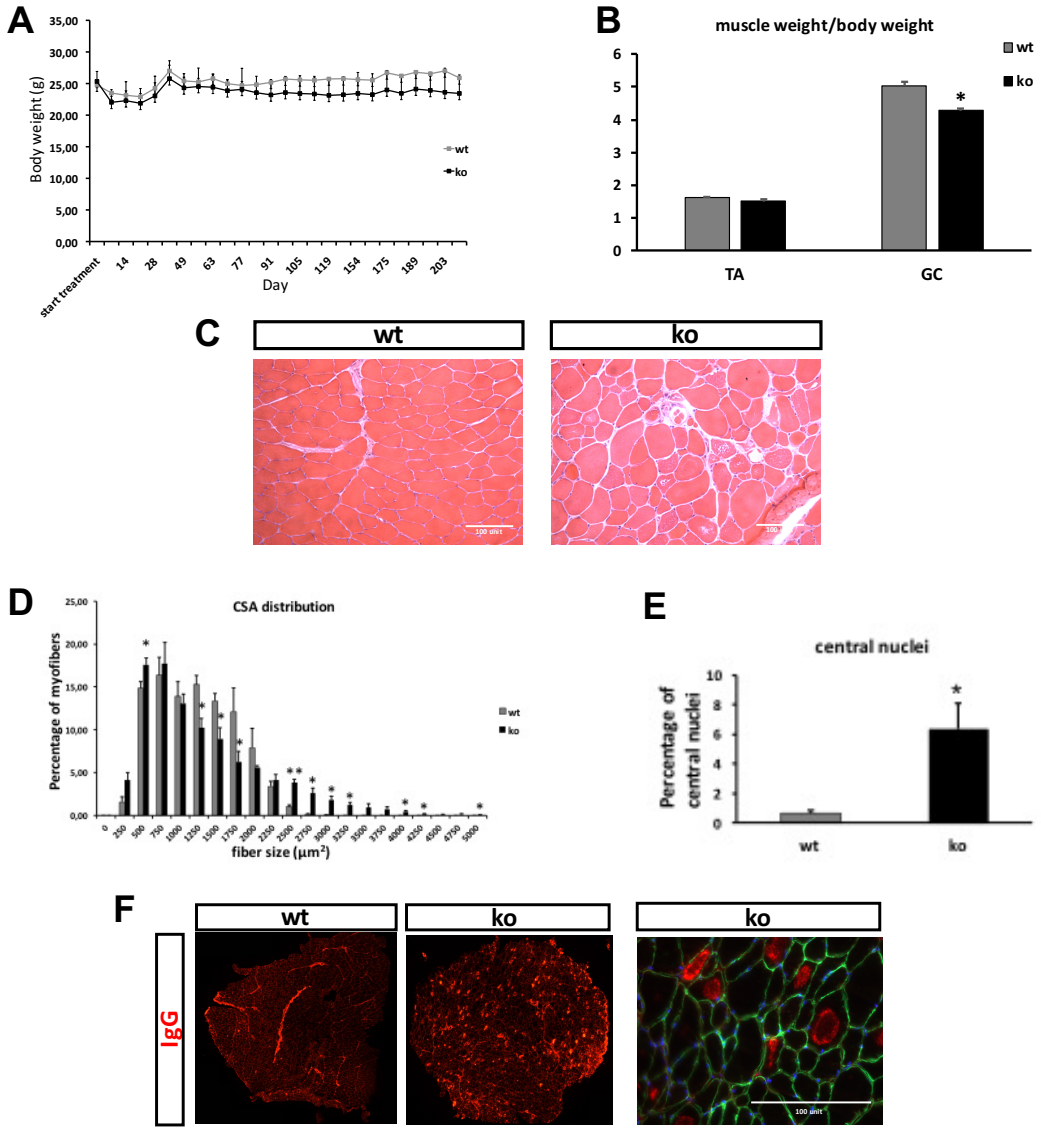

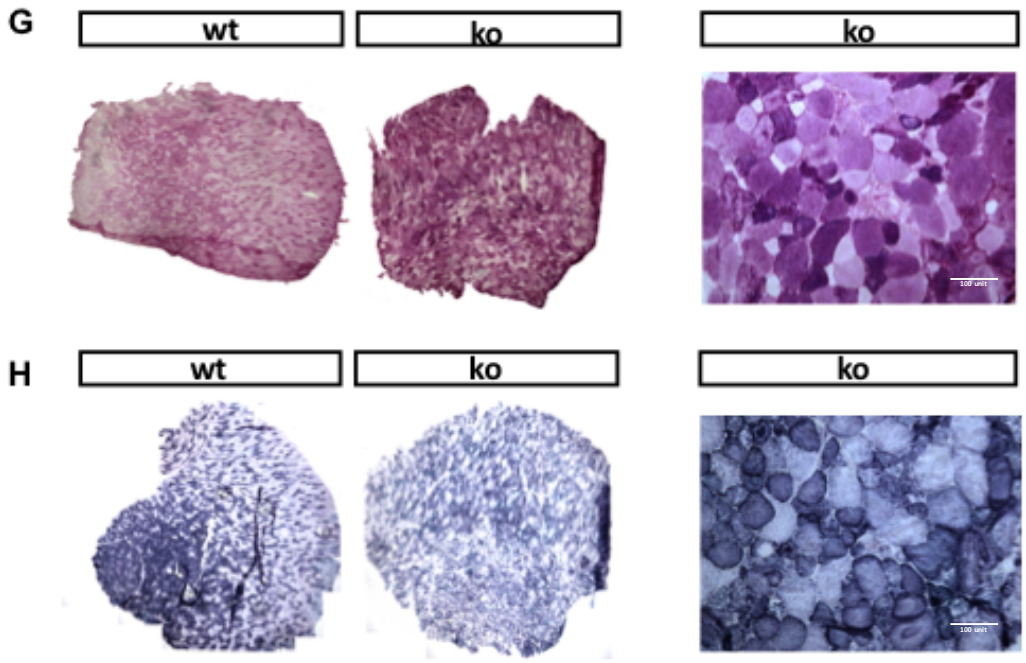

Fig. 8: Long-term deletion of Raptor results in myopathic features and glycogen accumulation. A) *Body weight measurements of control and Raptor ko mice. n=6 mice each group* ***B)*** *Muscle-weight/body-weight analysis of Tibialis Anterior and Gastrocnemius muscle in control and Raptor ko mice. n=6 mice each group* ***C)*** *Representative image of Hematoxylin and Eosin staining in control and Raptor ko Tibialis Anterior. n=6 mice each group* ***D)*** *Cross-Section Area (CSA) distribution of control and Raptor ko Tibialis Anterior. n=6 mice each group* ***E)*** *Centrally nucleated myofibers analysis on control and Raptor ko Tibialis Anterior. n=6 mice each group* ***F)*** *Representative image of IgG staining in control and Raptor ko Tibialis Anterior, with a high magnification of knock-out mouse. n=6 mice each group* ***G)*** *Representative image of PAS staining in control and Raptor ko Tibialis Anterior, with a high magnification of knock-out mouse. n=6 mice each group* ***H)*** *Representative image of SDH staining in control and Raptor ko Tibialis Anterior, with a high magnification of knock-out mouse. n=6 mice each group. *p≤0.05; **p≤0.01.*

When we looked at EDL and Soleus muscles, we found that muscle weight did not differ between wild-type and knock-out mice (fig. 9A). Moreover, similar to what we observed in Tibialis Anterior, muscle histology is compromised upon long-term Raptor deletion in both EDL and Soleus, with smaller and bigger fibers and centrally nucleated myofibers. Knock-out muscles displayed glycogen accumulation, which is higher in

EDL, and less SDH staining, which is on the contrary more pronounced in Soleus muscle (Fig. 9B and C).

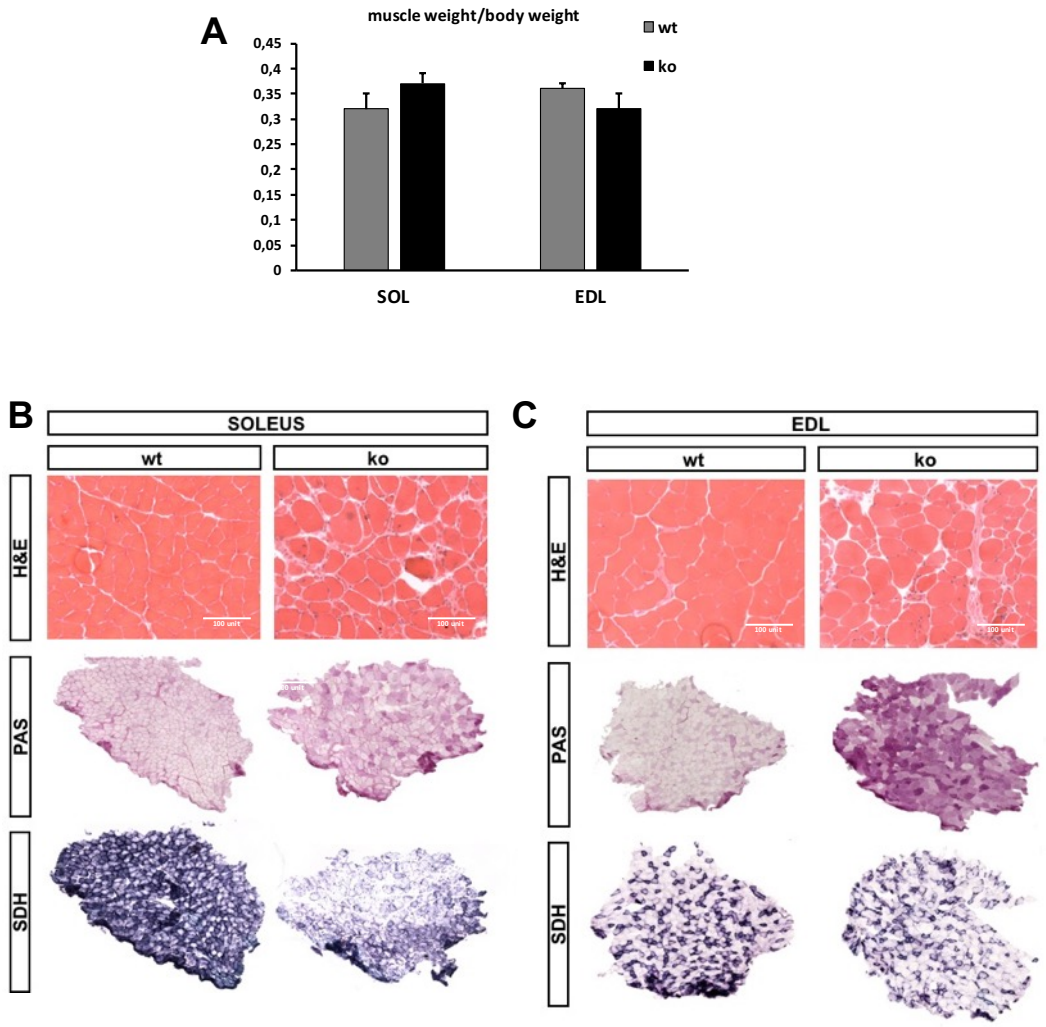

Fig. 9: Long-term deletion of Raptor affects also EDL and Soleus muscles. A) *Muscle-weight/body-weight analysis of Soleus and EDL muscles in control and Raptor ko mice. n=6 mice each group* ***B)*** *Representative image of Hematoxylin and Eosin, PAS and SDH staining of wild-type and knock-out soleus. n=6 mice each group* ***C)*** *Representative image of Hematoxylin and Eosin, PAS and SDH staining of wild-type and knock-out EDL. n=6 mice each group*

3.7. Long-term deletion of Raptor results in hyperphosphorylation of Akt and GSK3β

As we already observed in 1-month-treated knock-out mice, long-term

deletion of Raptor results in 50% decrease at mTOR protein levels, whereas no changes were found in mTOR mRNA expression levels between wild-type and knock-out animals, meaning that Raptor affects mTOR stability (Fig. 10A and B). Furthermore, when we checked mTOR localization upon long-term Raptor deletion, we observed that, in knock-out mice, it no longer co-localizes with lysosomes. Indeed, mTOR (red puncta) and the lysosomal marker LAMP1 (green puncta) were separately detectable in Raptor ko muscles (Fig. 10C).

In addition, we found that Akt is hyperphosphorylated and, thus, activated in knock-out mice, even to a higher extent when we compared long-term to 1-month-treated group. Therefore, Akt hyperactivation results in GSK3β phosphorylation and inhibition. This effect on GSK3β can, likely, explain glycogen accumulation observed in Raptor ko muscles. Surprisingly, mTORC1 downstream target S6 was slightly phosphorylated in knock-out animals. This phosphorylation might be a consequence of Akt hyperactivation (Fig. 10D).

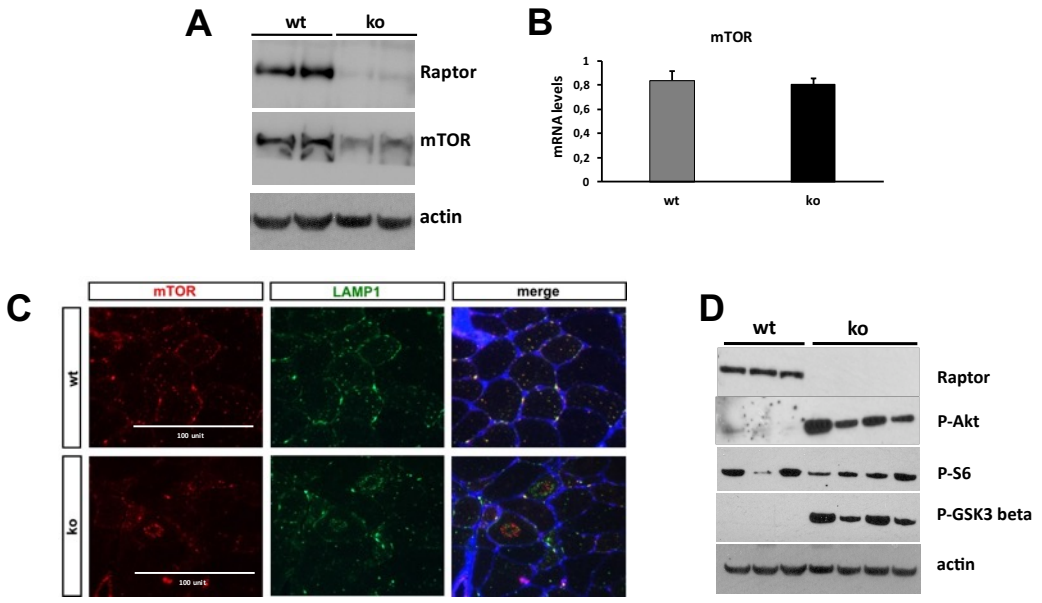

Fig. 10: Long-term deletion of Raptor affects mTOR stability and localization and results in hyperactivation of Akt. A) *Representative Western blot analysis of mTOR in*

wild-type and knock-out mice. n=4 mice each group ***B)*** *Quantitative RT-PCR for mTOR. n=6 mice each group* ***C)*** *Representative image of mTOR-LAMP1 co-staining (mTOR: red, LAMP1: green, co-localization: yellow, WGA: blue). n=3 mice each group* ***D)*** *Representative Western blot analysis of Akt-mTOR axis. n=6 mice each group.*

3.8. Long-term Raptor deletion induces a fiber-type switching from fast-to-slow

High glycogen content is indicative of fast-twitch (type II) muscle fibers. To test whether muscle in Raptor ko mice also changed their structural properties, we stained Tibialis Anterior muscle for type 1, type 2A and type 2B myosin heavy chain. Surprisingly, knock-out muscles displayed a decrease in fast myosin heavy chain (type 2B and 2X), and an increase in slow myosin heavy chain (type 1) and in fast-oxidative 2A content (Fig. 11A). Quantitative RT-PCR for the different myosin heavy chains revealed an increase in mRNA expression levels of MYH7, encoding for slow myosin heavy chain, and an increased transcription of gene encoding for 2X myosin whereas a decrease in mRNA expression levels of gene encoding for fast 2B myosin heavy chain was observed (Fig. 11B). Several signaling pathways control fiber-type gene transcription. The most known regulators of slow-twitch gene program are NFAT transcription factors. To understand if NFAT pathway is active in our inducible skeletal-specific Raptor knock-out mouse, we checked gene expression levels of a downstream target of NFATs, which is RCAN. Indeed, increased expression of RCAN is a well-established marker of activation of NFAT pathway. Moreover, high levels of RCAN protein regulates calcineurin-NFAT pathway through a negative feedback loop (Kingsbury and Cunningham, 2000). Quantitative RT-PCR showed a 5-fold increase in mRNA levels of RCAN in Raptor ko mice compared to control (Fig. 11C). Therefore, structural and metabolic properties changed in an opposite way upon Raptor deletion.

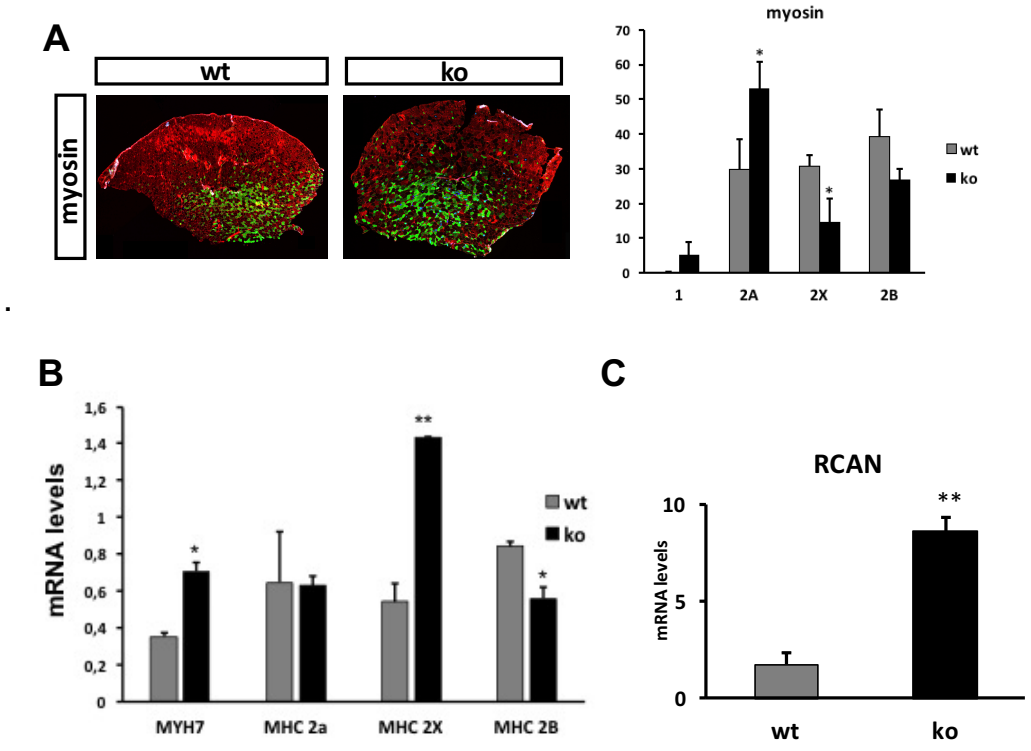

Fig. 11: Long-term Raptor deletion induces a fiber-type switching from fast-to-slow ***A)*** *Representative image of myosin heavy chain staining (type 1: blue; type 2A: green; type 2X: black; type 2B: red) in wild-type and knock-out Tibialis Anterior and relative quantification. n=3 mice each group* ***B)*** *Quantitative RT-PCR for myosin heavy chain genes. n=6 mice each group* ***C)*** *Quantitative RT-PCR for RCAN gene. n=6 mice each group. *p≤0.05; **p≤0.01.*

3.9. Loss of Raptor affects NeuroMuscular Junction (NMJ) in the long-term

Considering the shift from fast- to slow-twitch program and the myopathic features observed in Raptor ko mice, we decided to check whether the transmission nerve-muscle was impaired in these animals. In order to assess muscle innervation and NMJ function, we used Neural Cell Adhesion Molecule (NCAM) staining on Tibialis Anterior muscles. NCAM, generally, localizes in the NMJ, but when there is an impairment of neural transmission, it starts to diffuse throughout the fiber. Indeed, NCAM diffusion is a well-established marker of denervation. In fact, in wild-type

mice NCAM was strictly confined at NMJ level, whereas, in knock-out animals it started to be localized around the sarcolemma and, even, within the myofibers, resulting in 12% of NCAM-positive fibers (Fig. 12A). Moreover, fibers in which NCAM entered into cytoplasm showed a strong atrophy, as expected from the loss of innervation. To confirm the ongoing denervation, we performed electromyography analysis in order to record electrical activity produced by skeletal muscle in a basal state. Muscle tissue at rest is normally inactive. Indeed, wild-type mice showed no electrical activity, while knock-out animals displayed fibrillation potentials, confirming what we observed with NCAM staining (Fig.12B). Muscle denervation induced by Raptor deletion is a time-dependent process. Indeed, when we performed NCAM staining on 1-month-treated mice and on 3-months-treated animals, chosen as intermediate treatment time, we found that NCAM was present at NMJ level in 1-month group whereas it started to diffuse along the sarcolemma in the middle-term, without entering into myofibers (Fig. 12C).

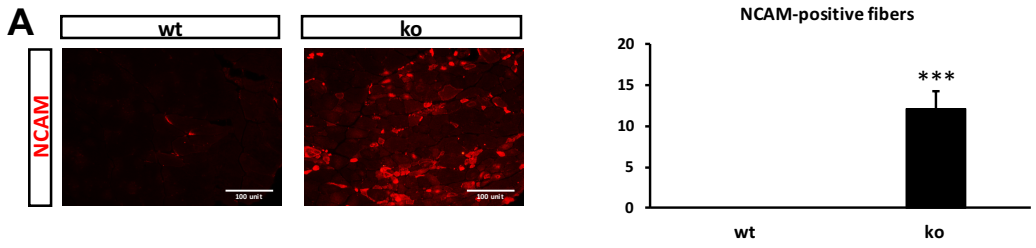

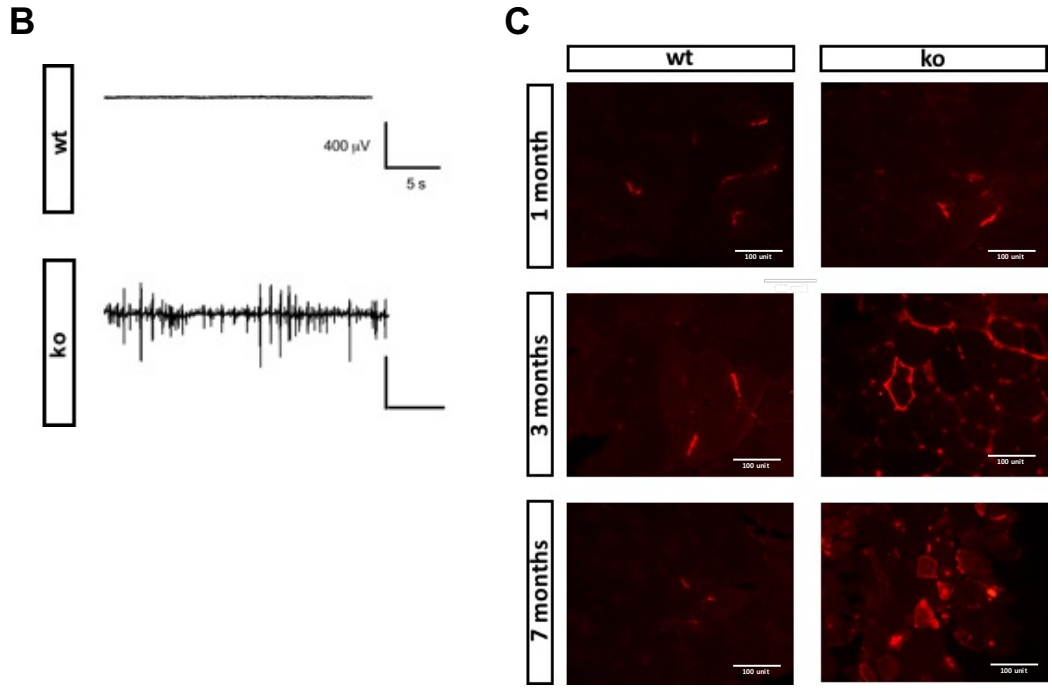

Fig. 12: Loss of Raptor affects NMJ in the long-term. A) *Representative image of NCAM staining in Tibialis Anterior of wild-type and knock-out mice and relative quantification. n=6 mice each group* ***B)*** *Electromyography analysis on Tibialis Anterior of wild-type and knock-out mice. n=4 mice each group* ***C)*** *Representative image of NCAM staining in Tibialis Anterior of wild-type and knock-out mice at different time-points. n=2 mice for 1-month and 3-months group. ***p≤0.001.*

3.10. Muscle performance is compromised in 7-months-treated Raptor ko mice

To test whether metabolic and structural changes and ongoing denervation of knock-out mice affected muscle performance, we analyzed *in vivo* strength of Gastrocnemius muscle. Maximal absolute force (tetanic force) was significantly reduced in knock-out mice, and, importantly, also the absolute force normalized for muscle mass (normalized force) was affected by Raptor long-term deletion (Fig. 13A and B). Surprisingly, despite fiber type switching from fast to slow, analysis of time to peak, half time to peak and relaxation time of the twitch were unaltered in long-term Raptor ko mice (Fig. 13C). The drop in muscle force can be due to

alterations of Ca^{2+} homeostasis or to dysfunctions in contractile apparatus. To understand the main cause of muscle weakness of knock-out mice, we measured force production in skinned muscle fibers, exposed to a solution in which Ca^{2+} concentration was controlled by EGTA. Maximal force was normalized to cross-section area of muscle fibers. Interestingly, knock-out mice displayed lower muscle tension compared to control animals (Fig. 13D), meaning that Raptor long-term deletion can directly affect the contractile machinery.

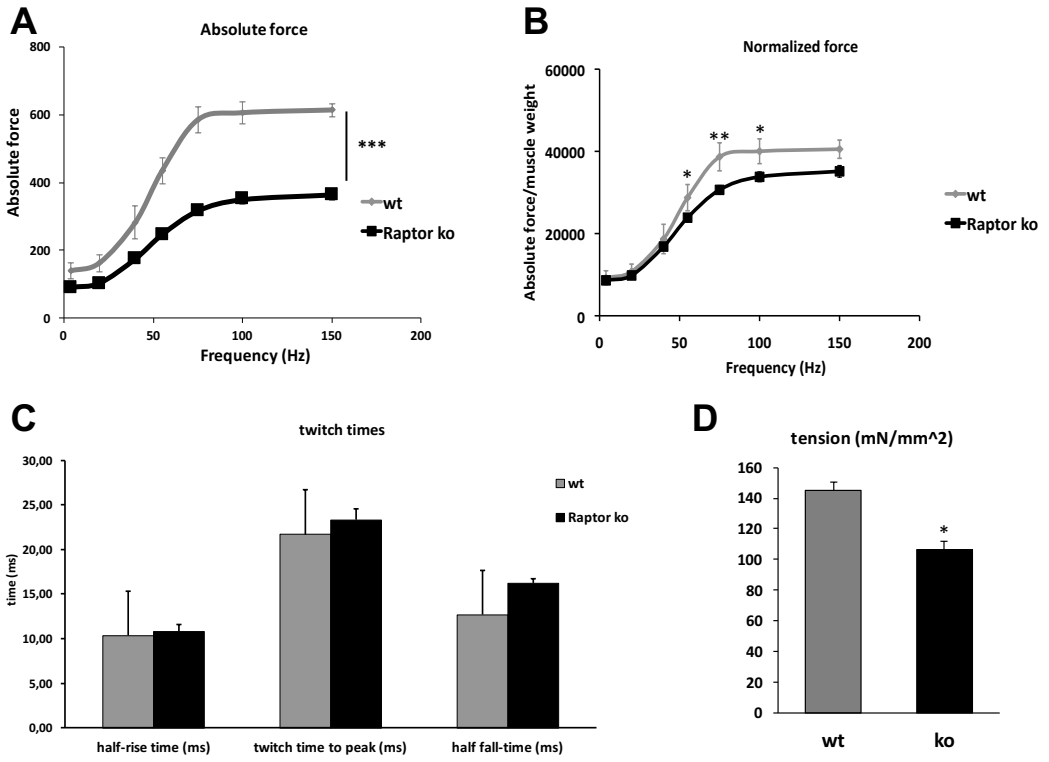

Fig. 13: Long-term deletion of Raptor affects muscle performance. A) *Absolute force of Gastrocnemius muscle in wild-type and knock-out mice. n=2 wt and n=6 ko* ***B)*** *Normalized force of Gastrocnemius muscle in wild-type and knock-out mice. n=2 wt and n=6 ko* ***C)*** *Twitch times analysis of wild-type and knock-out mice. n=2 wt and n=6 ko* ***D)*** *Force measurements on skinned fibers from wild-type and knock-out Gastrocnemius. n=2 wt GC and n=13 wt fibers; n=6 ko GC and n=33 ko fibers. *p≤0.05; **p≤0.01; ***p≤0.001.*

3.11. Long-term Raptor deletion results in mitochondrial deficit

SDH staining of knock-out mice showed a possible alteration in mitochondria. So, we decided to investigate mitochondrial content and function after a long-term deletion of Raptor. Western blot analysis for SDH and for the mitochondrial import receptor subunit TOM20 did not reveal significant changes between control and knock-out mice, whereas a small decrease in mitochondrial outer membrane protein porin1 was observed in Raptor ko animals (Fig. 14A). Moreover, levels of the different complexes of mitochondrial respiratory chain were comparable between wild-type and knock-out mice (Appendix Fig. 1). Proteomics analysis on control and Raptor-deficient mice revealed that many proteins involved in mitochondria functionality is significantly reduced in knock-out animals (Appendix Fig. 2). So, we decided to evaluate mitochondrial respiration efficiency. Interestingly, we found that Complex III and Complex IV activity was severely compromised upon Raptor deletion (Fig. 14B). Based on these results, we therefore decided to evaluate the capability to maintain mitochondrial membrane potential. We performed TMRM assay on FDB fibers from control and knock-out mice. After the addition of oligomycin, an inhibitor of F_1F_0-ATPase (Grumati et al., 2010), Raptor ko fibers showed a high content of depolarized mitochondria, whereas control mitochondria maintain membrane potential (Fig. 14C).

A deficit in mitochondria functionality is strictly correlated with muscle weakness and exercise intolerance. Thus, we decided to evaluate exercise performance of control and knock-out mice, placing them on a treadmill and let them run until exhaustion. We found that Raptor-deficient animals run about half of the distance of wild-type mice (Fig. 14D), confirming the mitochondrial dysfunction.

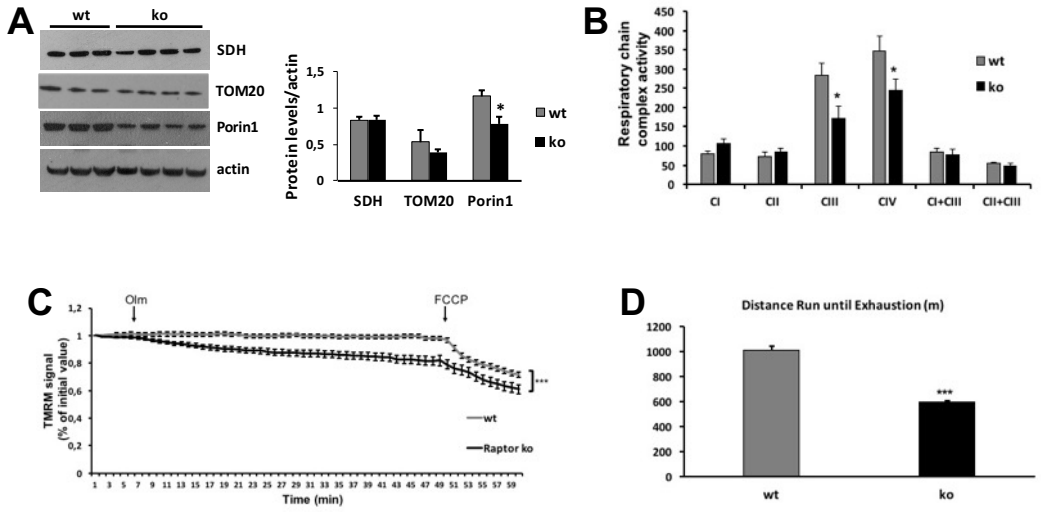

Fig. 14: Lack of Raptor results in mitochondrial deficiency and exercise intolerance. A) *Representative Western blot analysis for mitochondrial proteins SDH, TOM20 and Porin1 in wild-type and knock-out mice. n=3 wt and n=4 ko* ***B)*** *Activity of respiratory chain complexes in wild-type and knock-out quadriceps. n=4 wt and n=6 ko* ***C)*** *TMRM analysis in wild-type and knock-out FDB fibers. n=19 fibers from wt and n=31 fibers from ko* ***D)*** *Distance run until exhaustion in wild-type and knock-out. n=2 wt and n=4 ko. *p≤0.05; **p≤0.01; ***p≤0.001.*

3.12. Long-term deletion of Raptor affects autophagy regulation

Both denervation and mitochondrial dysfunction are linked to autophagy impairment. Moreover, glycogen accumulation can be associated with lysosomal storage disorders, like Pompe disease, in which autophagic vescicles accumulate inside myofibers (Shea and Raben, 2009). Therefore, we stained Raptor ko Tibialis Anterior for the autophagosomal marker LC3 and for the lysosomal protein LAMP1. We found that some glycogen puncta localized with autophagosomes and lysosomes in central core-like structures (Fig. 15A). Looking at autophagy, we observed that p62 accumulated within myofibers with a different pattern compared to that of LC3 and, as expected, transcription factor TFEB translocated into the nucleus where it is active (Fig. 15B and C). TFEB exerts a positive effect on its own transcription, through an autoregulatory feedback loop, and,

moreover, it controls mRNA expression of lysosomal genes, such as LAMP1 (Settembre et al., 2013). Surprisingly, quantitative RT-PCR showed a strong reduction in both TFEB and LAMP1 mRNAs upon Raptor deletion (Fig. 15D). Furthermore, expression levels of other *bona-fide* TFEB targets were downregulated in knock-out mice (Fig. 15E). TFEB controls also the expression of autophagy-related genes. To check what happens to UPS and to autophagy-lysosome system, we performed quantitative RT-PCR for different E3-ubiquitin ligases and for several "atrogenes". Atrogin-1 mRNA is significantly reduced in Raptor ko mice, whereas other E3-ubiquitin ligases, such as Murf-1, Fbxo21 and Ambra1 mRNAs only tend to decrease in knock-out animals (Fig. 15F). Moreover, among the different "atrogenes", the most affected by Raptor deletion were Ulk1 and BNIP3 (Fig. 15G). Surprisingly, Western blot analysis revealed an accumulation of the lipidated form of LC3 in knock-out muscles. No differences were, instead, found either in p62 protein content (Fig. 15H) or in levels of both lysine-48 and lysine-63 polyubiquitin proteins (Appendix Fig. 3).

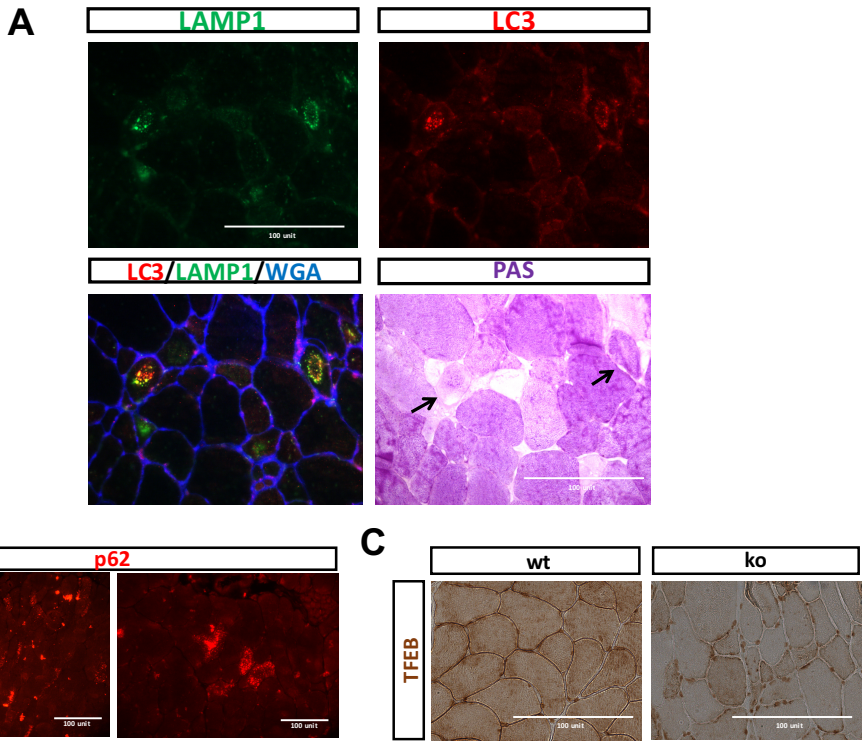

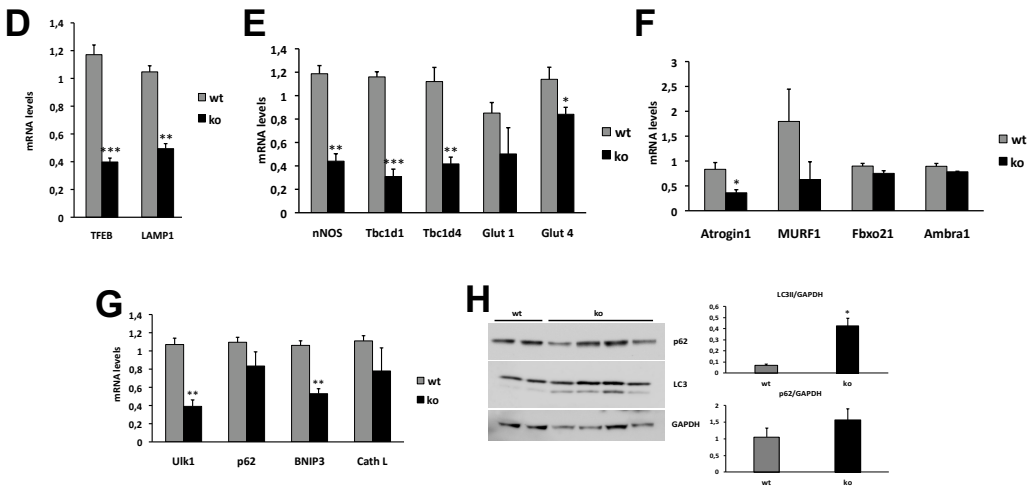

Fig. 15: Long-term deletion of Raptor affects autophagy regulation A) *Representative image of LAMP1-LC3 co-staining in Tibialis Anterior of knock-out mice (LAMP1: green; LC3: red; WGA: blue) and representative image of PAS staining of the same area (black arrows indicate fibers positive for LAMP1 and LC3). n=4 wt and n=6 ko* ***B)*** *Representative image of p62 staining in knock-out Tibialis Anterior at different magnifications. n=2 wt and n=2 ko* ***C)*** *Representative image of TFEB staining in wild-type and knock-out Tibialis Anterior. n=2 wt and n=4 ko* ***D)*** *Quantitative RT-PCR for TFEB and LAMP1. n=6 mice each group* ***E)*** *Quantitative RT-PCR for TFEB targets nNOS, Tbc1d1, Tbc1d4, Glut1, Glut4. n=6 mice each group* ***F)*** *Quantitative RT-PCR for E3-ubiquitin ligases Atroogin-1, Murf-1; Fbxo21 and Ambra1. n=6 mice each group* ***G)*** *Quantitative RT-PCR for "atrogenes" Ulk1, p62, BNIP3 and Cathepsin L. n=6 mice each group* ***H)*** *Representative Western blot analysis of LC3 and p62 in wild-type and knock-out and relative quantification. n=5 wt and n=8 ko. *p≤0.05; **p≤0.01; ***p≤0.001.*

PART II

3.13. Generation of Akt-Raptor ko mouse line

Akt overexpression results in skeletal muscle hypertrophy and increased muscle performance (Blaauw et al., 2009). Akt-induced growth is significantly reduced after treatment with the mTORC1 inhibitor rapamycin (Bodine et al., 2001b). However, deletion of the downstream target of mTORC1, S6K1, does not affect muscle hypertrophy induced by the upstream kinase Akt whereas it is required for muscle functionality (Marabita et al., 2016). To better understand the role of mTORC1 in skeletal muscle growth and performance, we decided to generate a mouse line in which Akt is overexpressed when Raptor is deleted (Akt-Raptor ko). So, we crossed floxed Raptor mouse line with mice expressing Akt only after the deletion of an upstream DNA sequence by the Cre recombinase. In this model, the Akt coding sequence is fused to a modified estrogen receptor-binding domain. Intramuscular injection of AAV9 for the Cre recombinase results in the cleavage of loxP sites on Raptor gene and on Akt gene, leading to Raptor deletion and Akt expression. In a basal state, Akt is degraded because the heat-shock protein complex, which is bound to the ER domain of Akt, marks it for the degradation. Tamoxifen treatment leads to Akt activation in muscles in which Raptor has been already deleted. So, we injected the virus for the Cre in gastrocnemius muscles, then we waited 1 month in order to delete Raptor and express Akt. After this period, we treated mice for 3 weeks with tamoxifen to activate Akt.

Western blot analysis revealed that Raptor is strongly reduced in Raptor ko and Akt-Raptor ko muscles compared to Akt mice (Fig. 16A). Moreover, immunofluorescence for P-Akt showed the high efficiency of infection, validating therefore the model (Fig. 16B).

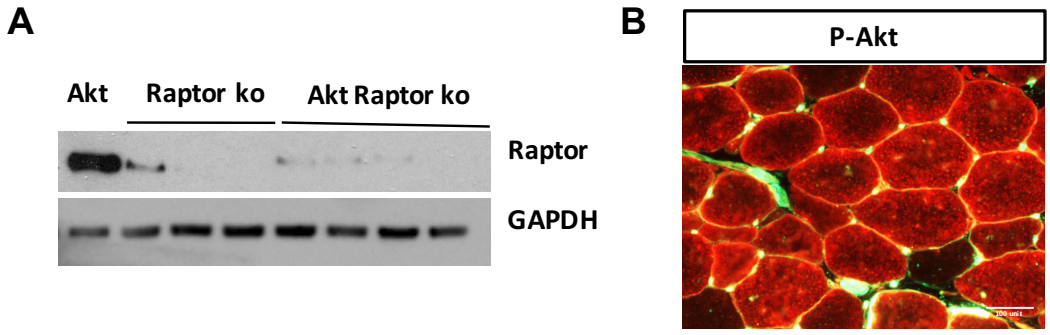

Fig. 16: Validation of Akt-Raptor ko model. A) *Representative Western blot for Raptor in Akt, Raptor ko and Akt-Raptor ko Gastrocnemius muscles injected with the AAV9-Cre virus. n=4 Akt mice; n=9 Raptor ko, n=10 Akt-Raptor ko* ***B)*** *Immunofluorescence for P-Akt in Akt-Raptor ko Gastrocnemius muscles. n=10 Akt-Raptor ko.*

3.14. Akt induces muscle hypertrophy also in the absence of Raptor

To understand what happens to muscle mass in Akt-Raptor ko mice, we firstly analyzed muscle weight over body weight in different models. Akt overexpression results in a significant muscle hypertrophy either in the presence (Akt) or in the absence of Raptor (Akt-Raptor ko) compared to wild-type and Raptor ko mice (Fig. 17A). Next, we checked myofibers size by measuring the Cross-Sectional Area (CSA) of infected and non-infected fibers of Akt and Akt-Raptor ko mice. Through P-Akt immunofluorescence, we could distinguish between the infected myofibers (red) and the non-infected ones surrounding them (black fibers). CSA measurements revealed that fibers only expressing Akt displayed a 2.5 fold increase in fiber size, whereas this growth is slightly but significantly reduced in fibers expressing Akt in the absence of Raptor (Fig. 17 B and C).

In addition, Western blot analysis showed an increase in phosphorylation of Akt downstream target, GSK3β in both Akt and Akt-Raptor ko group, as expected. Surprisingly, we also found that Raptor deletion did not affect S6 phosphorylation upon Akt activation (Fig. 17D).

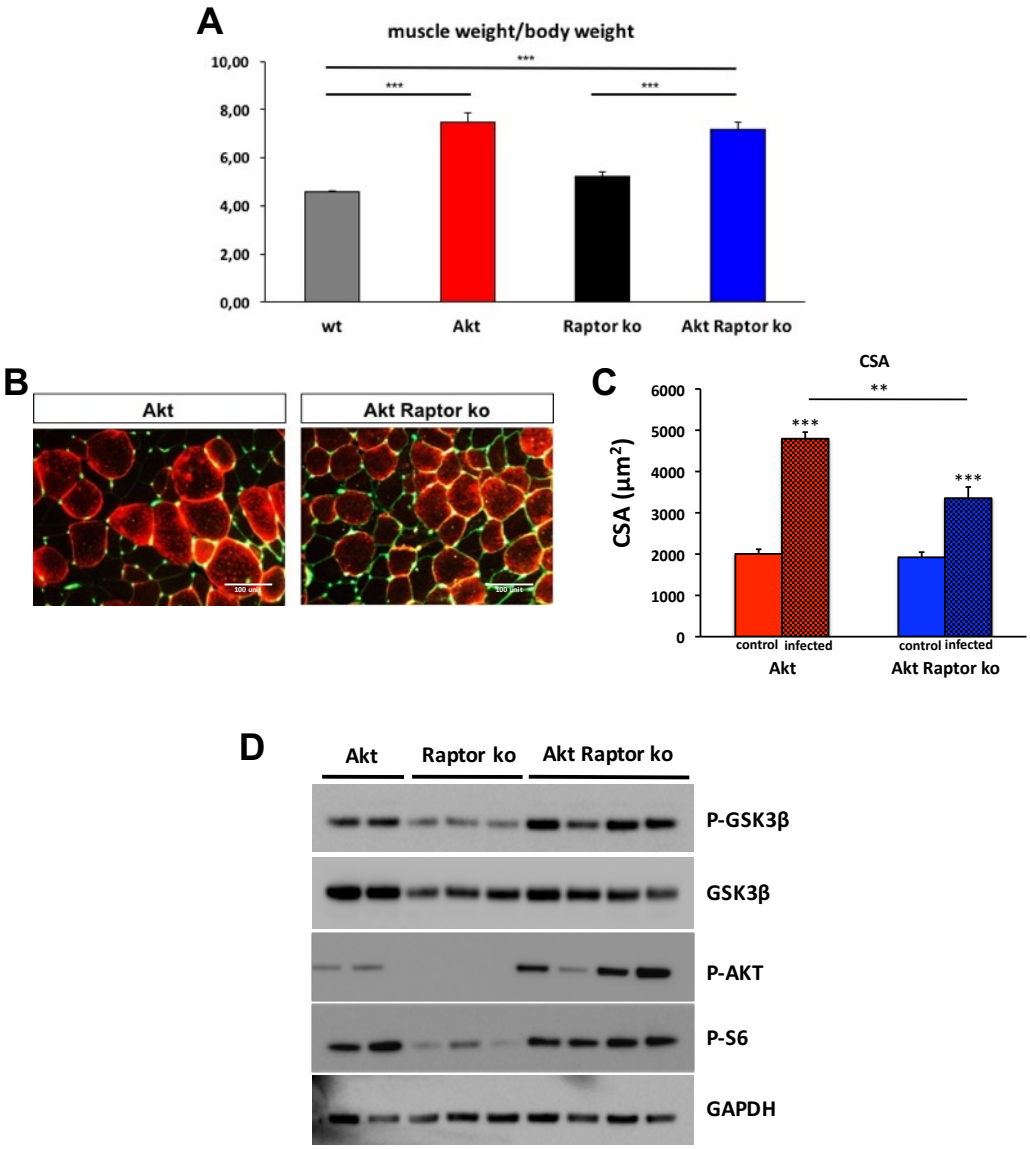

Fig. 17: Deletion of Raptor only slightly affects Akt-induced hypertrophy. A) *Muscle weight over body weight measurements of Gastrocnemius muscles of wild-type, Akt, Raptor ko and Akt-Raptor ko mice. n=3 wt mice; n=4 Akt mice; n=6 Raptor ko, n=7 Akt-Raptor ko* ***B)*** *P-Akt immunofluorescence of Gastrocnemius muscles of Akt and Akt-Raptor ko mice. n=4 Akt mice; n=7 Akt-Raptor ko* ***C)*** *CSA analysis of infected and control fibers in Akt and Akt-Raptor ko mice. n=4 Akt mice; n=7 Akt-Raptor ko* ***D)*** *Representative Western blot for Akt-mTOR axis in Akt, Raptor ko and Akt-Raptor ko Gastrocnemius muscles. n=4 Akt mice; n=6 Raptor ko, n=7 Akt-Raptor ko. **p≤0.01; ***p≤0.001.*

3.15. Rapamycin prevents Akt-induced hypertrophy in Akt-Raptor ko mice and results in muscle weakness

As previously told, Akt-induced hypertrophy is blunted after rapamycin administration. Since this compound acts inhibiting the interaction between Raptor and mTOR, we wondered what happens in Akt-Raptor ko mice. So, we injected muscles with AAV9 for the Cre and then we waited 1 month. After this period, we treated animals for 3 weeks both with tamoxifen to activate Akt and with rapamycin to inhibit mTORC1. To check if the treatment worked, we analyzed phosphorylation levels of mTORC1 downstream target S6. Western blot revealed that S6 phosphorylation was prevented upon rapamycin administration in Akt-Raptor ko mice, confirming the efficacy of the treatment (Fig. 18A). P-Akt immunofluorescence was used to measure CSA of infected and control fibers (Fig. 18B). In vehicle-treated Akt-Raptor ko mice, Akt induced fiber hypertrophy, as expected. Surprisingly, the increase in fiber size was significantly blunted by rapamycin administration (Fig. 18C).

It has been reported that Akt induces a functional growth; indeed muscle hypertrophy is accompanied by an increase in tetanic force in Akt overexpressing mice (Blaauw et al., 2009). Recently, we demonstrated that S6K1, one of the downstream target of mTORC1, is required for maintaining proper muscle function during hypertrophy. Indeed the lack of S6K1 leads to a drop in normalized tetanic muscle force, which can be preserved treating Akt-S6K1 ko mice with rapamycin (Marabita et al., 2016). In order to evaluate muscle performance of Akt-Raptor ko mice, we measured *in vivo* strength of Gastrocnemius muscle. Wild-type mice with or without rapamycin and vehicle-treated Raptor ko animals displayed normal muscle performance, whereas rapamycin-treated Raptor ko mice appeared significantly weaker. Interestingly, Akt-Raptor ko animals showed a drop in normalized muscle force which cannot be rescued by rapamycin treatment (Fig. 18D). We confirmed these data also measuring force production on skinned muscle fibers, placed in a solution in which

Ca^{2+} concentration is controlled by EGTA. Fiber tension was, then, normalized for myofiber CSA. A significant reduction was observed either in rapa-treated groups or in vehicle-treated Akt-Raptor ko fibers (Fig. 18E).

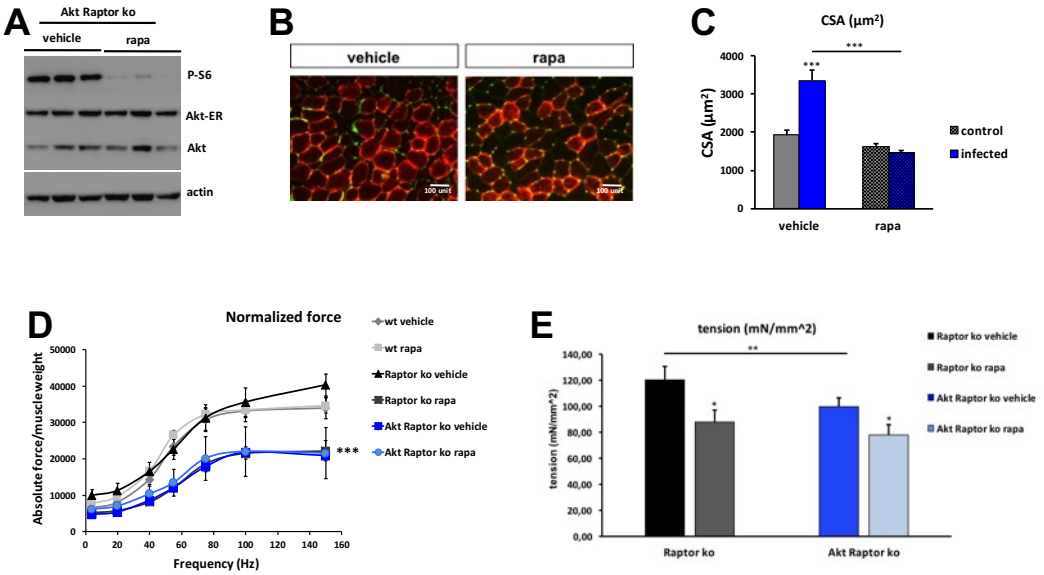

Fig.18: Rapamycin prevents Akt-induced hypertrophy and results in muscle weakness in the absence of Raptor. A) *Representative Western blot for P-S6 in Akt-Raptor ko mice with or without rapamycin (rapa). n=6 vehicle- and n=6 rapa-treated Akt-Raptor ko mice* ***B)*** *P-Akt immunofluorescence on Gastrocnemius muscle of vehicle- and rapa-treated Akt-Raptor ko mice. n=6 vehicle- and n=6 rapa-treated Akt-Raptor ko mice* ***C)*** *CSA analysis of control and infected fibers in vehicle- and rapa-treated Akt-Raptor ko mice. n=6 vehicle- and n=6 rapa-treated Akt-Raptor ko mice* ***D)*** *Normalized muscle force in vehicle- and rapa-treated wild-type, Raptor ko and Akt-Raptor ko mice. n=2 vehicle- and n=3 rapa-treated wt; n=5 vehicle- and n=5 rapa-treated Raptor ko; n=6 vehicle- and n=6 rapa-treated Akt-Raptor ko mice* ***E)*** *Force production on skinned fibers in vehicle- and rapa-treated Raptor ko and Akt-Raptor ko mice. n=3 vehicle- and n=2 rapa-treated Raptor ko; n=4 vehicle- and n=3 rapa-treated Akt-Raptor ko mice *p≤0.05; **p≤0.01; ***p≤0.001.*

3.16. Protein synthesis and protein ubiquitination are increased in Akt-Raptor ko mice

To understand if muscle hypertrophy in Akt-Raptor ko mice is

accompanied by an increase in protein synthesis, we took advantage of SUnSET technique (Schmidt et al., 2009). Importantly, vehicle-treated Akt-Raptor ko animals showed a 3-fold increase in protein synthesis compared to wild-type or Raptor ko mice. Moreover, higher protein formation was strongly blunted by rapamycin administration as shown by Western blot analysis (Fig. 19A).

Since skeletal muscle mass is the result of an equilibrium between protein synthesis and protein breakdown, we decided also to evaluate protein degradation. So, we performed Western blot for lysine-48 and lysine-63 polyubiquitin proteins. Interestingly, Akt-Raptor ko mice treated with vehicle displayed, for both the degradative pathways, an increase in ubiquitinated proteins, which can be partially prevented by rapamycin treatment (Fig. 19B and C). The same pattern was observed in Western blot analysis for p62, which accumulated in vehicle-treated Akt-Raptor ko mice and decreased in rapamycin-treated group (Fig. 19D).

To understand if muscle weakness can be due to misfolded proteins, we analyzed ER stress in these animals. So, we performed Western blots for two proteins involved in the Unfolded Protein Response (UPR). UPR aims are to degrade misfolded proteins, to restore normal function of the cell and to increase the production of molecular chaperones involved in protein folding. Akt-Raptor ko mice treated with vehicle showed an increased phosphorylation of eIF2α, whose inhibition is correlated with a downregulation of protein synthesis rate, and an accumulation of the chaperone BIP. Both these effects were blunted by rapamycin treatment in Akt-Raptor ko animals (Fig. 19E).

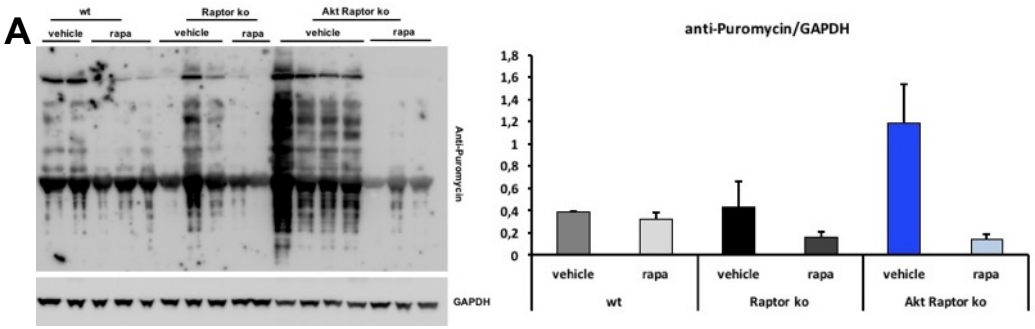

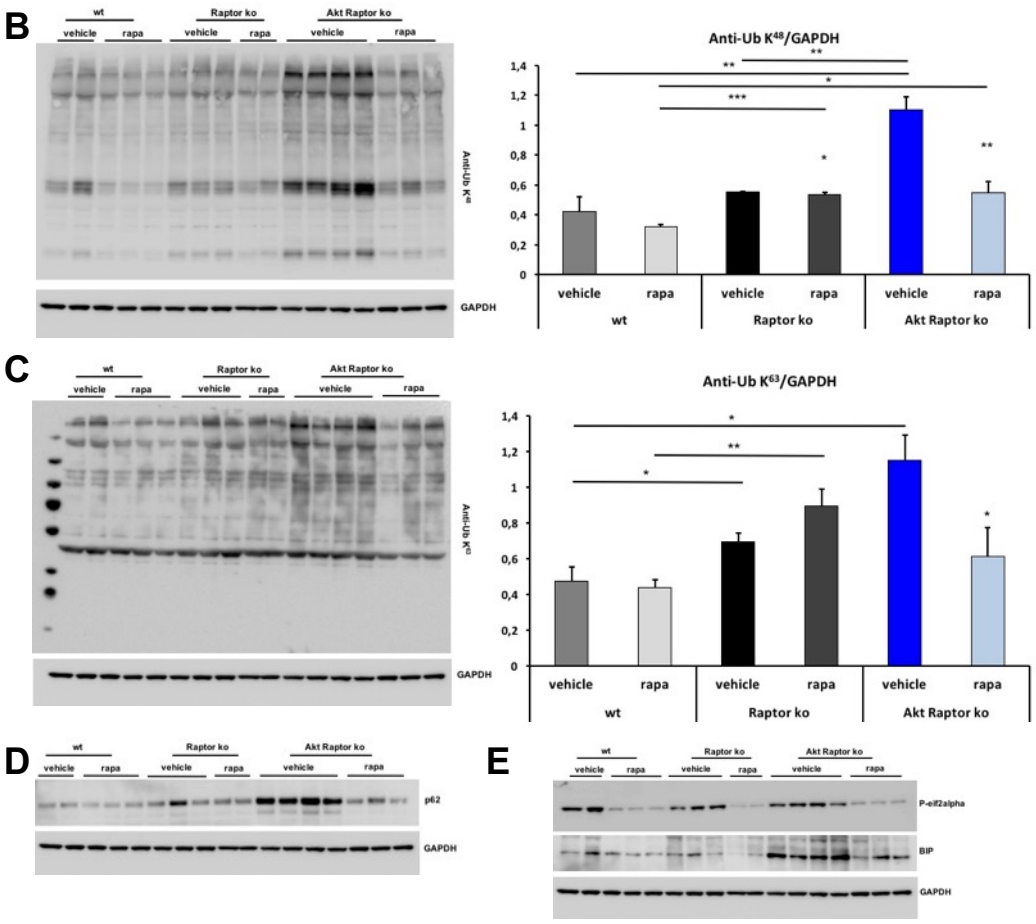

Fig. 19: Akt-Raptor ko mice show increased protein synthesis and activation of UPR. A) *In vivo SUnSET technique in vehicle- and rapa-treated wild-type, Raptor ko and Akt-Raptor ko mice and relative quantification. n=2 vehicle- and n=3 rapa-treated wt; n=3 vehicle- and n=2 rapa-treated Raptor ko; n=4 vehicle- and n=3 rapa-treated Akt-Raptor ko mice* ***B)*** *Western blot for Lys48 polyubiquitin protein in vehicle- and rapa-treated wild-type, Raptor ko and Akt-Raptor ko mice and relative quantification. n=2 vehicle- and n=3 rapa-treated wt; n=3 vehicle- and n=2 rapa-treated Raptor ko; n=4 vehicle- and n=3 rapa-treated Akt-Raptor ko mice* ***C)*** *Western blot for Lys63 polyubiquitin protein in vehicle- and rapa-treated wild-type, Raptor ko and Akt-Raptor ko mice and relative quantification. n=2 vehicle- and n=3 rapa-treated wt; n=3 vehicle- and n=2 rapa-treated Raptor ko; n=4 vehicle- and n=3 rapa-treated Akt-Raptor ko mice* ***D)*** *Representative Western blot for p62 in vehicle- and rapa-treated wild-type, Raptor ko and Akt-Raptor ko mice and relative quantification. n=2 vehicle- and n=3 rapa-treated wt; n=6 vehicle- and n=2 rapa-treated Raptor ko; n=8 vehicle- and n=3 rapa-treated Akt-Raptor ko mice* ***E)*** *Representative Western blot for UPR proteins in vehicle- and rapa-treated wild-type, Raptor ko and Akt-Raptor ko mice and relative quantification. n=2 vehicle- and n=3 rapa-treated wt; n=6 vehicle- and n=2 rapa-treated Raptor ko; n=8 vehicle- and n=3 rapa-treated Akt-Raptor ko mice*

4. DISCUSSION

PART I

Muscle atrophy is a systemic response that occurs during ageing and in various diseases. No therapeutic approaches are available to counteract muscle wasting. For this reason, understanding the key players in the regulation of muscle mass and function is of great importance. The two main pathways controlling muscle growth are the Akt-mTOR axis and the BMP signaling cascade. Indeed, Akt overexpression or BMP stimulation results in muscle hypertrophy. In both cases, muscle growth is strongly blunted after treatment with the mTORC1 inhibitor, rapamycin. These results highlight a key role for mTORC1 in the regulation of skeletal muscle mass.

Under anabolic condition, mTOR is activated, stimulating protein synthesis through the phosphorylation of S6K and 4EBP1, and blocking protein degradation through the inhibition of Ulk1.

mTOR exists as two multiprotein complex: mTORC1, when it is bound to Raptor, and mTORC2, when it is bound to Rictor. Muscle-specific inactivation of mTOR results in severe myopathy, leading to premature death. Moreover, mTOR-deficient muscles show impaired oxidative metabolism and altered mitochondrial regulation (Risson et al., 2009). Similar results have been observed in mice lacking Raptor in skeletal muscle from birth (RAmKO). Indeed, while muscle-specific Rictor knock-out mice appear normal throughout adulthood, RAmKO animals display myopathic features and start to loose body weight around 2 months of age resulting in premature death at 6 months (Bentzinger et al., 2008). These results suggest that mTOR function in skeletal muscle require only mTORC1.

On the other hand, inhibition of mTORC1 through the pharmacological treatment of adult mice with rapamycin, results in improved mice performance and increased lifespan (Harrison et al., 2009). To better understand the role of Raptor in adult skeletal muscle, we generated an

inducible muscle-specific Raptor knock-out mouse line (Raptor ko). We found that one month-treated Raptor ko mice are comparable to control littermates. However, when these mice are treated with rapamycin, they start to display signs of inflammation and weakness. This could be due to a stronger inhibition of mTORC1, likely acting on the small amount of Raptor left at this time point. Indeed, a longer period of deletion results in myopathic features, such as central nucleated fibers, an high amount of small fibers and hypertrophic ones, inflammation and muscle weakness. Also the results obtained by overexpression of Akt in Raptor ko mice support the interpretation that little Raptor is sufficient to maintain much of the signaling intact. Hypertrophy by Akt overexpression is only slightly altered after Raptor deletion; however, treatment with rapamycin completely prevents fiber hypertrophy. These results are suggestive that all Akt-dependent muscle growth requires mTORC1-dependent signaling. This is in line with the findings that rapamycin acts only on mTOR when blunting muscle growth (Goodman et al., 2011a).

Recently, it has been published that mTORC1 is a key upstream regulator of the transcriptional and metabolic stress responses identified in mitochondrial diseases, by contributing to the progression of the pathology (Khan et al., 2017). On the other hand, mTORC1 controls a subset of mitochondria-related mRNAs, mainly involved in mitochondrial activity and dynamics, via 4EBP1 inhibition (Morita et al., 2013) (Morita et al., 2017). TMRM analysis on our Raptor ko mouse reveal an impairment in the maintenance of mitochondrial membrane potential when ATP synthase is blocked. Mitochondria depolarization can be due either to a decrease in the activity of Complex III and IV, that likely are no longer able to pump protons outside the mitochondria, or to PTP opening, similar to what happens in myopathic mice with Collagen VI deficiency (Irwin et al., 2003). Cyclosporin treatment is planned on Raptor ko mice to better evaluate this hypothesis.

Mitochondrial dysfunction has been associated to NeuroMuscular Junction (NMJ) impairment (Tezze et al., 2017). Indeed, NCAM staining on our

Raptor ko muscles reveal a severe denervation, which is confirmed by electromyography analysis showing fibrillation potential spikes in resting condition. Moreover, muscle denervation occurs in all the fiber types, without differences between slow and fast-twitch fibers (data not shown).

Mitochondrial dysfunction and NMJ impairment result in muscle weakness and exercise intolerance in knock-out animals. An hypothesis is that decreased muscle strength may be correlated to a damage in contractile machinery since force measurement on skinned fibers is reduced upon Raptor deletion.

We thought that the absence of the negative feedback loop from S6K to IRS-1 in Raptor-deficient mice could result in Akt hyperactivation. Wang et al., however, recently suggested that the enhancement of Akt phosphorylation in Raptor ko mice and, in general, in animals treated with rapamycin is unlikely due to relief of S6K1-mediated inhibition of IRS1 (Wang et al., 2017). Nevertheless, Akt activation leads to GSK3β inhibition in knock-out mice. This leads to glycogen accumulation, meaning that Raptor deletion cause a shift of the metabolic properties from oxidative to glycolytic. Moreover, glycogen puncta sometimes co-localize with autophagosomes and lysosomes, similar to what happens in lysosomal storage diseases, like Pompe disease. GSK3β inhibition likely results in NFAT activation, as measured by RCAN mRNA expression levels. NFAT transcription factors are the main regulators of genes involved in slow-twitch program. Therefore, NFAT activation leads to a structural shift of muscle fibers from fast to slow, in contrast with metabolic properties, even if no changes in time to peak, half time to peak and relaxation time of the twitch have been observed. This lack of change in contractile properties is likely due to the fact that the change in fiber type is only partial, and therefore not sufficient to modify whole muscle contractile properties.

In skeletal muscle, autophagy is suggested to be controlled by FoxO3, by promoting “atrogenes” transcription (Mammucari et al., 2007). However, activation of mTORC1 results in an autophagy block, despite FoxO3 activation, while abrogation of mTORC1 signaling in RAmKO mice leads

to autophagy induction, regardless of FoxO inhibition (Bentzinger et al., 2008) (Castets et al., 2013). Thus, mTORC1 acquires a key role in autophagy induction in skeletal muscle. Nevertheless, many of the features that we observed in our inducible Raptor ko model, such as the mitochondrial dysfunction, the NMJ degeneration and the central structures, are often associated to an autophagy block (Carnio et al., 2014). Moreover, this would be in line also with mRNA expression of E3 ubiquitin ligases and autophagy-related genes observed in Raptor ko mice, whose reduction is likely linked to Akt hyperactivation and, thus, FoxO inhibition (Fig.1). In addition, we observed that in the absence of mTORC1, TFEB transcription factor goes into the nucleus, where it is active. However, TFEB target genes are downregulated in knock-out animals, suggesting that it maybe requires a co-factor, such as FoxO, to act. To test these hypothesis, future plans involve autophagic flux measurements and ChiP analysis for TFEB and FoxO. In conclusion, mTORC1 is important for maintaining muscle homeostasis also during adulthood.

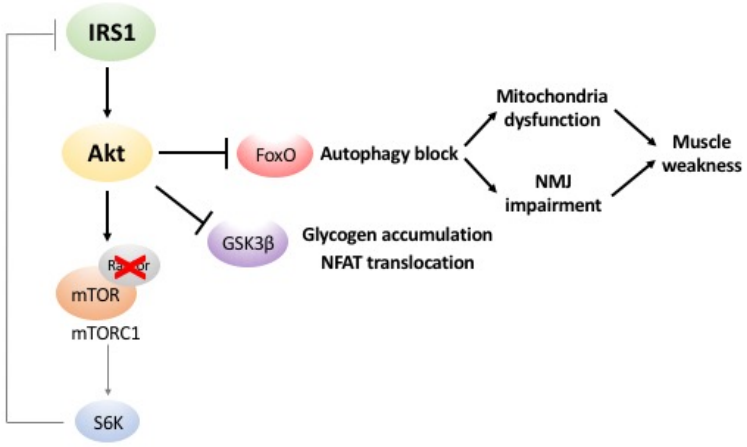

Fig.1: Proposed mechanism of muscle myopathy caused by Raptor deletion

PART II

So far, our results highlight the role of Raptor in the maintenance of muscle homeostasis. However, to evaluate its role in the regulation of muscle mass and especially in Akt-induced hypertrophy, we generated the Akt-Raptor ko mouse model. Akt overexpression results in a significant muscle hypertrophy, which is partially reduced upon rapamycin administration. Moreover, similar results were obtained in mice lacking S6K1/2 or transfected with a constitutive active form of 4EBP1 (4EBP1-4A). However, rapamycin treatment in S6K1 knock-out mice transfected with 4EBP1-4A did not further reduce fiber hypertrophy, suggesting that S6K1 and 4EBP1 are the rapamycin-sensitive targets that control skeletal muscle hypertrophy (Marabita et al., 2016). Raptor deletion partially decreases Akt-induced hypertrophy in our inducible model. Surprisingly, the increase in fiber size found in Akt-Raptor ko mice is completely prevented by rapamycin treatment. Muscle growth in Akt-Raptor ko mice is accompanied with increased S6 phosphorylation, similar to what observed in long-term Raptor ko animals in which Akt is hyperactivated. These results arise the question of a possible effect on S6 activity which is dependent from Akt, but either independent from Raptor or requires very little Raptor to be effective. S6 phosphorylation, in turn, reflects the increased protein synthesis observed in Akt-Raptor ko mice.

We recently demonstrated that, in contrast to Akt mice, Akt-S6K1 ko animals show a non-functional hypertrophy, suggesting that S6K1 is required for skeletal muscle function. Moreover, rapamycin treatment preserves the drop of normalized force observed, by preventing the formation of p62-positive protein aggregates (Marabita et al., 2016). Akt-Raptor ko mice show a reduced muscle strength, accompanied by increased ER stress and p62 accumulation. However, despite rapamycin administration prevents p62 accumulation and reduces ER stress levels, it does not restore normal muscle performance. Further investigations on rapamycin effects on both Raptor ko and Akt-Raptor ko mouse models

have to be done.

To conclude, Raptor is partially controlling Akt-induced muscle hypertrophy, but it is certainly required for maintaining a proper muscle function. These results underline the importance of better understanding the key factors involved in muscle performance. Indeed, in many pathologies reduction in muscle mass is accompanied with a decrease in the specific force. Moreover, understanding the key players in the regulation of muscle mass could be of therapeutic interest for diseases involving muscle wasting.

5. APPENDIX

Fig.1: Mitoprofile

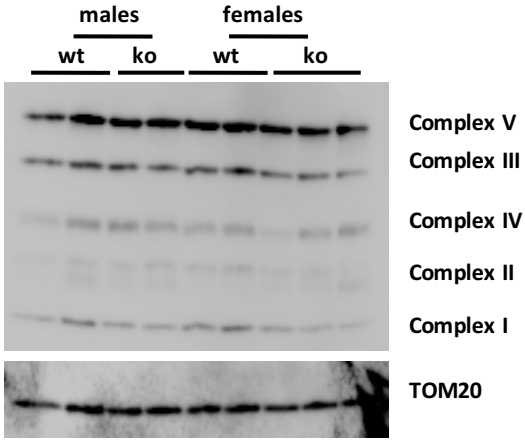

Western blot analysis for the different respiratory chain complexes in wild-type and knock-out long-term mice. n=2 each group

Fig.2: Proteomic data

-Log t-test p value_7month_KO_ vs_WT	log2 ratio_7month_KO_v s_WT	Protein names	Gene names
3,303	-1,821	Glycerophosphocholine phosphodiesterase GPCPD1	Gpcpd1
3,896	-1,743	Glutathione S-transferase Mu 2	Gstm2
2,404	-1,608	Serine beta-lactamase-like protein LACTB, mitochondrial	Lactb
4,070	-1,604	Branched-chain-amino-acid aminotransferase;Branched-chain-amino-acid aminotransferase, mitochondrial	Bcat2
2,578	-1,597	Proline-rich protein 33	Prr33
4,882	-1,585	NAD(P)H dehydrogenase [quinone] 1	Nqo1
1,962	-1,480	Geranylgeranyl transferase type-2 subunit beta	Rabggtb
2,451	-1,425	Glutamine synthetase	Glul
1,578	-1,425	2-oxoisovalerate dehydrogenase subunit beta, mitochondrial	Bckdhb
5,878	-1,395	2-oxoisovalerate dehydrogenase subunit alpha, mitochondrial	Bckdha

3,193	-1,361	Glutathione S-transferase Mu 1	Gstm1
5,010	-1,352	Succinyl-CoA:3-ketoacid coenzyme A transferase 1, mitochondrial;Succinyl-CoA:3-ketoacid-coenzyme A transferase	Oxct1
3,243	-1,325	Cytosolic 5-nucleotidase 1A	Nt5c1a
3,737	-1,316	NADP-dependent malic enzyme;Malic enzyme	Me1
2,611	-1,305	AMP deaminase 1	Ampd1
6,887	-1,300	Glycerol-3-phosphate dehydrogenase, mitochondrial;Glycerol-3-phosphate dehydrogenase	Gpd2
3,300	-1,248	Short/branched chain specific acyl-CoA dehydrogenase, mitochondrial	Acadsb
3,919	-1,162	Propionyl-CoA carboxylase alpha chain, mitochondrial	Pcca
2,721	-1,150	Sulfite oxidase, mitochondrial	Suox
3,002	-1,122	NADP-dependent malic enzyme, mitochondrial	Me3
3,172	-1,088	Phosphorylase b kinase regulatory subunit alpha, skeletal muscle isoform	Phka1
3,966	-1,055	UPF0317 protein C14orf159 homolog, mitochondrial	9030617O03Rik
1,794	-1,020	Glycogenin-1	Gyg1;Gyg
2,581	-1,009	Carboxylesterase 1D	Ces1d
2,713	-1,006	Phosphorylase b kinase regulatory subunit beta	Phkb
2,813	-1,000	Mitochondrial dynamics protein MID49	Mief2
2,342	-0,999	NADH dehydrogenase [ubiquinone] 1 beta subcomplex subunit 2, mitochondrial	Ndufb2
4,248	-0,991	Methylmalonate-semialdehyde dehydrogenase [acylating], mitochondrial	Aldh6a1
2,868	-0,984	Glycogen phosphorylase, muscle form;Alpha-1,4 glucan phosphorylase	Pygm
3,523	-0,975	Atlastin-2	Atl2
0,885	-0,971	Collagen alpha-1(I) chain	Col1a1
4,891	-0,952	5-oxoprolinase	Oplah
3,662	-0,952	NADH-ubiquinone oxidoreductase chain 1	Mtnd1
1,814	-0,949	Methylcrotonoyl-CoA carboxylase beta chain, mitochondrial	Mccc2
1,177	-0,940	Protein phosphatase 1 regulatory subunit 1A	Ppp1r1a
2,876	-0,940	Kynurenine--oxoglutarate transaminase 3	Ccbl2
1,866	-0,936	Selenium-binding protein 1;Selenium-binding protein 2	Selenbp1;Selenbp2
2,906	-0,931	Acetyl-coenzyme A synthetase 2-like, mitochondrial	Acss1
2,484	-0,918	Chloride channel protein;Chloride channel protein 1	Clcn1
2,677	-0,915	Trans-1,2-dihydrobenzene-1,2-diol dehydrogenase	Dhdh
2,482	-0,906	Endoplasmic reticulum resident protein 44	Erp44
2,280	-0,905	Protein 4.1	Epb4.1;Epb41
2,835	-0,878	Riboflavin kinase	Rfk
2,217	-0,877	OCIA domain-containing protein 2	Ociad2
4,169	-0,877	Propionyl-CoA carboxylase beta chain, mitochondrial	Pccb
2,219	-0,807	NADH dehydrogenase [ubiquinone] 1 beta subcomplex subunit 8, mitochondrial	Ndufb8
1,580	-0,796	Hydroxyacid-oxoacid transhydrogenase, mitochondrial	Adhfe1
2,535	-0,775	Fructose-2,6-bisphosphatase TIGAR	Tigar
6,670	-0,774	Long-chain fatty acid transport protein 1	Slc27a1

2,134	-0,770	Selenide, water dikinase 2	Sephs2
2,375	-0,758	ATP-binding cassette sub-family F member 2	Abcf2
2,669	-0,751	Phosphoglycerate mutase 2	Pgam2
2,242	-0,749	Myozenin-1	Myoz1
3,585	-0,739	Myosin light chain kinase 2, skeletal/cardiac muscle	Mylk2
3,623	-0,718	NADH dehydrogenase [ubiquinone] 1 beta subcomplex subunit 9	Ndufb9
3,252	-0,713	Serine/threonine-protein kinase Nek7	Nek7
2,779	-0,710	Parvalbumin alpha	Pvalb
2,289	-0,706	FAD-linked sulfhydryl oxidase ALR	Gfer
0,497	-0,688	Myosin light chain 4	Myl4
1,776	-0,686	Dehydrogenase/reductase SDR family member 7C	Dhrs7c
3,009	-0,670	Phosphoglucomutase-1	Pgm1
1,576	-0,665	Lipoamide acyltransferase component of branched-chain alpha-keto acid dehydrogenase complex, mitochondrial	Dbt
2,422	-0,665	[Pyruvate dehydrogenase [acetyl-transferring]]-phosphatase 1, mitochondrial	Pdp1
2,452	-0,662	NADH dehydrogenase [ubiquinone] 1 beta subcomplex subunit 11, mitochondrial	Ndufb11
1,901	-0,659	Apolipoprotein O	Apoo
2,182	-0,657	Methylcrotonoyl-CoA carboxylase subunit alpha, mitochondrial	Mccc1
3,513	-0,648	Citrate synthase, mitochondrial	Cs
2,729	-0,634	L-lactate dehydrogenase A chain;L-lactate dehydrogenase	Ldha
3,011	-0,624	Trifunctional purine biosynthetic protein adenosine-3;Phosphoribosylamine--glycine ligase;Phosphoribosylformylglycinamidine cyclo-ligase;Phosphoribosylglycinamide formyltransferase	Gart
3,109	-0,623	Glyceraldehyde-3-phosphate dehydrogenase	Gapdh
3,247	-0,621	Protein deglycase DJ-1	Park7
1,750	-0,594	NADH dehydrogenase [ubiquinone] 1 alpha subcomplex subunit 3	Ndufa3

Fig.3: Western blot for polyubiquitin proteins

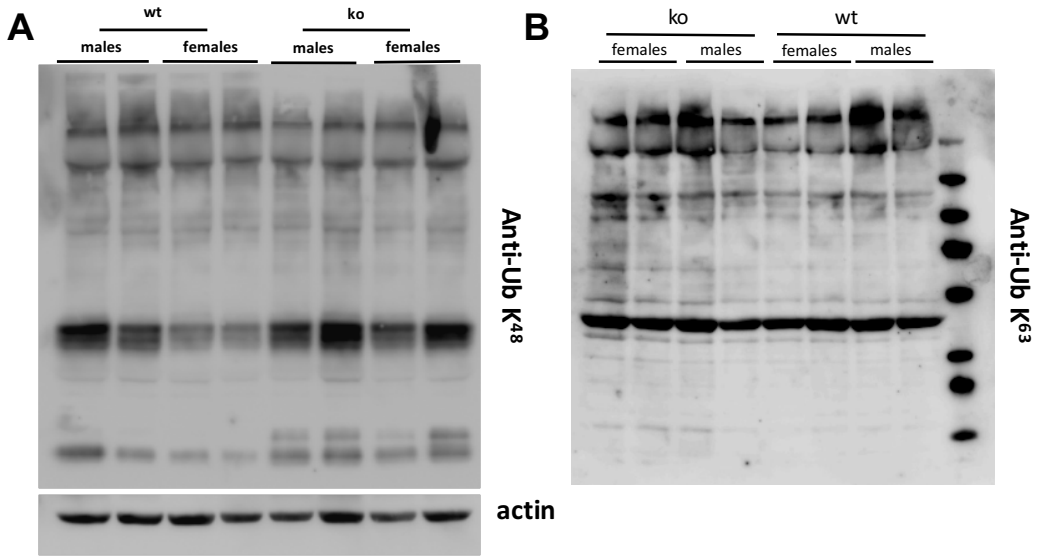

Western blot analysis for Lys48 (A) and Lys63 (B) polyubiquitin proteins in wild-type and knock-out long-term mice. n=2 each group

6. BIBLIOGRAPHY

Alain, T., Morita, M., Fonseca, B.D., Yanagiya, A., Siddiqui, N., Bhat, M., Zammit, D., Marcus, V., Metrakos, P., Voyer, L.A., et al. (2012). eIF4E/4E-BP ratio predicts the efficacy of mTOR targeted therapies. Cancer Res *72*, 6468-6476.

Amthor, H., Macharia, R., Navarrete, R., Schuelke, M., Brown, S.C., Otto, A., Voit, T., Muntoni, F., Vrbova, G., Partridge, T., et al. (2007). Lack of myostatin results in excessive muscle growth but impaired force generation. Proc Natl Acad Sci U S A *104*, 1835-1840.

Barrett K.E., Boitano S., Barman S.M., Brooks H.L. (2010). Chapther 5 – Excitable tissue: muscle, in "*Ganong's review of medical physiology*" twenty-third edition.

Bdolah, Y., Segal, A., Tanksale, P., Karumanchi, S.A., and Lecker, S.H. (2007). Atrophy-related ubiquitin ligases atrogin-1 and MuRF-1 are associated with uterine smooth muscle involution in the postpartum period. Am J Physiol Regul Integr Comp Physiol *292*, R971-976.

Beals, C.R., Sheridan, C.M., Turck, C.W., Gardner, P., and Crabtree, G.R. (1997). Nuclear export of NF-ATc enhanced by glycogen synthase kinase-3. Science *275*, 1930-1934.

Bentzinger, C.F., Romanino, K., Cloetta, D., Lin, S., Mascarenhas, J.B., Oliveri, F., Xia, J., Casanova, E., Costa, C.F., Brink, M., et al. (2008). Skeletal muscle-specific ablation of raptor, but not of rictor, causes metabolic changes and results in muscle dystrophy. Cell Metab *8*, 411-424.

Bjorkoy, G., Lamark, T., Brech, A., Outzen, H., Perander, M., Overvatn, A., Stenmark, H., and Johansen, T. (2005). p62/SQSTM1 forms protein aggregates degraded by autophagy and has a protective effect on huntingtin-induced cell death. J Cell Biol *171*, 603-614.

Blaauw, B., Canato, M., Agatea, L., Toniolo, L., Mammucari, C., Masiero, E., Abraham, R., Sandri, M., Schiaffino, S., and Reggiani, C. (2009). Inducible activation of Akt increases skeletal muscle mass and force without satellite cell activation. FASEB J *23*, 3896-3905.

Blaauw, B., Mammucari, C., Toniolo, L., Agatea, L., Abraham, R., Sandri, M., Reggiani, C., and Schiaffino, S. (2008). Akt activation prevents the force drop induced by eccentric contractions in dystrophin-deficient skeletal muscle. Hum Mol Genet *17*, 3686-3696.

Bodine, S.C., Latres, E., Baumhueter, S., Lai, V.K., Nunez, L., Clarke, B.A., Poueymirou, W.T., Panaro, F.J., Na, E., Dharmarajan, K., et al. (2001a). Identification of ubiquitin ligases required for skeletal muscle atrophy. Science *294*, 1704-1708.

Bodine, S.C., Stitt, T.N., Gonzalez, M., Kline, W.O., Stover, G.L., Bauerlein, R., Zlotchenko, E., Scrimgeour, A., Lawrence, J.C., Glass, D.J., et al. (2001b). Akt/mTOR pathway is a crucial regulator of skeletal muscle hypertrophy and can prevent muscle atrophy in vivo. Nat Cell Biol *3*, 1014-1019.

Bogdanovich, S., Perkins, K.J., Krag, T.O., Whittemore, L.A., and Khurana, T.S. (2005). Myostatin propeptide-mediated amelioration of dystrophic pathophysiology. FASEB J *19*, 543-549.

Carnio, S., LoVerso, F., Baraibar, M.A., Longa, E., Khan, M.M., Maffei, M., Reischl, M., Canepari, M., Loefler, S., Kern, H., et al.

(2014). Autophagy impairment in muscle induces neuromuscular junction degeneration and precocious aging. Cell Rep *8*, 1509-1521.

Castets, P., Lin, S., Rion, N., Di Fulvio, S., Romanino, K., Guridi, M., Frank, S., Tintignac, L.A., Sinnreich, M., and Ruegg, M.A. (2013). Sustained activation of mTORC1 in skeletal muscle inhibits constitutive and starvation-induced autophagy and causes a severe, late-onset myopathy. Cell Metab *17*, 731-744.

Chen, D., and Dou, Q.P. (2010). The ubiquitin-proteasome system as a prospective molecular target for cancer treatment and prevention. Curr Protein Pept Sci *11*, 459-470.

Ciciliot, S., Rossi, A.C., Dyar, K.A., Blaauw, B., and Schiaffino, S. (2013). Muscle type and fiber type specificity in muscle wasting. Int J Biochem Cell Biol *45*, 2191-2199.

Cohen, P., and Frame, S. (2001). The renaissance of GSK3. Nat Rev Mol Cell Biol *2*, 769-776.

Eskelinen, E.L., and Saftig, P. (2009). Autophagy: a lysosomal degradation pathway with a central role in health and disease. Biochim Biophys Acta *1793*, 664-673.

Flynn, J.M., O'Leary, M.N., Zambataro, C.A., Academia, E.C., Presley, M.P., Garrett, B.J., Zykovich, A., Mooney, S.D., Strong, R., Rosen, C.J., et al. (2013). Late-life rapamycin treatment reverses age-related heart dysfunction. Aging Cell *12*, 851-862.

Frezza, C., Cipolat, S., and Scorrano, L. (2007). Organelle isolation: functional mitochondria from mouse liver, muscle and cultured fibroblasts. Nat Protoc *2*, 287-295.

Fusi, L., Huang, Z., and Irving, M. (2015). The Conformation of Myosin Heads in Relaxed Skeletal Muscle: Implications for Myosin-Based Regulation. Biophys J *109*, 783-792.

Gomes, M.D., Lecker, S.H., Jagoe, R.T., Navon, A., and Goldberg, A.L. (2001). Atrogin-1, a muscle-specific F-box protein highly expressed during muscle atrophy. Proc Natl Acad Sci U S A *98*, 14440-14445.

Goodman, C.A., Frey, J.W., Mabrey, D.M., Jacobs, B.L., Lincoln, H.C., You, J.S., and Hornberger, T.A. (2011a). The role of skeletal muscle mTOR in the regulation of mechanical load-induced growth. J Physiol *589*, 5485-5501.

Goodman, C.A., Mabrey, D.M., Frey, J.W., Miu, M.H., Schmidt, E.K., Pierre, P., and Hornberger, T.A. (2011b). Novel insights into the regulation of skeletal muscle protein synthesis as revealed by a new nonradioactive in vivo technique. FASEB J *25*, 1028-1039.

Grumati, P., Coletto, L., Sabatelli, P., Cescon, M., Angelin, A., Bertaggia, E., Blaauw, B., Urciuolo, A., Tiepolo, T., Merlini, L., et al. (2010). Autophagy is defective in collagen VI muscular dystrophies, and its reactivation rescues myofiber degeneration. Nat Med *16*, 1313-1320.

Guertin, D.A., Stevens, D.M., Thoreen, C.C., Burds, A.A., Kalaany, N.Y., Moffat, J., Brown, M., Fitzgerald, K.J., and Sabatini, D.M. (2006). Ablation in mice of the mTORC components raptor, rictor, or mLST8 reveals that mTORC2 is required for signaling to Akt-FOXO and PKCalpha, but not S6K1. Dev Cell *11*, 859-871.

Hara, K., Maruki, Y., Long, X., Yoshino, K., Oshiro, N., Hidayat, S., Tokunaga, C., Avruch, J., and Yonezawa, K. (2002). Raptor, a

binding partner of target of rapamycin (TOR), mediates TOR action. Cell *110*, 177-189.

Harrison, D.E., Strong, R., Sharp, Z.D., Nelson, J.F., Astle, C.M., Flurkey, K., Nadon, N.L., Wilkinson, J.E., Frenkel, K., Carter, C.S., et al. (2009). Rapamycin fed late in life extends lifespan in genetically heterogeneous mice. Nature *460*, 392-395.

Hay, N., and Sonenberg, N. (2004). Upstream and downstream of mTOR. Genes Dev *18*, 1926-1945.

He, C., Bassik, M.C., Moresi, V., Sun, K., Wei, Y., Zou, Z., An, Z., Loh, J., Fisher, J., Sun, Q., et al. (2012). Exercise-induced BCL2-regulated autophagy is required for muscle glucose homeostasis. Nature *481*, 511-515.

Hilioti, Z., Gallagher, D.A., Low-Nam, S.T., Ramaswamy, P., Gajer, P., Kingsbury, T.J., Birchwood, C.J., Levchenko, A., and Cunningham, K.W. (2004). GSK-3 kinases enhance calcineurin signaling by phosphorylation of RCNs. Genes Dev *18*, 35-47.

Irwin, W.A., Bergamin, N., Sabatelli, P., Reggiani, C., Megighian, A., Merlini, L., Braghetta, P., Columbaro, M., Volpin, D., Bressan, G.M., et al. (2003). Mitochondrial dysfunction and apoptosis in myopathic mice with collagen VI deficiency. Nat Genet *35*, 367-371.

Ju, J.S., Varadhachary, A.S., Miller, S.E., and Weihl, C.C. (2010). Quantitation of "autophagic flux" in mature skeletal muscle. Autophagy *6*, 929-935.

Kang, S.A., Pacold, M.E., Cervantes, C.L., Lim, D., Lou, H.J., Ottina, K., Gray, N.S., Turk, B.E., Yaffe, M.B., and Sabatini, D.M.

(2013). mTORC1 phosphorylation sites encode their sensitivity to starvation and rapamycin. Science *341*, 1236566.

Khan, N.A., Nikkanen, J., Yatsuga, S., Jackson, C., Wang, L., Pradhan, S., Kivela, R., Pessia, A., Velagapudi, V., and Suomalainen, A. (2017). mTORC1 Regulates Mitochondrial Integrated Stress Response and Mitochondrial Myopathy Progression. Cell Metab *26*, 419-428 e415.

Kim, D.H., Sarbassov, D.D., Ali, S.M., King, J.E., Latek, R.R., Erdjument-Bromage, H., Tempst, P., and Sabatini, D.M. (2002). mTOR interacts with raptor to form a nutrient-sensitive complex that signals to the cell growth machinery. Cell *110*, 163-175.

Kim, J., Kundu, M., Viollet, B., and Guan, K.L. (2011). AMPK and mTOR regulate autophagy through direct phosphorylation of Ulk1. Nat Cell Biol *13*, 132-141.

Kingsbury, T.J., and Cunningham, K.W. (2000). A conserved family of calcineurin regulators. Genes Dev *14*, 1595-1604.

Light, N., and Champion, A.E. (1984). Characterization of muscle epimysium, perimysium and endomysium collagens. Biochem J *219*, 1017-1026.

Liu, C.W., Li, X., Thompson, D., Wooding, K., Chang, T.L., Tang, Z., Yu, H., Thomas, P.J., and DeMartino, G.N. (2006). ATP binding and ATP hydrolysis play distinct roles in the function of 26S proteasome. Mol Cell *24*, 39-50.

Lopez, R.J., Mosca, B., Treves, S., Maj, M., Bergamelli, L., Calderon, J.C., Bentzinger, C.F., Romanino, K., Hall, M.N., Ruegg, M.A., et al. (2015). Raptor ablation in skeletal muscle decreases Cav1.1

expression and affects the function of the excitation-contraction coupling supramolecular complex. Biochem J *466*, 123-135.

Lowe, D.A., Surek, J.T., Thomas, D.D., and Thompson, L.V. (2001). Electron paramagnetic resonance reveals age-related myosin structural changes in rat skeletal muscle fibers. Am J Physiol Cell Physiol *280*, C540-547.

Luo, Y., Liu, L., Wu, Y., Singh, K., Su, B., Zhang, N., Liu, X., Shen, Y., and Huang, S. (2015). Rapamycin inhibits mSin1 phosphorylation independently of mTORC1 and mTORC2. Oncotarget *6*, 4286-4298.

Mammucari, C., Milan, G., Romanello, V., Masiero, E., Rudolf, R., Del Piccolo, P., Burden, S.J., Di Lisi, R., Sandri, C., Zhao, J., et al. (2007). FoxO3 controls autophagy in skeletal muscle in vivo. Cell Metab *6*, 458-471.

Marabita, M., Baraldo, M., Solagna, F., Ceelen, J.J.M., Sartori, R., Nolte, H., Nemazanyy, I., Pyronnet, S., Kruger, M., Pende, M., et al. (2016). S6K1 Is Required for Increasing Skeletal Muscle Force during Hypertrophy. Cell Rep *17*, 501-513.

Masiero, E., Agatea, L., Mammucari, C., Blaauw, B., Loro, E., Komatsu, M., Metzger, D., Reggiani, C., Schiaffino, S., and Sandri, M. (2009). Autophagy is required to maintain muscle mass. Cell Metab *10*, 507-515.

Milan, G., Romanello, V., Pescatore, F., Armani, A., Paik, J.H., Frasson, L., Seydel, A., Zhao, J., Abraham, R., Goldberg, A.L., et al. (2015). Regulation of autophagy and the ubiquitin-proteasome system by

the FoxO transcriptional network during muscle atrophy. Nat Commun *6*, 6670.

Mizushima, N., and Yoshimori, T. (2007). How to interpret LC3 immunoblotting. Autophagy *3*, 542-545.

Morita, M., Gravel, S.P., Chenard, V., Sikstrom, K., Zheng, L., Alain, T., Gandin, V., Avizonis, D., Arguello, M., Zakaria, C., et al. (2013). mTORC1 controls mitochondrial activity and biogenesis through 4E-BP-dependent translational regulation. Cell Metab *18*, 698-711.

Morita, M., Prudent, J., Basu, K., Goyon, V., Katsumura, S., Hulea, L., Pearl, D., Siddiqui, N., Strack, S., McGuirk, S., et al. (2017). mTOR Controls Mitochondrial Dynamics and Cell Survival via MTFP1. Mol Cell *67*, 922-935 e925.

Murgia, M., Serrano, A.L., Calabria, E., Pallafacchina, G., Lomo, T., and Schiaffino, S. (2000). Ras is involved in nerve-activity-dependent regulation of muscle genes. Nat Cell Biol *2*, 142-147.

Nakamura, S., and Yoshimori, T. (2017). New insights into autophagosome-lysosome fusion. J Cell Sci *130*, 1209-1216.

Nandi, D., Tahiliani, P., Kumar, A., and Chandu, D. (2006). The ubiquitin-proteasome system. J Biosci *31*, 137-155.

Patursky-Polischuk, I., Stolovich-Rain, M., Hausner-Hanochi, M., Kasir, J., Cybulski, N., Avruch, J., Ruegg, M.A., Hall, M.N., and Meyuhas, O. (2009). The TSC-mTOR pathway mediates translational activation of TOP mRNAs by insulin largely in a raptor- or rictor-independent manner. Mol Cell Biol *29*, 640-649.

Pette, D., and Heilmann, C. (1979). Some characteristics of sarcoplasmic reticulum in fast- and slow-twitch muscles. Biochem Soc Trans *7*, 765-767.

Pfaffl, M.W. (2001). A new mathematical model for relative quantification in real-time RT-PCR. Nucleic Acids Res *29*, e45.

Pickart, C.M., and Fushman, D. (2004). Polyubiquitin chains: polymeric protein signals. Curr Opin Chem Biol *8*, 610-616.

Risson, V., Mazelin, L., Roceri, M., Sanchez, H., Moncollin, V., Corneloup, C., Richard-Bulteau, H., Vignaud, A., Baas, D., Defour, A., et al. (2009). Muscle inactivation of mTOR causes metabolic and dystrophin defects leading to severe myopathy. J Cell Biol *187*, 859-874.

Rommel, C., Bodine, S.C., Clarke, B.A., Rossman, R., Nunez, L., Stitt, T.N., Yancopoulos, G.D., and Glass, D.J. (2001). Mediation of IGF-1-induced skeletal myotube hypertrophy by PI(3)K/Akt/mTOR and PI(3)K/Akt/GSK3 pathways. Nat Cell Biol *3*, 1009-1013.

Sacheck, J.M., Hyatt, J.P., Raffaello, A., Jagoe, R.T., Roy, R.R., Edgerton, V.R., Lecker, S.H., and Goldberg, A.L. (2007). Rapid disuse and denervation atrophy involve transcriptional changes similar to those of muscle wasting during systemic diseases. FASEB J *21*, 140-155.

Schiaffino, S., and Mammucari, C. (2011). Regulation of skeletal muscle growth by the IGF1-Akt/PKB pathway: insights from genetic models. Skelet Muscle *1*, 4.

Schiaffino, S., and Reggiani, C. (1996). Molecular diversity of myofibrillar proteins: gene regulation and functional significance. Physiol Rev *76*, 371-423.

Schiaffino, S., and Reggiani, C. (2011). Fiber types in mammalian skeletal muscles. Physiol Rev *91*, 1447-1531.

Schiaffino, S., Sandri, M., and Murgia, M. (2007). Activity-dependent signaling pathways controlling muscle diversity and plasticity. Physiology (Bethesda) *22*, 269-278.

Schmidt, E.K., Clavarino, G., Ceppi, M., and Pierre, P. (2009). SUnSET, a nonradioactive method to monitor protein synthesis. Nat Methods *6*, 275-277.

Schuler, M., Ali, F., Metzger, E., Chambon, P., and Metzger, D. (2005). Temporally controlled targeted somatic mutagenesis in skeletal muscles of the mouse. Genesis *41*, 165-170.

Sehgal, S.N. (1998). Rapamune (RAPA, rapamycin, sirolimus): mechanism of action immunosuppressive effect results from blockade of signal transduction and inhibition of cell cycle progression. Clin Biochem *31*, 335-340.

Settembre, C., De Cegli, R., Mansueto, G., Saha, P.K., Vetrini, F., Visvikis, O., Huynh, T., Carissimo, A., Palmer, D., Klisch, T.J., et al. (2013). TFEB controls cellular lipid metabolism through a starvation-induced autoregulatory loop. Nat Cell Biol *15*, 647-658.

Settembre, C., Di Malta, C., Polito, V.A., Garcia Arencibia, M., Vetrini, F., Erdin, S., Erdin, S.U., Huynh, T., Medina, D., Colella, P., et

al. (2011). TFEB links autophagy to lysosomal biogenesis. Science *332*, 1429-1433.

Shea, L., and Raben, N. (2009). Autophagy in skeletal muscle: implications for Pompe disease. Int J Clin Pharmacol Ther *47 Suppl 1*, S42-47.

Shende, P., Plaisance, I., Morandi, C., Pellieux, C., Berthonneche, C., Zorzato, F., Krishnan, J., Lerch, R., Hall, M.N., Ruegg, M.A., et al. (2011). Cardiac raptor ablation impairs adaptive hypertrophy, alters metabolic gene expression, and causes heart failure in mice. Circulation *123*, 1073-1082.

Spinazzi, M., Casarin, A., Pertegato, V., Salviati, L., and Angelini, C. (2012). Assessment of mitochondrial respiratory chain enzymatic activities on tissues and cultured cells. Nat Protoc *7*, 1235-1246.

Tezze, C., Romanello, V., Desbats, M.A., Fadini, G.P., Albiero, M., Favaro, G., Ciciliot, S., Soriano, M.E., Morbidoni, V., Cerqua, C., et al. (2017). Age-Associated Loss of OPA1 in Muscle Impacts Muscle Mass, Metabolic Homeostasis, Systemic Inflammation, and Epithelial Senescence. Cell Metab *25*, 1374-1389 e1376.

Wang, X., Yue, P., Tao, H., and Sun, S.Y. (2017). Inhibition of p70S6K does not mimic the enhancement of Akt phosphorylation by rapamycin. Heliyon *3*, e00378.

Winbanks, C.E., Chen, J.L., Qian, H., Liu, Y., Bernardo, B.C., Beyer, C., Watt, K.I., Thomson, R.E., Connor, T., Turner, B.J., et al. (2013). The bone morphogenetic protein axis is a positive regulator of skeletal muscle mass. J Cell Biol *203*, 345-357.

Xu, P., Duong, D.M., Seyfried, N.T., Cheng, D., Xie, Y., Robert, J., Rush, J., Hochstrasser, M., Finley, D., and Peng, J. (2009). Quantitative proteomics reveals the function of unconventional ubiquitin chains in proteasomal degradation. Cell *137*, 133-145.

Yang, Z., Huang, J., Geng, J., Nair, U., and Klionsky, D.J. (2006). Atg22 recycles amino acids to link the degradative and recycling functions of autophagy. Mol Biol Cell *17*, 5094-5104.

Yao, T.P. (2010). The role of ubiquitin in autophagy-dependent protein aggregate processing. Genes Cancer *1*, 779-786.

Zhao, J., Brault, J.J., Schild, A., Cao, P., Sandri, M., Schiaffino, S., Lecker, S.H., and Goldberg, A.L. (2007). FoxO3 coordinately activates protein degradation by the autophagic/lysosomal and proteasomal pathways in atrophying muscle cells. Cell Metab *6*, 472-483.